

University of Alberta

Experimental Tests of the Light-Use Efficiency Model in Alfalfa

by

Saulo Manuel Castro

A thesis submitted to the Faculty of Graduate Studies and Research
in partial fulfillment of the requirements for the degree of

Master of Science

Department of Earth and Atmospheric Sciences

©Saulo Manuel Castro-Contreras

Fall 2013

Edmonton, Alberta

Permission is hereby granted to the University of Alberta Libraries to reproduce single copies of this thesis and to lend or sell such copies for private, scholarly or scientific research purposes only. Where the thesis is converted to, or otherwise made available in digital form, the University of Alberta will advise potential users of the thesis of these terms.

The author reserves all other publication and other rights in association with the copyright in the thesis and, except as herein before provided, neither the thesis nor any substantial portion thereof may be printed or otherwise reproduced in any material form whatsoever without the author's prior written permission.

Abstract

This study explored ways of integrating optical and flux measurements in the context of the Light Use Efficiency (LUE) model in an alfalfa (*Medicago sativa*) field. Narrow-band spectrometers and low cost two-band radiometers provided alternate ways to measure NDVI and estimate the APAR term of the LUE model. The high temporal resolution of two-band sensors system accurately tracked seasonal carbon flux dynamics ($R^2 = 0.96$) demonstrating the value of automated, low cost approaches to monitoring NDVI and canopy light absorption, which was the dominant term in the LUE model for this agricultural field. At the seasonal scale PRI correlations with LUE varied with the LUE formulation, and suggested that seasonal PRI patterns were primarily driven by canopy structure changes. However, at the diurnal level, Δ PRI correlated with changing efficiency. Combined optical and flux sampling can help partition flux data, gap-fill data, and add insights into the controls of carbon fluxes.

Acknowledgements

Funding for this project was provided in the form of research grants to Dr. John Gamon from the Natural Science and Engineering Research Council of Canada (NSERC Discovery), and Alberta Innovates (iCORE). Additional support was provided by the Queen Elizabeth II Graduate Scholarship and the Mary Louise Imrie Graduate Student Award.

I would like to thank Dr. Lawrence Flanagan for the guidance and excellent scholarly advice he provided me during our short but productive meetings, and for his role in my Master's committee. I am also grateful for role Dr. Alex Wolf had in providing valuable additional perspectives for my thesis, as well as for his participation in my committee. I am indebted to my supervisor, Dr. John Gamon, whose amazing support and guidance throughout my Master's program went beyond expectations. I thank you for always challenging me to do my best and for helping me achieve one of the most meaningful life experiences thus far. I would also like gratefully acknowledge all the help provided to me by several very hard-working field assistants, including Morgan Randall, Chris Wong, Peter Carlson, and Enrica Nestola.

Thank you to my incredible friends Ernest (El Viejo), Nata (sabe TODO), Kiki (Ux), Michelle, Vir, Don, Sammy, and many others who provided me with endless support, encouragement and inspiration. Last but not least, I would like to thank my amazing Set and Nita who always told me I could accomplish anything. Los amo!!

Table of Contents

CHAPTER 1 – INTRODUCTION: BACKGROUND, CONTEXT.....	1
References Cited	11
CHAPTER 2– SENSORMONITORING AND COMPARISON	18
2.1 Introduction.....	18
2.2 Methods	20
2.2.1 Study site.....	20
2.2.2 Experimental design.....	22
2.2.3 Micrometeorology measurements.....	22
2.2.3.1 Eddy covariance instrumentation	22
2.2.3.2 NEE calculations	23
2.2.3.3 GPP and total ecosystem respiration calculations	25
2.2.4 Reflectance measurements	26
2.2.4.1 Hyperspectral data from tram system	26
2.2.4.2 Broadband data from phenology station	28
2.2.4.3 Calculation of reflectance indices	29
2.2.5 Direct fA_{PAR} measurements.....	30
2.3 Results	31
2.3.1 Monitoring through meteorological instruments	31
2.3.2 Monitoring through remote sensing instruments	35
2.3.3 Empirical comparison of broadband vs. narrow-band NDVI- fA_{PAR} relationships	40
2.4 Discussion	41
2.5 References Cited.....	46
CHAPTER 3 – TESTING PRI AS A PROXY OF LUE	51
3.1 Introduction	51
3.2 Methods	54
3.2.1 Study site.....	54
3.2.2 Hyperspectral tram reflectance	54

3.2.3 fA_{PAR} calculation.....	56
3.2.4 Continuous fA_{PAR} and A_{PAR} measurements.....	57
3.2.5 LUE derivations	58
3.2.6 Linear mixing model	59
3.2.7 Seasonal analysis of optical, fA_{PAR} and flux measurements.....	59
3.2.8 Diurnal Analysis of PRI as an LUE proxy	60
3.3 Results	62
3.3.1 Analysis of seasonal patterns.....	62
3.3.2 Seasonal PRI comparison to PAR, fA_{PAR} , and A_{PAR}	66
3.3.3 Linear mixing model and correlations to canopy structure.....	67
3.3.4 Diurnal evaluation of PRI as a proxy of LUE	69
3.4 Discussion.....	73
3.5 References Cited	79

CHAPTER 4 – EFFECTS OF TEMPORAL AGGREGATION ON LUE

MODEL ACCURACY	82
4.1 Introduction	82
4.2 Methods	84
4.2.1 Study site.....	84
4.2.2 Eddy-covariance derived GPP	84
4.2.3 Vegetation indices.....	85
4.2.4 fA_{PAR} and A_{PAR} values and derivations	87
4.2.5 Temporal aggregation of LUE model variables	88
4.3 Results	93
4.3.1 Temporal aggregation of each LUE model variable	93
4.3.2 Optical vs. flux productivity comparisons based on optimal aggregation.....	97
4.4 Discussion.....	101
4.5 References Cited	107

CHAPTER 5 – GENERAL DISCUSSION AND CONCLUSION

References Cited	118
------------------------	-----

List of Tables

Table 2-1: Description and notation of the various greenness indices derived from broadband data	30
Table 2-2: Correlations (R^2) of broadband derived NDVI proxies and GPP during the dormancy, green-up, and mature growth stages.	38
Table 4-1: Resulting optimal aggregation periods for each of the aggregation methods. Individual periods were calculated for each of the three growth cycles within the 2010 growth season and a composite of the entire growth season.	97

List of Figures

Figure 2-1: Alfalfa field located at the University of Alberta South Campus agricultural research farm and locations of tram, phenology and eddy covariance monitoring systems.....	21
Figure 2-2: Corresponding phenological stages designated for GPP and NDVI _{Huemmrich_II} greenness proxy for the 2010 growth season	33
Figure 2-3: Comparison of seasonal time series of mid-day GPP with total precipitation, PPFD temperature, VPD, and relative humidity.....	34
Figure 2-4: Composite of midday NDVI time series calculated through hyperspectral and broadband NDVI proxy indices compared to midday GPP	36
Figure 2-5: Time series of midday GPP and corresponding the various expressions of NDVI	37
Figure 2-6: Time series and simple correlations between narrow-band derived NDVI _{680,800} and broad-band NDVI proxies for the 2010 growing season	39
Figure 2-7: NDVI- fA_{PAR} relationships derived from mid-day hyperspectral spectrometer data and broadband spot radiometers data.....	41
Figure 3-1: Comparison of time series of midday GPP with irradiance, temperature, VPD, PRI _{531,570} , fA_{PAR} , LUE _{Inc} , and LUE _{Abs}	64
Figure 3-2: Comparison of hourly collected fA_{PAR} , midday LUE _{Inc} , and midday LUE _{Abs} to hourly collected PRI _{531,570} seasonal time series.....	65

Figure 3-3: One-to-one correlation of seasonal LUE_{Abs} and LUE_{Inc} showing a negative exponential correlation.....	65
Figure 3-4: One-to-one correlation of $PRI_{531,570}$ and PPFD, A_{PAR} , and fA_{PAR} for the entire 2010 growing season.....	67
Figure 3-5: Spectral reflectance results from the linear mixing model for various percentages of canopy closure.....	68
Figure 3-6: Seasonal correlation of LUE vs. PRI and LUE vs. fA_{PAR}	69
Figure 3-7: Time place of collection days <i>A</i> , <i>B</i> , <i>C</i> , and <i>D</i> used for diurnal analysis on the GPP and PRI seasonal time series.....	71
Figure 3-8: Analysis of diurnal patterns of light response curves and diurnal changes in PRI as a function of PPFD, for collection days <i>A</i> , <i>B</i> , <i>C</i> and <i>D</i>	72
Figure 3-9: Correlation between delta LUE and delta $PRI_{531,570}$ derived from diurnal analysis.....	73
Figure 4-1: Flow chart depicting the method used to calculate continuous fA_{PAR} derived from the measured $NDVI_{680,800}$ - fA_{PAR} relationship.....	88
Figure 4-2: Conceptual model showing how $NDVI_{proxy}$ data were associated with fA_{PAR} measurements during the calculation of continuous fA_{PAR} values.....	91
Figure 4-3: Work flows for aggregation of PAR, fA_{PAR} , A_{PAR} , GPP, and all variables combined	93

Figure 4-4: Comparison of the effect of aggregation through averaging on the time series of PAR, fA_{PAR} , A_{PAR} , and GPP.....	95
Figure 4-5: LUE model R^2 changes due to changing aggregation period in PAR, fA_{PAR} , A_{PAR} , GPP and all variables combined.....	96
Figure 4-6: Comparison between measured GPP and optically derived representation of productivity through PAR, $NDVI_{proxy}$, fA_{PAR} , and A_{PAR}	98
Figure 4-7: Seasonal comparison of GPP and optically derived representation of productivity for all combined growth cycles.....	99
Figure 4-8: Time series of measured GPP and A_{PAR} derived productivity	101
Figure 5-1: Hypothesized funnel concept describing the progress of integrating different data sources.....	113

List of Abbreviations

- α – LUE defined as the initial slope of the light response curve, also called “photon yield” or “quantum yield”(mol CO₂ mol⁻¹ PPFD).
- A_{PAR} – Absorbed photosynthetically active radiation ($\mu\text{mol m}^{-2} \text{s}^{-1}$).
- A_{max} – GPP at maximum PPFD ($\mu\text{mol m}^{-2} \text{s}^{-1}$).
- ϵ – Light use efficiency (mol CO₂ mol⁻¹ PPFD) when expressing “instantaneous” efficiency as opposed to time-integrated efficiency.
- EVI2 – Two band Enhanced Vegetation Index.
- fA_{PAR} – Fraction of absorbed photosynthetically active radiation.
- GPP – Gross primary productivity ($\mu\text{mol CO}_2\text{m}^{-2} \text{s}^{-1}$) when expressing “instantaneous” productivity.
- H – Sensible heat flux (W m^{-2}).
- IRGA – Infra-red gas analyzer.
- LE – Latent heat flux (W m^{-2}).
- LUE – Light use efficiency (mol CO₂ mol⁻¹ PPFD).
- MODIS – Moderate Resolution Imaging Spectroradiometer.
- NDVI_{680,800} – Normalized Differential Vegetation Index derived using 680nm and 800nm spectral bands.
- NDVI_{proxy} – Substitute Normalized Differential Vegetation Index derived from two-band sensors.
- NEE – Net ecosystem exchange ($\mu\text{mol CO}_2 \text{m}^{-2} \text{s}^{-1}$) when expressed on an “instantaneous” basis.
- ρ_a – The density of dry air (mol m^{-3}).
- ρ_{PAR} – Reflectance of photosynthetically active radiation (dimensionless).
- $\rho_{\text{corrected}}$ – Corrected reflectance normalized with 99% reflective white standard.
- ρ_{PYR} – Reflectance of solar radiation (dimensionless).

PAR – Photosynthetically active radiation (400-700 nm). Often used in remote sensing literature as a synonym for PPFD. In its original definition, PAR refers to the *quality* of light, not the flux of light.

PPFD – Photosynthetically-active photon flux density ($\mu\text{mol photons m}^{-2} \text{s}^{-1}$).

PRI_{531,570} – Photochemically Reflectance Index derived using 531nm and 570nm spectral bands.

Q₁₀ – Temperature sensitivity coefficient for TER (dimensionless).

R₁₀ – The rate of TER at 10°C ($\mu\text{mol m}^{-2} \text{s}^{-1}$).

RH – Relative humidity (%).

s' – Molar mixing ratio fluctuation (mol mol^{-1} dry air).

T – Air temperature (°C).

TER – Total ecosystem respiration ($\mu\text{mol m}^{-2} \text{s}^{-1}$).

VPD – Vapor pressure deficit (KPa).

w' – Vertical wind velocity fluctuation (m s^{-1}).

Chapter 1 – Introduction: Background and Context

The accurate assessment of global biosphere-atmosphere carbon exchange remains a major challenge for ecosystem scientists. Not only do we have to account for the size of the biospheric-atmospheric fluxes, but interpreting the ecological dynamics within each biome introduces a higher level of complexity that is responsible for our incomplete understanding of some of the carbon cycle mechanisms (Field et al., 1998, Running, 2008). Over the years, a goal of ecologists has been to develop consistent global ecosystem measurements that properly describe and integrate ecosystem dynamics (Schimel, 1995). Early methods attempted to model global productivity through various approaches that included the assessment of productivity through climate (Leith, 1975), soil, and nutrient availability (Schimel et al. 1994), distribution of assumed homogeneous biomes (Leith and Whittaker, 1975, Atjay et al., 1979), or by determining light interception by vegetation (Ruimy et al., 1994). Each conceptual model attempted to characterize the biosphere as a whole, however, each one contained errors due to oversimplifications of ecosystem dynamics or the lack of available spatially and temporally suitable data. To address ecosystem dynamics, methodical studies looking at temporal patterns within individual ecosystems need to be conducted. Characterizing ecosystem processes allows us to create regional models that characterize the challenges, limitations, and feasibility of global-scale models (Field et al., 1995). As such, we can think of ecosystem studies as being a key to

correctly informing global carbon models (Schimel, 1995; Braswell et al., 1997; Reich et al., 1999; Running et al., 2004; Turner et al. 2005).

The eddy covariance technique has become a valuable tool for assessing ecosystem mechanisms related to ecosystem-atmosphere gas fluxes. Eddy covariance allows the direct *in situ* measurement of carbon exchange between vegetated canopies and the atmosphere (Baldocchi et al. 1988). Carbon flux measurements quantify the total carbon accumulated by an ecosystem as the net gain or loss when both photosynthesis and respiration are considered, and is expressed as net ecosystem exchange (NEE) (Randerson et al., 2002). By providing real-time, non-invasive measurements of NEE, the eddy covariance technique has become the standard method for accessing ecosystem carbon fluxes. Partitioning net carbon fluxes into gross primary productivity (GPP), defined as the carbon fixed during photosynthesis over a period of time and respiration provides further insight into ecosystem functioning (Baldocchi, 2003).

Despite the wide acceptance of the eddy covariance method (Baldocchi et al., 2001; Baldocchi, 2008), there are some drawbacks to this technique. Measurements of fluxes are assumed to be in ecosystems under steady state atmospheric conditions, with homogenous vegetation in flat terrain (Baldocchi et al., 1988; Aubinet et al., 2000). Implementation of this technique in non-ideal conditions requires accounting for complex effects of atmospheric storage, wind divergence and advection which can lead to significant errors in the ecosystem carbon budget (Baldocchi et al., 1988; Baldocchi et al., 2000; Foken & Wichura, 1995; Massman & Lee; 2002). To correctly quantify local and global

carbon budgets, accurate measurements of carbon fluxes at stand scale that allow us to resolve the spatial and temporal variability of carbon exchange are required.

Remote sensing has provided the prospect to measure ecosystem productivity at scales ranging from local to global. One of the biggest benefits of remote sensing is its ability to sample across a wide range of spatial and temporal scales. Additionally, remote sensing gives us the ability to gather a wide range of data from locations that were previously inaccessible and to do this in a non-destructive way. Most remote sensing methods for ecosystem carbon flux assessment have involved the light-use efficiency (LUE) model.

The LUE model was first proposed by Monteith (1972, 1977), and in its simplest form states that the amount of plant growth is a function of a structural term determining light absorption and a physiological efficiency term. In more specific terms, Monteith determined that the amount of productivity can be quantified by measuring the amount of photosynthetically active radiation (PAR) absorbed by the canopy, and the efficiency by which that absorbed radiation is transformed to fixed carbon (dry biomass) during a specific time period. This can be expressed as

$$\text{Total Yield} = \epsilon_0 \int A_{PAR} dt \quad (1)$$

where A_{PAR} ($\mu\text{mol m}^{-2} \text{s}^{-1}$) is the absorbed photosynthetically available radiation (PAR) ($\mu\text{mol m}^{-2} \text{s}^{-1}$) and ϵ represents the light use efficiency (LUE). In its original formulation, ϵ was expressed in g MJ (grams of dry matter per mega

joule of solar radiation, integrated over a growing season, Monteith, 1977), but recent applications have often applied a more instantaneous definition and units (e.g. mol CO₂mol⁻¹ PPFD, or μmol CO₂μmol⁻¹ PPFD). Depending upon the application it can be integrated over an annual cycle, although other periods (e.g., instantaneous, daily, weekly or monthly) are also used.

A principal advantage of this model is that it can be applied at a wide range of spatial scales (*i.e.* at leaf-level, at canopy-level, or stand level) and time periods across all vegetation types. Furthermore, the LUE model can be directly linked to remote sensing, allowing the required data to be collected, even over large areas, by non-destructive methods. When driven by remote sensing, the LUE model is conventionally expressed in terms of gross primary production (GPP) expressed as follows:

$$GPP = \sum_{i=1}^n A_{PAR} \times \epsilon \quad (2)$$

where $\sum A_{PAR}$ refers to the integration of absorbed photosynthetic available radiation over time frame (Monteith, 1977; Asrar et al., 1984; Sellers 1985). Traditionally, light absorption is integrated temporally into seasonally or yearly time periods. However, conceptually, the LUE model expressed by equation (2) can describe various temporal scales, including “instantaneous” measurements (Gamon et al., 2001). In this thesis, an LUE model was derived using instantaneous light absorption measurements as a basis for examining the processes influencing the terms in the model. Primary productivity is often

measured in terms of *net* instead of gross values. This requires the addition of a respiration term to the model (Prince and Goward, 1995; Ruimy et al., 1994). Alternatively, respiration is sometimes integrated into the model (Gamon and Qiu, 1999).

In the remote sensing community, PAR is sometimes used as a synonym of photosynthetic photon flux density (PPFD) when discussing the LUE model. Throughout this thesis, PPFD will be used to describe the flux of downwelling radiation from 400 to 700 nm, and PAR will be used to refer to the expression of PPFD in the context of the LUE model equation, following this remote sensing convention. The relationship between optical remote sensing and the LUE model is based on the principle that PAR measurements can be combined with the fraction of PAR absorbed by vegetation (fA_{PAR}) to determine the A_{PAR} term, providing a measure of *potential* photosynthetic activity (Sellers, 1985, Sellers et al., 1987; Myneni and Williams, 1994). More specifically, A_{PAR} is the product of the fraction of the photosynthetic available radiation absorbed by the *green portions* of the plant (green fA_{PAR}) and the total downwelling irradiance, or PPFD. Typically, green fA_{PAR} is assessed using a vegetation index, usually the normalized difference vegetation index (NDVI). The relationship between the normalized difference vegetation index (NDVI) and green fA_{PAR} has been explored both theoretically (Kumar & Monteith, 1981; Sellers et al., 1987; Prince, 1991; Goward & Huemmrich, 1992) and empirically (Daughtry et al., 1983; Gallo et al., 1985; Gamon et al., 1995), showing that NDVI and green fA_{PAR} are closely correlated.

Light use efficiency provides a physiological measure of how plants respond to changing environmental conditions (Monteith, 1972; 1977). Its complexity, relating to the large number of factors that can possibly be encompassed within this term, has led to different ways of treating this variable. Monteith (1977) first proposed that the efficiency term should be relatively constant for all plant functional types across all ecosystems, and this view has sometimes been supported by the observation that most unstressed vegetation has a similar photosynthetic photon yield (Manchow, 1985; Garcia et al. 1988; Field, 1991). However, exceptions have been observed in canopies under water, temperature, and nutrient stresses, and efficiency can vary with ontogeny, season, and functional types (Runyon et al., 1994; Gamon et al., 1995; Landsberg and Waring, 1997; Huemmrich et al., 2010). Many researchers using the LUE model have, therefore, adopted the approach of estimating a variable efficiency term that accounts for variability between vegetation types as well as the seasonal variability within an ecosystem.

The NASA Moderate-Resolution Imaging Spectroradiometer (MODIS) satellite instrument for calculating GPP/NPP (MOD17A2/A3) products follows this approach (Heinsch et al., 2003). To quantify the range of efficiency across biomes, MODIS algorithms use a biome parameter look-up table (BPLUT) that starts with a maximum efficiency for each biome type. This efficiency is further modified by temperature and vapor pressure deficit (VPD) derived from gridded (interpolated) meteorological data (Running et al., 2004). However, these meteorological data are collected at much coarser spatial resolutions (1° latitude x

1.25° longitude) than the MODIS pixel (250m), leading to a significant loss of information due to the degradation of the intrinsic spatial variability within ecosystems (Running et al., 2004; Turner et al., 2005; Zhao et al., 2005; Heinsch et al., 2006). Consequently, a more direct assessment of LUE at a finer scale is needed.

One proposed method to reduce inaccuracies within the LUE model is to exclude all externally derived meteorological data and instead estimate efficiency solely from remote sensing data (Gamon and Qiu, 1999; Sims et al., 2006; Strachan et al., 2008; Grace et al., 2007; Coops et al., 2010). Advances in the spectral resolution of remote sensing tools have provided some new opportunities for estimating LUE. One possible method involves the photochemical reflectance index (PRI), typically derived from narrow band reflectance at 531 and 570 nm (Gamon et al., 1990, 1992, 1993; Peñuelas et al., 1995; Filella et al., 1996). Over certain conditions, this index can serve as a proxy for the activity of the xanthophyll cycle, which is closely linked to photosystem II (PSII) photochemical efficiency (Gamon et al., 1990, 1992; Peñuelas et al., 1995). A useful tool for defining these conditions is the concept of “excess light energy”. This can be visualized through commonly used light response curves where departure from the linear, light limited region indicates light saturation and excess energy (Björkman and Demmig-Adams 1994). Under excess light, the majority of PSII centers remain in a reduced (closed) state, leaving them susceptible to photoinhibitory damage. To prevent damage, carotenoid pigments composing the xanthophyll cycle undergo chemical changes and quench excess energy. The

general mechanism for the xanthophyll cycle involves the conversion of violaxanthin to the photoprotective pigment zeaxanthin, via antheraxanthin as a response to exposure to excess light (Bjorkman and Demming-Adams, 1994; Demming-Adams et al., 1995, 1996). This mechanism provides a sink for excess energy and thus a method for light regulation, and can be detected optically via the PRI (Gamon et al. 1992, 1997, Gamon and Surfus 1999).

It should be noted that PRI was originally defined in the context of diurnal changing light levels and photosynthetic rates (Gamon et al. 1992, 1993, Peñuelas et al., 1995). Since then, many remote sensing studies have used the PRI as an indicator of changing photosynthesis. However, most of these studies have been correlative in nature, and have not explicitly examined the *cause* of changing PRI over time and space. PRI interpretation becomes particularly problematic over large time scales (e.g. seasonal change) or spatial scales (e.g. regional or global satellite measurements), where many confounding factors including canopy structure, view and illumination angles can affect PRI (Barton & North, 2001). Additionally, across seasons or multiple canopies, PRI often provides a measure of canopy greenness or chlorophyll:carotenoid ratios (Sims & Gamon 2002, Stylinski et al. 2002, Filella et al. 2004 & 2009, Garrity et al. 2011, Gamon & Berry 2012), which may also scale with light-use efficiency, although this relationship between pigment pool sizes and LUE has received less attention than the effect of xanthophyll cycle epoxidation state. Perhaps for these reasons, attempts to compare satellite based PRI and photosynthetic efficiency across ecosystems have typically demonstrated contrasting PRI-LUE relationships for

different ecosystems (Nichol et al. 2002; Goerner et al. 2011), calling into question PRI's ability to accurately measure LUE when used in a remote sensing context. Consequently, the utility of PRI as a remote-sensing measure of LUE remains an open question.

One challenge of testing the LUE model for individual ecosystems is that the necessary data are often not easily available at the appropriate temporal or spatial scales. For this reason, there is a need to apply field spectrometers within the flux tower footprint, sometimes periodically or continuously over time (Gamon et al. 2006a, 2010). These studies are beginning to yield insights into factors affecting the terms of the LUE model, but principle challenges include obtaining accurate and cost effective data with comparable methods. In recent years, a variety of methods have been developed to address these challenges (Huemmrich et al 1999, Gamon et al., 2006b; Leuning et al., 2006; Vierling et al. 2006; Hilker et al., 2007; Richardson et al., 2007). Recently, low-cost methods involving simple broadband radiometers (Huemmrich et al., 1999) or two-band radiometers (Eklundh et al. 2011) have also been explored as alternative ways to estimate the terms of the LUE model. The assessment of vegetation at the ecosystem scale, allows us to address the strengths and weaknesses of the model and develop an operational model that can be scaled spatially and temporally. Ideally, this working model would not focus only on one data source, but would take advantage of different data resources. For example, much information could be gathered through the comparison and integration of different optical data sources, ranging from hyperspectral to broadband.

For this study we utilized proximal remote sensing collected from a tram system (Gamon et al., 2006b), automated, tower-mounted broadband sensors, and eddy covariance data to assess crop productivity using the LUE model. The objectives of the study were to 1) determine the feasibility of using two-band sensors to derive an A_{PAR} term that is comparable to one derived from standard narrow-band data; 2) determine if PRI can be used as a proxy of LUE and, if so, to evaluate the mechanisms driving this association; 3) determine the effect of temporal aggregation on the accuracy of productivity estimates; and 4) develop a working framework for deriving an operational LUE model driven entirely from optical remote sensing. We hypothesize that 1) 2-channel broadband sensors data will produce a LUE model that predicts fluxes with accuracy; 2) seasonal PRI values will be affected by changing canopy structure throughout the season; and 3) the integration analysis of flux and optical data can provide a novel way to partition flux data, gap fill missing flux data, and gain valuable insight into the controls of ecosystem carbon fluxes.

References Cited:

Asrar, G., Fuchs, M., Kanemasu, E. T., and Hatfield, J. L. (1984). Estimating absorbed photosynthetic radiation and leaf area index from spectral reflectance in wheat. *Agronomy Journal*, 76:300-306.

Atjay, G. L., Ketner, P., and Duvigneaud, P. (1979). Terrestrial primary production and phytomass, in *The Global Carbon Cycle* (B. Bolin, E. T. Degens, S. Kempe, and P. Ketner, Eds.), Wiley, New York, pp. 129-182.

Aubinet M., Aubinet, M., Grelle, A., Ibrom, A., Rannik, Ü., Moncrieff, J., Foken, T., Kowalski, A.S., Martin, P.H., Berbigier, P., Bernhofer, Ch., Clement, R., Elbers, J., Granier, A., Grünwald, T., Morgenstern, K., Pilegaard, K., Rebmann, C., Snijders, W., Valentini, R., Vesala, T. (2000). Estimates of the annual net carbon and water exchange of forests: The EUROFLUX methodology. *Advances in Ecological Research* 30: 113-176.

Baldocchi D.D., Hicks B.B., and Meyers T.D. (1988). Measuring biosphere-atmosphere exchanges of biologically related gases with micrometeorological methods. *Ecology*, 69: 1331-1340.

Baldocchi D.D., Finnigan J.J., Wilson K.W. et al., (2000). On measuring net ecosystem carbon exchange in complex terrain over tall vegetation. *Boundary Layer Meteorology*, 96: 257-291.

Baldocchi, D.D., Falge, E., Gu, L., Olson, R., Hollinger, D., Running, S., Anthoni, P., Bernhofer, Ch., Davis, K., Evans, R., Fuentes, J., Goldstein, A., Katul, G., Law, B., Lee, X., Malhi, Y., Meyers, T., Munger, W., Oechel, W., Paw, U.K.T., Pilegaard, K., Schmid, H.P., Valentini, R., Verma, S., Vesala, T., Wilson, K., and Wofsy, K. (2001). FLUXNET: A new tool to study the temporal and spatial variability of ecosystem-scale carbon dioxide, water vapor, and energy flux densities. *Bulletin of the American Meteorological Society*, 82: 2415-2434.

Baldocchi D.D. (2003). Assessing the eddy covariance technique for evaluating carbon dioxide exchange rates of ecosystems: past, present and future. *Global Change Biology*, 9: 479-492.

Baldocchi, D.D. (2008). Breathing of the terrestrial biosphere: Lessons learned from a global network of carbon dioxide flux measurement systems, *Australian J. Botany*, 56: 1-26.

Barton, C.V.M., & North, P.R.J. (2001). Remote Sensing of canopy light use efficiency using the Photochemical Reflectance Index. Model and analysis. *Remote Sensing of Environment*, 78:264-273.

Björkman, O. and Demmig-Adams, B. (1994) Regulation of photosynthetic light energy capture, conversion and dissipation in leaves of higher plants. In: Schulze E-D and Caldwell MM (eds) *Ecophysiology of Photosynthesis*, pp 17-47. Ecological Studies 100. Springer-Verlag, Berlin.

Braswell, B.H., Schimel, D.S., Linder, E., and Moore III, B. (1997). The response of global terrestrial ecosystems to interannual temperature variability. *Science*, 278:870-873.

Coops, C., Hilker, T., Hall, F.G., Nichol, C.J., Drolet G.G. (2010). Estimation of light-use efficiency of terrestrial ecosystems from space: a status report. *Bioscience*, 60: 788-797.

Daughtry, C.S.T., Gallo K.P., and Bauer M.E. (1983). Spectral estimates of solar radiation intercepted by corn canopies. *Agronomy Journal*, 75: 527–531.

Demming-Adams, B., et al. (1995). Xanthophyll cycle-dependent energy dissipation and flexible photosystem II efficiency in plants acclimated to light stress. *J. Plant Physiol*, 22: 249-60

Demming-Adams, B., et al. (1996). The role of xanthophyll cycle carotenoids in the protection of photosynthesis. *Trends in Plant Science*, 1: 21-26

Eklundh, L., Jin, H., Schubert, P., Guzinski, R., Heliasz, M. (2011). An optical sensor network for vegetation phenology monitoring and satellite data calibration. *Sensors*, 11: 7678-7709.

Field, C. B. (1991). Ecological scaling of carbon gain to stress and resource availability. pp 35-65 in H. A. Mooney, W. E. Winner, and E. J. Pell, editors. *Responses of plants to multiple stresses*. Academic Press, London, England.

Field C.B., Randerson J.T., and Malmstrom C.M. (1995) Global net primary production: combining ecology and remote sensing. *Remote Sensing of Environment*, 51:74-88.

Field C.B., Behrenfeld M.J., Randerson J.T. and Falkowski P. (1998). Primary production of the biosphere: Integrating terrestrial and oceanic components. *Science*, 281: 237-240.

Filella, I., Amaro, T., Araus, J., L., and Peñuelas, J. (1996) Relationship between photosynthetic radiation-use efficiency of barley canopies and the photochemical reflectance index (PRI). *Physiol Plant*, 96: 211–216.

Foken, T.H., Wichura, B., (1995). Tools for quality assessment of surface-based flux measurements. *Agricultural and Forest Meteorology*, 78: 83-105.

Gallo, K.P., Daughtry, C.S.T., Bauer, M.E. (1985). Spectral estimation of absorbed photosynthetically active radiation in corn canopies. *Remote Sensing of Environment*, 17:221-232.

Gamon, J.A., Field, C.B., Bilger, W., Björkman, O., Fredeen, A.L., and Peñuelas, J. (1990). Remote sensing of the xanthophyll cycle and chlorophyll fluorescence in sunflower leaves and canopies. *Oecologia*, 85: 1–7.

Gamon, J.A., Peñuelas J., and Field C.B. (1992). A narrow-waveband spectral index that tracks diurnal changes in photosynthetic efficiency. *Remote Sensing of Environment*, 41: 35-44.

Gamon, J.A., Filella, I., Peñuelas, J. (1993) The dynamic 531-nanometer Δ reflectance signal: a survey of twenty angiosperm species. Yamamoto HY , Smith CM (Eds). *Photosynthetic Responses to the Environment*. American Society of Plant Physiologists, Rockville. pp. 172-177.

Gamon, J. A., Field, C.B., Goulden, M., Griffin, K., Hartley, A., Joel, G., Peñuelas, J., Valentini, R. (1995). Relationship between NDVI, canopy structure, and photosynthesis in three Californian vegetation types. *Ecological Applications*, 5: 28-41.

Gamon, J. A., Serrano, L., and Surfus, J. S. (1997) The photochemical reflectance index: An optical indicator of photosynthetic radiation use efficiency across species, functional types and nutrient levels. *Oecologia*, 112: 492–501.

Gamon, J. A., and Surfus, J. S. (1999) Assessing leaf pigment content and activity with a reflectometer. *New Phytologist*, 143: 105–117.

Gamon, J.A. and Qiu, H.L. (1999) Ecological applications of remote sensing at multiple scales. In: Pugnaire FI and Valladares F (eds) *Handbook of Functional Plant Ecology*, pp 805–846. Marcel Dekker, New York.

Gamon, J.A., Field, C.B., Fredeen, A.L., Thayer, S. (2001). Assessing photosynthetic downregulation in sunflowers stands with an optically-based model. *Photosynthesis Research*, 67: 113-125.

Gamon, J.A., Rahman, A.F., Dungan, J.L., Schildhauer, M., and Huemmrich, K.F. (2006a). Spectral Network (SpecNet): what is it and why do we need it? *Remote Sensing of Environment*, 103: 227–235.

Gamon, J. A., Cheng, Y., Claudio, H., MacKinney, L., Sims, D. A. (2006b). A mobile tram system for systematic sampling of ecosystem optical properties. *Remote Sensing of Environment*, 103: 246-254.

Gamon, J.A., Coburn, C., Flanagan, L.B., Huemmrich, K.F., Kiddle, C., Sanchez-Azofeifa, G.A., Thayer, D.R., Vescovo, L., Gianelle, D., Sims, D.A., Rahman, A.F., and Pastorello, G.Z. (2010). SpecNet revisited: bridging flux and remote sensing communities, *Can. J. Remote Sensing*, Vol. 36, Suppl. 2, pp. S376–S390

Garcia, R., Kanemasu, E. T., Blad, B. L., Bauer, A., Hatfield, L., Major, D., Reginato, R., and Hubbard, K. G. (1988). Interception and use efficiency of light in winter wheat under different nitrogen regimes. *Agricultural and Forest Meteorology*, 44: 175-186.

Goerner, A., Reichstein, M., Tomelleri, E., Hanan, N., Rambal, S., Papale, D., Dragoni, D., Schimmlus, C. (2011). Remote sensing of ecosystem light use efficiency with MODIS-based PRI. *Biogeosciences*, 8: 189-202.

Goward, S. N., & Huemmrich, K. F. (1992). Vegetation canopy PAR absorbance and the Normalized Difference Vegetation Index: An assessment using the SAIL model. *Remote Sensing of Environment*. 39: 119–140.

Grace J., Nichol, C., Disney, M., Lewis, P., Quaife, T., Bowyer, P. (2007). Can we measure terrestrial photosynthesis from space directly, using spectral reflectance and fluorescence? *Global Change Biology*, 13:1487-1497

Heinsch, F. A., Reeves, M., Bowker, C. F., Votava, P., Kang, S., Milesi, C., et al. (2003). User's Guide: GPP and NPP (MOD17A2/A3) Products. NASA MODIS Land Algorithm. Version 2.0. Available online at: <http://www.ntsg.umt.edu/modis/MOD17UsersGuide.pdf>

Heinsch F. A., Zhao, M., Running, S. W., Kimball, J. S., Nemani, R. R., Davis, K. J., et al. (2006). Evaluation of remote sensing based terrestrial productivity from MODIS using regional tower eddy flux network observations, *IEEE Trans. Geosci. Remote Sens.*, 44: 1908-1925.

Hilker, T., Coops, N.C., Nestic, Z., Wulder, M.A., and Black, A.T. (2007). Instrumentation and approach for unattended year round tower based measurements of spectral reflectance. *Computers and Electronics in Agriculture*, 56: 72-84.

Huemmrich, K. F., Black, T. A., Jarvis, P. G., McCaughey, J. H., & Hall, F. G. (1999). High temporal resolution NDVI phenology from micrometeorological radiation sensors. *Journal of Geophysical Research*, 104: 935-944.

Huemmrich K.F., Gamon, J.A., Tweedie, C.E., Oberbauer, S.F., Kinoshita, G., Houston, S., Kuchy, A., Hollister, R.D., Kwon, H., Mano, M., Harazono, Y., Webber, P.J., and Oechel, W.C. (2010). Remote sensing of tundra ecosystems productivity and light use efficiency under varying temperature and moisture conditions. *Remote Sensing of Environment*, 114: 481-489.

Kumar, M., & Monteith, J. L. (1981). Remote sensing of crop growth. In H. Smith (Ed.), *Plants in the daylight spectrum*. New York: Academic Press. 134-144.

Landsberg L. L., Waring R. H., (1997). A generalized model of forest productivity using simplified concepts of radiation-use efficiency, carbon balance and partitioning. *Forest Ecology and Management*, 95:209-228.

Leith, H., (1975). Modeling the primary productivity of the world, in *Primary Productivity of the Biosphere* (H. Leith and R. H. Whittaker, Eds.), Springer-Verlag, Berlin and New York, pp. 237-263.

Leith H., and Whittaker R. H., (Eds.), (1975). *Primary Productivity of the Biosphere*, Springer, New York.

Leuning, R., Hughes, D., Daniel, P., Coops, N.C., and Newnham, G. (2006). A multi-angle spectrometer for automatic measurement of plant canopy reflectance spectra. *Remote Sensing of Environment*, 103: 236-245.

Munchow, R C. (1985). An analysis of the effects of water deficits on grain legumes grown in a semiarid tropical environment in terms of radiation interception and its efficiency of use. *Field Crop Res.* 11: 309-323.

Massman W.J., Lee X., (2002). Eddy covariance flux correlations and uncertainties in long term studies of carbon and energy exchanges. *Agricultural and Forest Meteorology*, 113: 121-144.

Monteith, J.L. (1972). Solar radiation and productivity in tropical ecosystems. *Journal of Applied Ecology*, 9: 747-766.

Monteith, J.L. (1977). Climate and the efficiency of crop production in Britain. *Phil. Trans. R. Soc. Lond. B.*, 281: 277-294.

Myneni, R.B., & Williams, D.L., (1994). On the relationship between FAPAR and NDVI. *Remote Sensing of Environment*, 49:200-211.

Nichol, C.J., Lloyd, J., Shibistova, O., Arneth, A., Roser, C., Knohl, A., Matsubara, S., and Grace, J. (2002). Remote sensing of photosynthetic light-use efficiency of a Siberian boreal forest. *Tellus*, 54B, pp. 677-687.

Peñuelas, J., Gamon, J. A., Fredeen, A. L., Merino, J., and Field, C. B. (1994). Reflectance indices associated with physiological changes in nitrogen and water-limited sunflower leaves. *Remote Sensing of Environment*, 48:135-146.

Peñuelas, J., Filella, I., and Gamon, J. A. (1995). Assessment of photosynthetic radiation-use efficiency with spectral reflectance. *New Phytologist*, 131: 291–296.

- Prince, S. D., (1991). A model of regional primary production for use with coarse resolution satellite data. *International Journal of Remote Sensing*, 12:1312-1330.
- Prince, S.D. and Goward, S.N. (1995). Global primary production: a remote sensing approach. *Journal of Biogeography* 22: 815–835.
- Randerson J.T., Chapin, F.S., Harden, J.W., Neff, C., Harmon, M.E. (2002). Net ecosystem production: A comprehensive measure of net carbon accumulation by ecosystems. *Ecological Applications* 12 (4): 937-947.
- Reich, P.B., Turner, D.P., Bolstad, P. (1999). An approach to spatially distributed modeling of net primary production (NPP) at the landscape scale and its application in validation of EOS NPP products. *Remote Sensing of Environment*, 70: 69–81.
- Ruimy, A., Saugier, B., Dedieu, G. (1994). Methodology for the estimation of terrestrial net primary production from remotely sensed data. *Journal of Geophysical Research*, 99:5263-5283.
- Running S.W., Nemani, R.R., Heinsch, F.A., Zhao, M., Reeves, M., Hashimoto, H. (2004). A continuous satellite-derived measure of global terrestrial primary production. *Bioscience*, 54: 547-560.
- Running, S.W. (2008). Ecosystem disturbance, carbon, and climate. *Science* 321: 652–653.
- Runyon, J., Waring, R.H., Goward, S.N., Wells, J.M. (1994). Environmental limits on net primary productivity production and light-use efficiency across the Oregon transect. *Ecological Applications*. 4: 226-237.
- Schimel D.S., Brasswell, B. H., Jr., Holland, E. A., et al. (1994). Climatic, edaphic, and biotic controls over storage and turnover of carbon in soils. *Global Biogeochemical Cycles*, 8:279-293.
- Schimel D.S. (1995). Terrestrial biogeochemical cycles: global estimates with remote sensing. *Remote Sensing of Environment*, 51: 49–56
- Sellers, P.J. (1985). Canopy reflectance, photosynthesis, and transpiration. *International Journal of Remote Sensing*, 6:1335-1372.
- Sellers, P.J. (1987). Canopy reflectance, photosynthesis, and transpiration II. The role of biophysics in the linearity of their interdependence. *Remote Sensing of Environment*, 21: 143–183.

Sims, D. A., Rahman, A.F., Cordova, V.D., El-Masri, B.Z., Baldocchi, D.D., Flanagan, L.B., Goldstein, A.H., Hollinger, D.Y., Misson, L., Monson, R.K., Oechel, W.C., Schmid, H.P., Wofsy, S.C., Xu, L. (2006). On the use of MODIS EVI to assess gross primary productivity of North American ecosystems. *Journal of Geophysical Research*, 112: 1633-1646.

Strachan, I.B., Pattey, E., Salustro, C., and Miller, J.R. (2008). Use of hyperspectral remote sensing to estimate the gross photosynthesis of agricultural fields. *Canadian Journal of Remote Sensing*, 34: 333–341.

Turner, D. P., Ritts, W. D., Cohen, W. B., Maeirsperger, T. K., Gower, S. T., Kirschbaum, A. A., et al.(2005), Site-level evaluation of satellite-based global terrestrial GPP and NPP monitoring, *Global Change Biology*, 11: 666–684.

Vierling, L., Fersdahl, M., Chen, X., & Zimmerman, P. (2006). The Short Wave Aerostat-Mounted Imager (SWAMI): A novel platform for acquiring remotely sensed data from a tethered balloon. *Remote Sensing of Environment*, 103: 255-264.

Zhao, M., Heinsch, F.A., Nemani, R.R., and Running, S. W. (2005). Improvement of the MODIS terrestrial gross and net primary production global data set, *Remote Sensing of Environment*, 95: 164–176.

Chapter 2 –Seasonal dynamics monitored by meteorological and optical sensors

2.1 Introduction:

Phenological observations can elucidate climate-biosphere relationships within an ecosystem and can be used to better inform vegetation models (Schwartz, 1990; Schwartz, 1994). Links between plant life-cycle events and variations in weather and climate can reveal an assembly of feedback interactions associated with controls on green-up and senescence that define growth season length and represent a key constraint on primary productivity (Running and Nemani, 1991; Goulden et al., 1996; White et al. 1997; Churkina et al., 2005). With the onset of remote sensing, optical sampling has provided a non-invasive tool allowing the monitoring of vegetation phenology at a variety of spatial and temporal scales ranging from local to global. Seasonal dynamics observed through NDVI have been shown to properly describe vegetation phenological changes used to describe vegetation type and productivity (Huemmrich et al., 1999; Jenkins et al., 2002; Schwartz et al., 2002; Fisher et al., 2006).

Productivity assessment using remote sensing data is commonly done through the light use efficiency (LUE) model (Kumar & Monteith, 1981; Sellers, 1987, Field, 1991; Running et al., 2004). However, one of the biggest challenges in using remote sensing data for productivity assessments is the shortage of data at the appropriate temporal and spatial scales. To drive the LUE model, we need to achieve a balance between the temporal and spatial resolutions that allow us to interpret the ecological dynamics within each biome. Furthermore, we may also

need to match the scale of resolution between sensors. Many commonly used multiband and hyperspectral satellite optical datasets have the advantage of having global coverage and being relatively available. However, difficulties include low temporal resolution that can lead to a lack of data needed to accurately characterize subtle vegetation changes (Huemmrich et al. 1999). Additionally, large composite periods chosen to minimize errors sources from cloud contamination and atmospheric aerosols, gases and water vapor, can lead to a bias towards higher NDVI values during periods of change such as the start and end of the growing season (Los et al., 1994; Holbem, 1986). Further difficulty with multiband and hyperspectral remote sensing include limitations in spatial resolution making it difficult to properly define individual plant processes within a specific vegetation type at the scale of a flux tower (Huemmrich et al., 1999). Addressing these challenges can impose costly solutions, forcing us to develop cost-efficient ways to obtain scale-appropriate optical measurements.

To solve these challenges, many people have been exploring the use of low-cost methods involving simple two-channel radiometers as alternative ways to derive proxy LUE model terms (Huemmrich et al., 1999; Jenkins et al., 2007; Richardson et al., 2007; Wilson and Meyers, 2007; Garrity et al., 2010). The high temporal resolution in automated optical sensor systems could allow improved tracking of diurnal and seasonal carbon flux dynamics within an ecosystem. Furthermore, the low cost of these sensors would enable them to be widely used by the scientific community, allowing a possible extensive spatial network of sensors as suggested by the SpecNet network and similar efforts (Gamon et al.,

2006; 2011; Eklundh et al. 2011). To achieve this, it is important to consider if data from simple two-band sensors can be used to drive a LUE model with the level of accuracy that one would achieve with high spectral resolution data. In this thesis chapter, we begin to explore comparisons of common meteorological and optical variables with measured gross primary productivity. We also explore the possibility of driving a LUE model from two-channel broadband data by defining the NDVI- fA_{PAR} relationship using various proxy greenness indices derived from broadband reflectance. These simple relationships were the initial steps needed to construct a more robust LUE model, later discussed in Chapter 4 of this thesis.

2.2. Methods

2.2.1 Study Site:

The study site was located at the University of Alberta South Campus agricultural research farm (53.497 N, -113.552 E) within in the city of Edmonton, Alberta, Canada (Figure 2-1). The individual parcel of land for this study had been cultivated with alfalfa (*Medicago sativa*) for a number of years, helping minimize any adverse influence from plant row structures usually encountered in croplands. The 250m wide x 500m long alfalfa parcel had a homogenous arrangement of plants with nearly flat topography. This site was monitored for three consecutive growing seasons starting in 2009 and continuing through 2011.

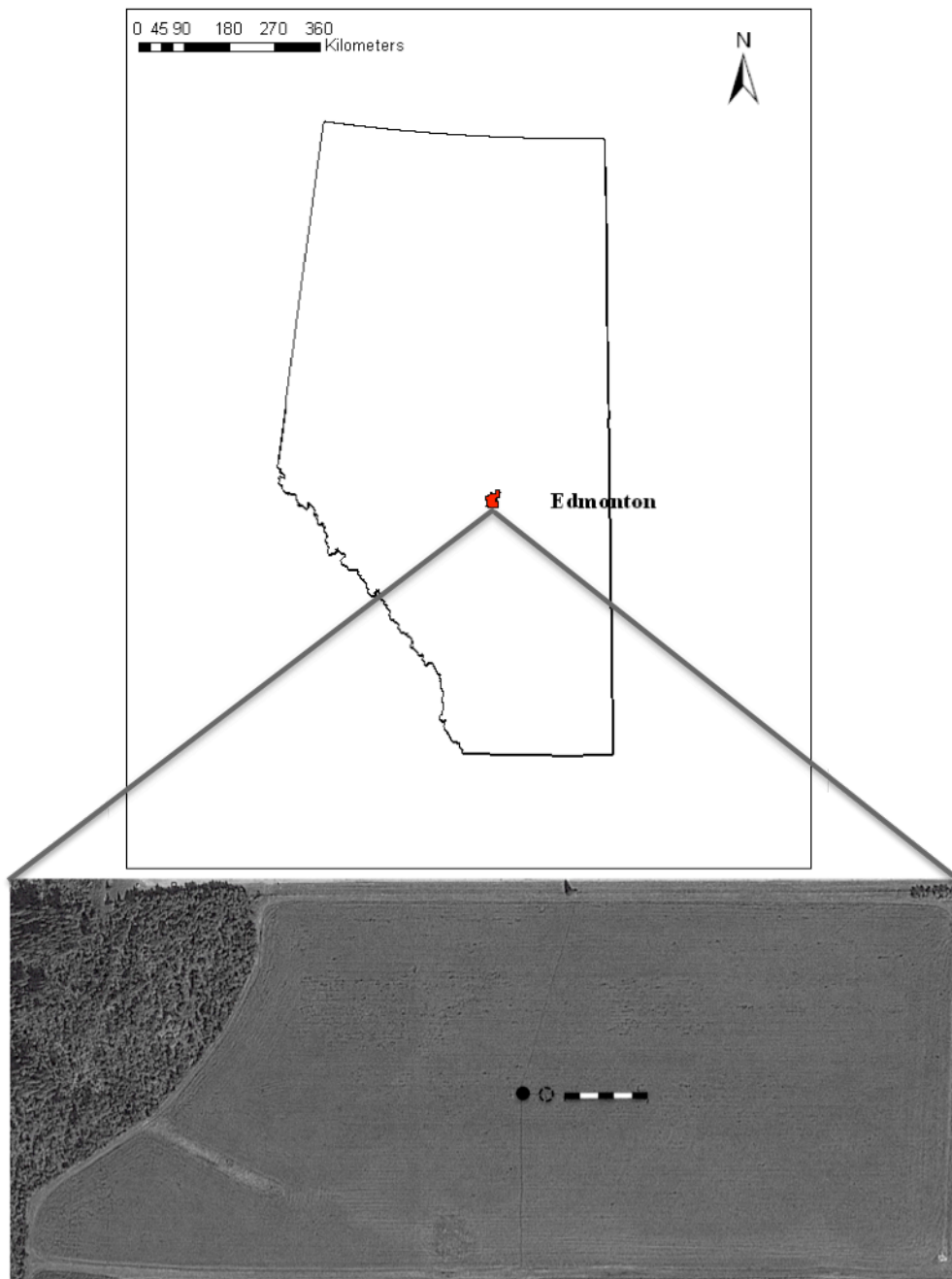


Figure 2-1: Alfalfa field located at the University of Alberta South Campus agricultural research farm in Edmonton, Alberta, Canada (53.497 N, -113.552 E). Monitoring systems include a 50m robotic tram system (black and white line), a 3m phenology/meteorology station (dotted circle), and a 2.5m eddy covariance flux tower (black circle).

2.2.2. Experimental design:

Of the three years of monitoring, the 2010 growth season saw the most rigorous data collection campaigns. The ecosystem at this site was monitored using three different systems: 1) a 50m Tram system (Gamon, et al., 2006b) oriented east to west, 2) a 3 m phenology/ meteorological station, and 3) a 2.5m eddy covariance flux tower (Figure 2-1). The homogenous nature of the field allowed direct comparison between all three systems. More specifically, the 50m track length of the tram system was designed to collect measurements comparable to those collected from the majority of the flux footprint. Optical sensors on the phenology tower contained cosine foreoptics, allowing hemispherical measurements of a large area of the field similar to the flux footprint. To construct a LUE model, fA_{PAR} measurements were included during all tram data collection campaigns. During the 2010 growth season, the field was harvested three times, partitioning the growth season into individual growth cycles, composed of separate green-up and mature growth stages, and followed by disturbance (through harvesting) events (Figure 2-2). Each of the growth cycles was treated as an independent growing event.

2.2.3 Micrometeorology measurements:

2.2.3.1 Eddy Covariance Instrumentation:

The eddy covariance (EC) flux technique (Baldocchi et al., 1988, Moncrieff et al., 1997; Aubinet et al., 2000; Baldocchi, 2003) was used to measure net ecosystem CO_2 ($\mu\text{mol m}^{-2} \text{s}^{-1}$), latent heat (LE) (W m^{-2}), and sensible

heat (H) (W m^{-2}) fluxes at the study alfalfa field. These were gathered during the 2009 and 2010 growing seasons.

A three-meter tower was equipped with a sonic anemometer (SAT; CSAT3, Campbell Scientific, Logan, UT, USA), used to measure three dimensional wind velocities, direction, and temperature fluctuations; along with a open-path infrared gas analyzer (IRGA; LI7500, LI-COR Inc., Lincoln, NE, USA), used to measure CO_2 and water vapor concentration fluctuations in air, within the boundary layer above the alfalfa field. These two instruments were mounted on separate horizontal support arms, oriented towards the direction of the prevailing winds (south-west direction) and having a separation of approx. 15cm between the center of the IRGA optical path and the center of the SAT instrument path. Both of the SAT and IRGA were programmed to have a sampling frequency of 10Hz, logged with a CR5000 data-logger (Campbell Scientific, Logan, UT, USA) and recorded using an industrial grade compact flash memory storage card.

Additional meteorological equipment was integrated into the flux tower, including a net radiometer (NR lite, Kip & Zonen, Delft, Holland), air temperature and humidity probe (HMP45C, Vaisala Inc., Helsinki, Finland) encased in a vented radiation shield (41003-5, Gill Multiprobe, R.M. Young Company, Traverse City, MI, USA).

2.2.3.2 NEE calculations:

High frequency eddy covariance data was processed using the post-acquisition software EdiRe (University of Edinburgh) program. Flux of CO_2 was

expressed as the product of mean air density and the covariance between instantaneous vertical wind velocity and concentration fluctuations.

$$F_c = - \rho_a \overline{w' s'} \quad (1)$$

where F_c represents the vertical CO_2 ($\mu\text{mol m}^{-2} \text{s}^{-1}$), ρ_a is the dry air density (mol m^{-3}), w is the instantaneous vertical wind speed (m s^{-1}), and s is the molar mixing ratio (mol mol^{-1} dry air). Over bars over the wind speed and mixing ratio terms indicate time averaging, while primes indicate fluctuations about the mean (over a 30 minute time aggregate), following Reynolds decomposition. The negative notation in the expression was added since a meteorological notation was adopted for representation of NEE, where negative NEE values represented net CO_2 uptake into an ecosystem and a positive values represent net CO_2 release into the atmosphere.

Sensor separation correction was applied to the 10Hz eddy covariance data to compensate for lost fluxes due to the inability of the IRGA and SAT instruments to sample the exact same volume (Moore, 1986). Also, coordinate rotations corrections (Baldocchi et al., 1988; Aubinet et al. 2000) were performed, allowing the proper alignment of the mean vertical wind direction to a position exactly perpendicular to the mean wind streamlines. To correct for the effect of changes in temperature and water vapor on air density (and CO_2 mixing ratio) (Webb et al. 1980), the Webb-Pearman-Leuning correction was applied.

2.2.3.3 GPP and total ecosystem respiration calculations:

Net ecosystem CO₂ exchange ($\mu\text{mol m}^{-2} \text{s}^{-1}$) is the sum of two competing processes and can be expressed as:

$$\text{NEE} = -\text{GPP} + \text{TER} \quad (2)$$

where GPP is the gross primary production ($\mu\text{mol m}^{-2} \text{s}^{-1}$) and TER is the total ecosystem respiration ($\mu\text{mol m}^{-2} \text{s}^{-1}$). The negative sign on the GPP term comes from adopting a meteorological convention indicating NEE as being negative where there is CO₂ uptake by an ecosystem.

Similarly, NEE can be conveyed in terms of light-response curves, relying on the ecological relationships between rate of photosynthesis and incident light (as photosynthetically active photon flux density; PPFD) (Landsberg, 1977) as well as temperature and respiration (Lloyd and Taylor, 1994). Using these relationships, NEE can be expressed as (Flanagan and Johnson, 2005; Glenn et al., 2006a; Glenn et al. 2006b; Syed et al., 2006; Adkinson et al., 2011):

$$\text{NEE} = - \frac{A_{max} \alpha \text{PPFD}}{A_{max} + \alpha \text{PPFD}} + R_{10} Q_{10}^{(T-10/10)} \quad (3)$$

where A_{max} is the maximum carbon assimilation ($\mu\text{mol m}^{-2} \text{s}^{-1}$), or GPP, at infinite PPFD ($\mu\text{mol m}^{-2} \text{s}^{-1}$); α is the apparent quantum yield derived from the initial slope of the light-response curve ($\text{mol CO}_2 \text{ mol}^{-1} \text{PPFD}$); R_{10} represents the ecosystem respiration rate at 10°C ($\mu\text{mol m}^{-2} \text{s}^{-1}$); Q_{10} is the respiration

temperature response coefficient during temperature changes of 10 °C; and T is the atmospheric temperature (°C). Using five-day aggregated diurnal meteorological ($PPFD$ and T) and NEE flux data, a series of non-linear least square, Gauss-Newton, regressions were applied, using the statistical package Systat10 (SPSS Inc. 2000), to calculate estimates of A_{max} , α , R_{10} and Q_{10} variables. The parameters were constrained over the following ranges: A_{max} between 1.0 and 60 $\mu\text{mol m}^{-2} \text{s}^{-1}$, α between 0.001 and 0.08 ($\text{mol CO}_2 \text{ mol}^{-1} \text{PPFD}$), R_{10} between 0.001 and 0.6 $\mu\text{mol m}^{-2} \text{s}^{-1}$, and Q_{10} between 1.4 and 2.2.

Resulting diurnal model parameters (A_{max} , α , R_{10} and Q_{10}) were combined and plotted over the course of each growth cycle. Polynomial relationships as a function of time were fitted for each parameter. These functions, combined with measured $PPFD$ and T , were used to estimate half-hourly values for GPP, TER, and modeled NEE. To determine the accuracy of the model, the modeled NEE was directly compared to measured NEE.

2.2.4 Reflectance measurements:

2.2.4.1 Hyperspectral data from Tram system:

A dual channel field spectrometer (Unispec-DC, PP-Systems, Amesbury, Massachusetts, USA) was used to collect hyperspectral optical measurements on a periodic (roughly weekly) basis, following the tram system collection method described by Gamon et al. (2006b). This involved the use of a dual channel field spectrometer (Unispec-DC, PP-Systems, Amesbury, Massachusetts, USA)

(spectral range of 305-1130nm) collecting data every 1m along the 50m-length tram track every hour throughout the collection day, as weather permitted.

All raw reflectance data collected from the hyperspectral tram runs was corrected to actual target reflectance using a 99% reflective white standard panel (Spectralon, Labsphere Inc., North Sutton, NH). The correction procedure can be mathematically expressed as:

$$\rho_{\text{corrected}} = (R_{\text{target}}/I_{\text{downwelling}}) \times (I_{\text{downwelling}}/R_{\text{standard}}) \quad (4)$$

where $\rho_{\text{corrected}}$ represents corrected reflectance. The first term ($R_{\text{target}}/I_{\text{downwelling}}$) represents the raw reflectance, expressed as a ratio of the upwelling radiance to the downwelling irradiance over the alfalfa field target. The second term ($I_{\text{downwelling}}/R_{\text{standard}}$) represents the cross calibration value, calculated as a ratio of the downwelling irradiance to the radiance of the standard panel (Gamon et al. 2006b). An assumption of this method is that the sky conditions are identical (or nearly identical) during target and panel readings. Using this formula, it is not necessary to apply a radiometric calibration, since the calibration coefficients would cancel.

Spectral measurements collected at an hourly basis were averaged over the length of the track and average values were used in all subsequent analyses. Hyperspectral tram measurements provided a “benchmark” against which two-band radiometer values were compared. Ideally, optical measurements were set out to be collected weekly including during the recovery period after major

disturbance events through harvesting, with each collection characterizing the diurnal reflectance of the canopy through hourly sampling. However, periodic precipitation events led to less extensive diurnal collections and seasonal coverage of these measurements.

2.2.4.2 Broadband data from phenology station

Broadband optical measurements from two-band radiometers provided fully automated continuous measurements of both the target reflectance and the sky conditions. The phenology tower allowed near continuous yearly measurements since first installed on June 6, 2009. Measurements included light conditions, through upward looking photosynthetic active radiation (PAR) and pyranometer (PYR) spot radiometers (Onset Computer Corporation, Bourne, Massachusetts, USA, Massachusetts), and canopy reflectance, through paired upward and downward-looking PAR and PYR sensors (Onset Computer Corporation, Bourne, Massachusetts, USA). Ancillary meteorological data included temperature and relative humidity (RH) measurements (HMP45C-L, Campbell Scientific Corp., Logan, UT, USA). Continuous optical measurements were logged at an interval of one minute throughout the entire growth seasons. Data was logged onto a HOBO H-21-011 Weather Station data-logger (Onset Computer Corporation, Bourne, Massachusetts, USA, Massachusetts) and downloaded every 15 days.

2.2.4.3 Calculation of reflectance indices

Vegetation indices were derived from tram hyperspectral reflectance measurements at both diurnal and seasonal temporal scales. The normalized difference vegetation index (NDVI) was used as a proxy of green biomass. The index were constructed as follows:

$$\text{NDVI}_{680,800} = (\rho_{800} - \rho_{680}) / (\rho_{800} + \rho_{680}) \quad (5)$$

where “ ρ ” refers to reflectance and the subscripts refers to the specific spectral wavelengths used (800 nm and 680nm).

To assess NDVI proxies using broadband data, five different indices for canopy greenness were derived using the two-band sensors mounted from the phenology station. These five NDVI proxies included the Jenkins NDVI proxy method (Jenkins et al., 2007), the Wilson method (Wilson et al., 2007), the Huemmrich method (Huemmrich et al., 1999), the two band enhanced vegetation index (EVI2) method (Rocha and Shaver, 2009), and a revised version of the Huemmrich method (Gamon et al. 2011). The revised Huemmrich index, hereafter called Huemmrich II, was constructed as follows:

$$\text{NDVI}_{\text{Huemmrich_II}} = (\rho_{\text{PYR}} - \rho_{\text{PAR}}) / (\rho_{\text{PYR}} + \rho_{\text{PAR}}) \quad (6)$$

where ρ_{PYR} is the solar radiation reflectance calculated from the ratio of upwelling to downwelling radiation using the pyranometers; and ρ_{PAR} is the total reflectance

of photosynthetically active radiation (PAR) calculated from the ratio of upwelling to downwelling PPF (Gamon et al. 2011). For clarity, we propose specific nomenclature that eases the identification of each proxy index as used throughout this thesis. This involves stating the index followed by a subscript that recognizes the original author who proposed the proxy calculation. Each term and the literature reference where they were first discussed are listed in Table 2-1.

Table 2-1: References and notation of the various greenness indices derived from broadband data.

Proxy Index	References
NDVI _{Jenkins}	NDVI proxy as outlined by Jenkins et al., 2007
NDVI _{Wilson}	NDVI proxy as outlined by Wilson et al., 2007
NDVI _{Huemmrich_I}	NDVI proxy as outlined by Huemmrich et al., 1999
NDVI _{Huemmrich_II}	Modified Huemmrich proxy outlined in Gamon et al. 2011
EVI2	Two band EVI as outlined by Rocha and Shaver, 2009

2.2.5 Direct fA_{PAR} measurements:

Light properties above and within the canopy were measured using a ceptometer (AccuPAR LP-80, Decagon, Pullman, Washington, USA). Light interaction with the canopy can be expressed as:

$$1 = fA_{PAR} + f_{trans} + f_{RefVeg} - f_{RefSoil} \quad (7)$$

where, fA_{PAR} is the fraction of absorbed PPF, f_{trans} is the fraction of transmitted radiation, f_{RefVeg} is the reflected radiation from the vegetation, and $f_{RefSoil}$ is the is the fraction reflected by soil. Operationally, fA_{PAR} is expressed following common convention:

$$fA_{PAR} = 1 - t - r + r_s \quad (8)$$

where, t is the fraction of transmitted radiation, r is the reflected radiation from the canopy, and r_s is the soil reflectance component. fA_{PAR} sampling periods correlated with hourly tram sampling events as measurements were gathered in concert with optical sampling. Individual canopy measurements were made every 5 meters along the tram track throughout the diurnal collection period.

2.3. Results:

2.3.1. Monitoring through meteorological instruments:

The evaluation of the midday (30 min about solar noon, 13:30 MDT) GPP time series for the entire 2010 growth season shows the progression through the phenological stages of dormancy, green-up and mature growth (Figure 2-2). Disturbance events, due to harvesting between growth cycles, are also distinguishable in the flux seasonal trends (grey bars, Figure 2-2). Gaps within the GPP dataset (Figure 2-2) are attributed to precipitation events that cause unreliable CO_2 concentration measurements due to the use of an open path IRGA (LI7500, LI-COR Inc., Lincoln, NE, USA). Overall, the GPP patterns correlated with several meteorological variables. Seasonal trends of temperature (Figure 2-3c) and VPD (Figure 2-3d) appear to have a strong association with that of GPP. Temperature increased during crop green-up and reached peak values during the second growth cycle where peak productivity occurred. VPD also increased

during green-up and, initially, appeared to continue this trend, however, the values decreased slightly during the beginning of the second growth cycle when frequent prolonged precipitation events occurred (Figure 2-3d). At the end of the season, both temperature and VPD seasonal declines coincided with a period of decreasing GPP and low precipitation. Time series of the incoming (downwelling) radiation shows a consistent pattern throughout growth cycles #1 and #2. A decline in crop productivity was observed during the third growth cycle, coinciding with a decline in PPFD (Figure 2-3b). Comparison between the seasonal patterns of relative humidity and GPP did not yield strong similarities (Figure 2-3e).

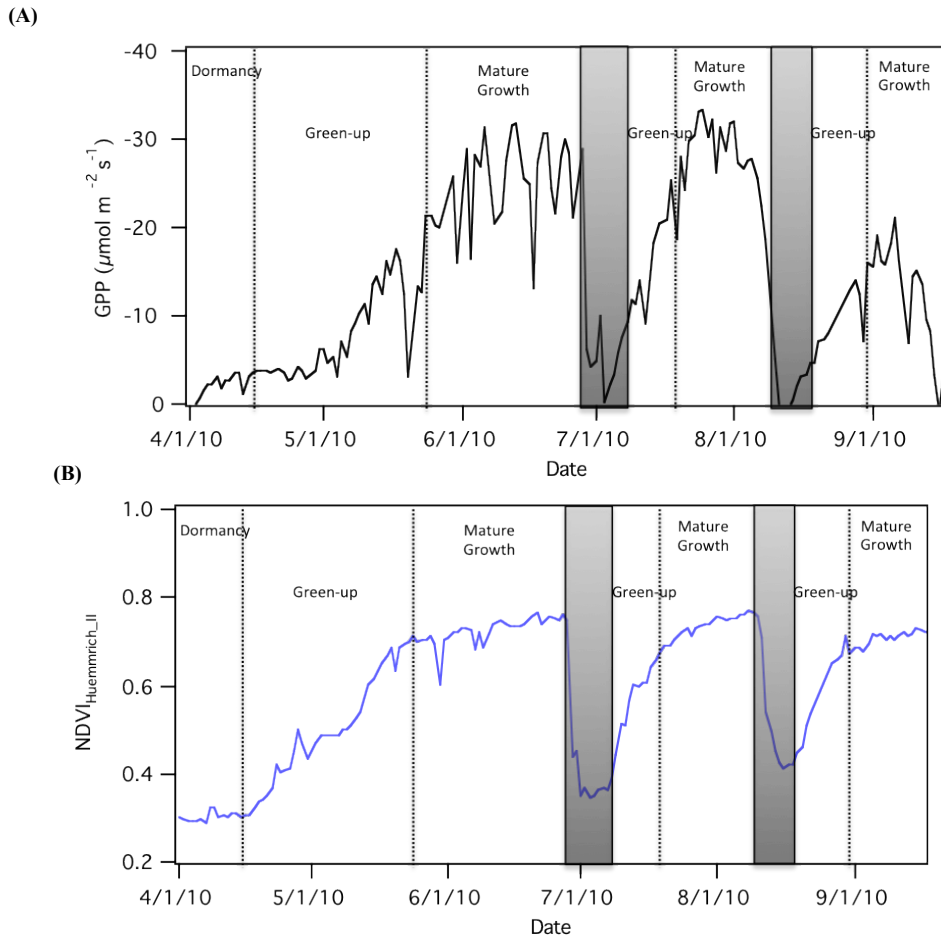


Figure 2-2: Corresponding phenologic stages designated for (A) the gross primary production (GPP), and (B) NDVI_{Huemrich_II} greenness proxy for the 2010 growth season. Individual stage delineation was chosen through rate of change analysis of the broadband phenology tower seasonal data.

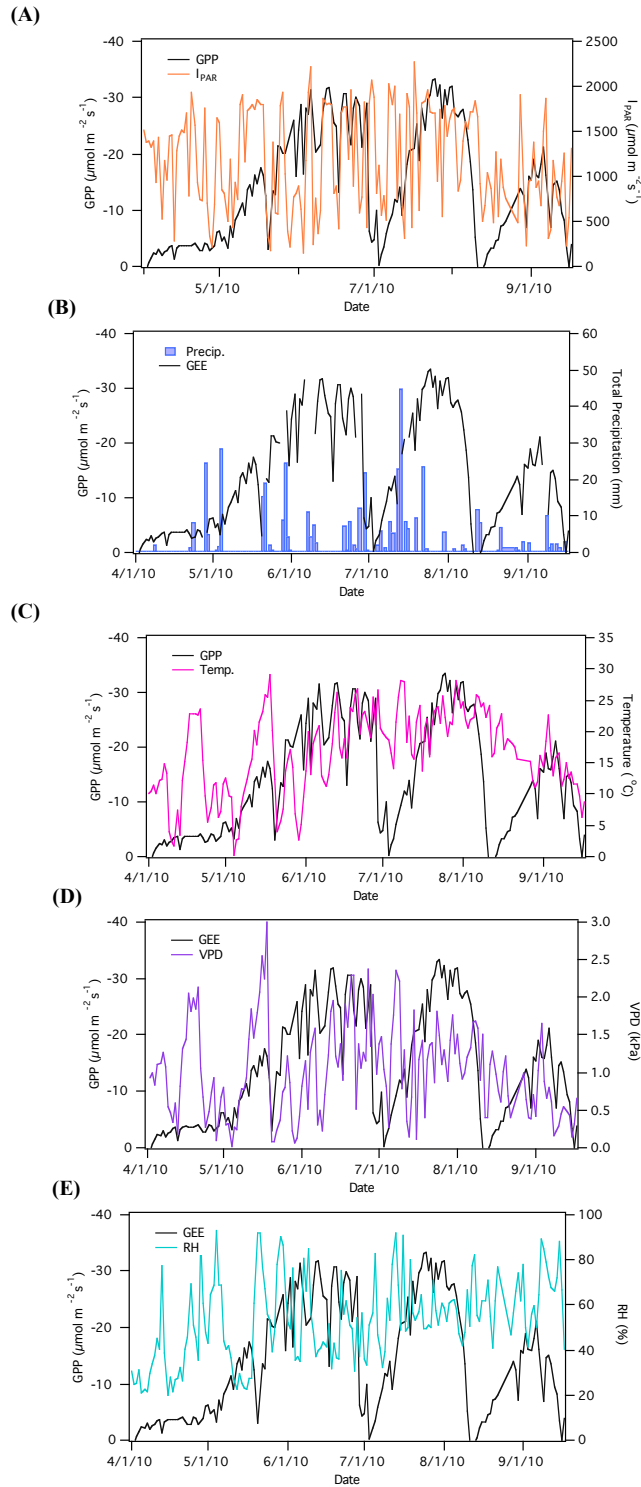


Figure 2-3: Seasonal time series of mid-day GPP and (A) total precipitation, (B) PPFD (C) temperature, (D) calculated VPD, and (E) relative humidity. GPP was calculated from eddy-covariance flux measurements.

2.3.2 Monitoring through remote sensing instruments:

Comparison of the seasonal time series of narrow band NDVI_{680,800} and that of midday GPP values showed similar patterns (Figure 2-4). Some of the seasonal variability observed in GPP was not apparent in NDVI_{680,800} due to the non-continuous nature of narrow-band measurements (collected once a week). However, we should note that the high frequency and resolving power of flux instrumentation lead to inherently noisier measurements than any optical expression, regardless of temporal resolution. This is because NDVI doesn't capture instantaneous variations due to wind and other stochastic processes that affect the fluxes. Additionally, tram data were not collected after the second harvesting event, thus no hyperspectral data is available for the third and final growth cycle.

Time series of each of the broadband greenness proxy methods were also compared to seasonal productivity changes. Resulting patterns from each index all followed the general seasonal trajectory of GPP (Figure 2-5 b-f). One-to-one comparisons between the each proxy index and GPP during individual phenological stages (dormancy, green-up, and mature growth) allowed us to identify where deviations occurred throughout the seasonal progression (Table 2-2). During dormancy all greenness indices showed very low correlations with GPP, with EVI2 and Huemmrich II having the best correlations. During green-ups, all proxies showed linear correlations to GPP, with NDVI_{Huemmrich_II} showing the best correlation ($R^2 = 0.663$). Through the mature growth stage, the phenology and flux datasets plateaued, leading to stable NDVI and GPP values that produce

deceptively low correlation coefficients. However, visual analysis (figure 2-5) showed their patterns to be quite similar. For the overall season (all growing phases combined), all proxies had high correlations with GPP, with EVI having the best relationship ($R^2 = 0.871$). The Huemmrich II proxy was shown to have the second highest correlation with GPP ($R^2 = 0.840$). Correlations during disturbance (through harvesting) events were not used due to the possible unreliability of flux measurements during this period associated with farm equipment emissions and higher than normal respiration rates associated with the decomposition of harvested biomass

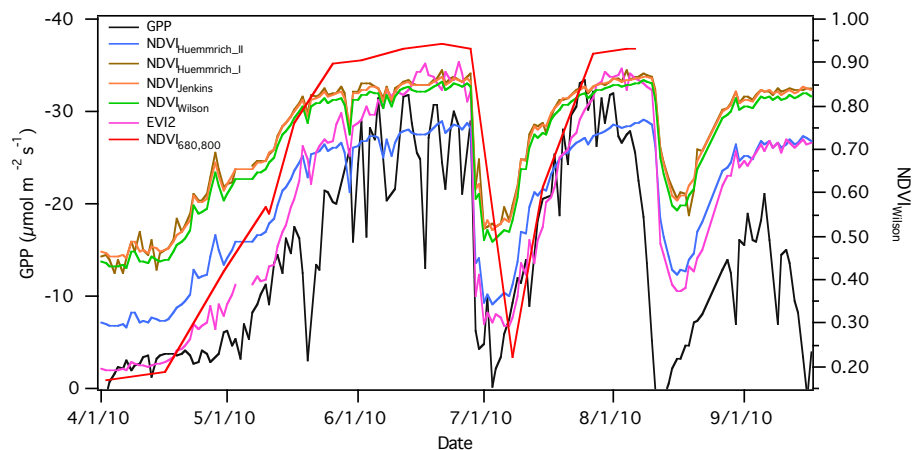


Figure 2-4: Composite of midday NDVI time series calculated through hyperspectral and broadband NDVI proxy indices compared to midday GPP.

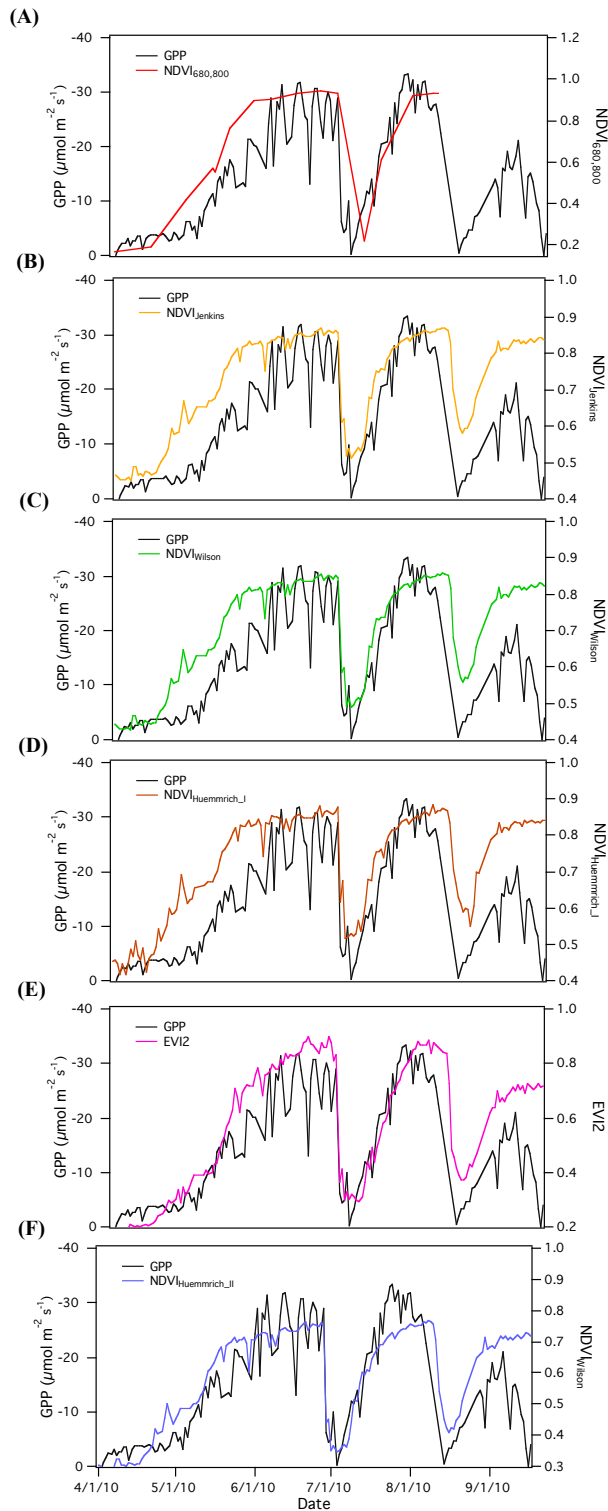


Figure 2-5: Time series of midday GPP and corresponding (A) $NDVI_{680,800}$, (B) $NDVI_{Jenkins}$, (C) $NDVI_{Wilson}$, (D) $NDVI_{Huemmerich_I}$, (E) $EVI2$, and (F) $NDVI_{Huemmerich_{II}}$. $NDVI_{680,800}$ was derived from narrow-band reflectance measurements from tram. All other NDVIs were derived from two-band sensors, where subscripts refer to the specific proxy method used.

Table 2-2: Correlations (R^2) of broadband derived NDVI proxies and GPP during the dormancy, green-up, and mature growth stages.

	Dormancy	Green-up	Mature Growth	Combined Season
NDVI Proxy	R^2	R^2	R^2	R^2
Jenkins	0.211	0.648	0.086	0.811
Huemmrich_I	0.164	0.634	0.074	0.799
Wilson	0.211	0.65	0.086	0.816
EVI2	0.379	0.637	0.253	0.871
Huemmrich_II	0.211	0.663	0.09	0.84

To evaluate the feasibility of using two-channel broadband data to track the seasonal changes in biomass, proxy NDVIs and EVI2 measurements were compared to measured $NDVI_{680,800}$ values calculated from the spectrometer (Figure 2-6). Statistical evaluation, through paired t-tests, of the broad-band vegetation indices shows them all as being significantly related to measured $NDVI_{680,800}$ ($p < 0.005$). Simple one-to-one correlations show all proxy NDVIs as being linearly correlated to $NDVI_{680,800}$; proxy calculation method Huemmrich II having the greatest correlation ($R^2 = 0.994$). EVI2 was observed to be non-linearly correlated to $NDVI_{680,800}$.

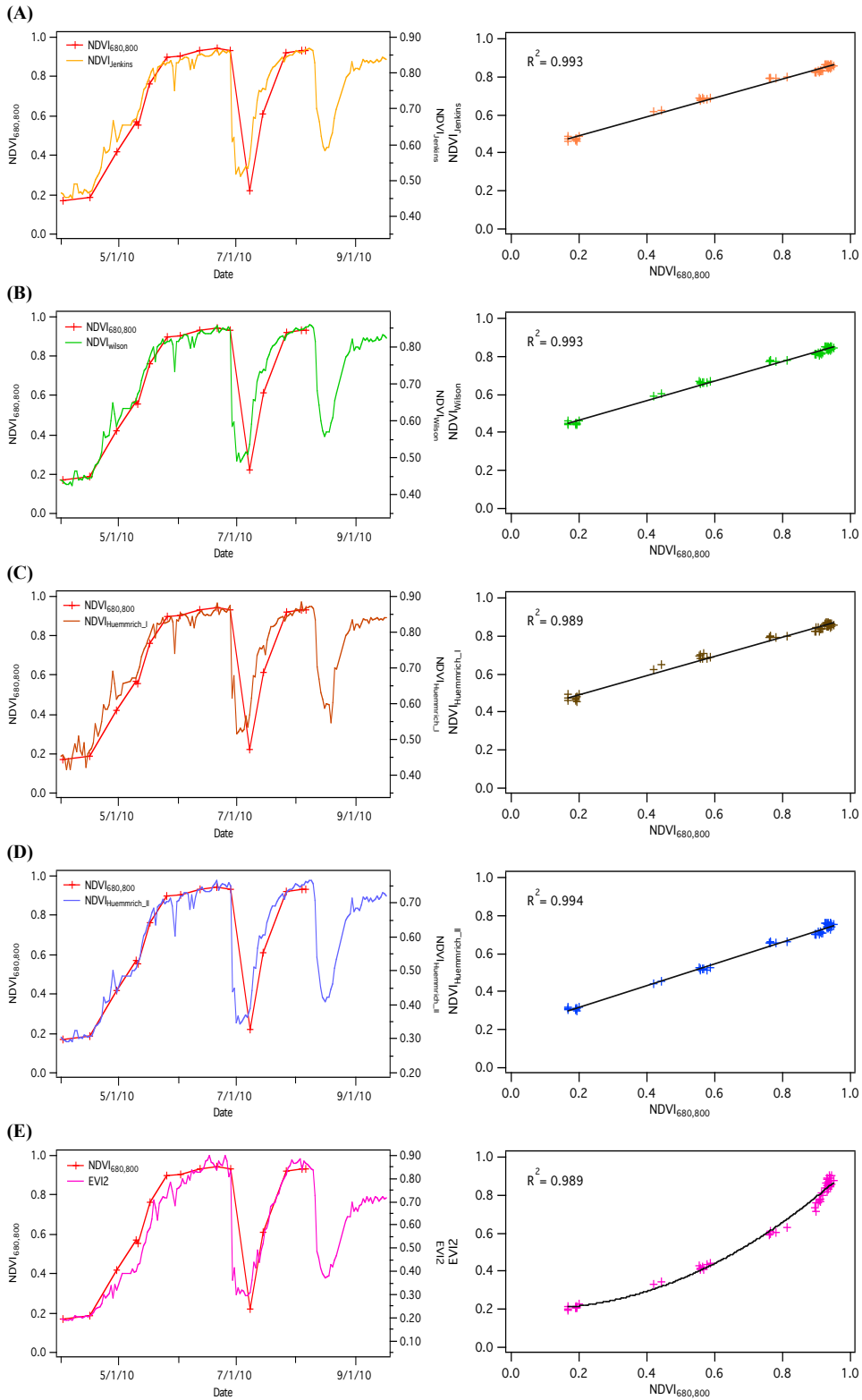


Figure 2-6: Time series and Simple correlations between narrow-band derived NDVI_{680,800} and broad-band NDVI proxies calculated using the (A) Jenkins, (B) Wilson, (C) Huemmrich I, (D) EVI2, and (E) Huemmrich II methods for the 2010 growing season.

2.3.3 Empirical comparison of broadband vs. narrow-band NDVI- fA_{PAR}

relationships:

Midday NDVI data values collected from the tram system during 2009, 2010, and 2011 were combined with fA_{PAR} measurements of green vegetation (green fA_{PAR}), collected at matching time periods under same light conditions, to determine an empirical relationship between the two (Figure 2-7a). The mathematical expression that characterized this relationship is:

$$fA_{PAR} = 1.02 (\text{NDVI}_{680,800})^{3.45} \quad (7)$$

This non-linear function showed a high correlation coefficient ($r^2=0.92$) and showed small interannual variability, which was attributed to the better characterization of the relationship with increasing data. To minimize the effects of canopy structure due to changes in diurnal sun angle, only midday values (30 minutes averaging window centered on solar noon, 13:30 MDT) were used to form this relationship. NDVI values between 2 and 3 represented the lower resolving limit of the spectrometer, thus values within this range could be less reliable than the rest.

Midday phenology data, collected during the same time period, was also used to determine the relationships between broadband vegetation indices and fA_{PAR} (Figure 2-7b). Comparison between broadband relationships showed variability in patterns, with Jenkins, Huemmrich I, and Wilson NDVI- fA_{PAR} functions all closely related to one another, while Huemmrich II and EVI2

showed similar curves that were different from the other proxy NDVI indices. All relationships derived from the proxies produced functions slightly offset compared to that of the tram-derived (Figure 2-7b). However, empirical normalization of broadband data to represent that of the hyperspectral signal resulted in all proxy NDVIs/EVI2- fA_{PAR} functions as being statistically comparable as equation (6) (t-test; $p < 0.05$) (Figure 2-7c).

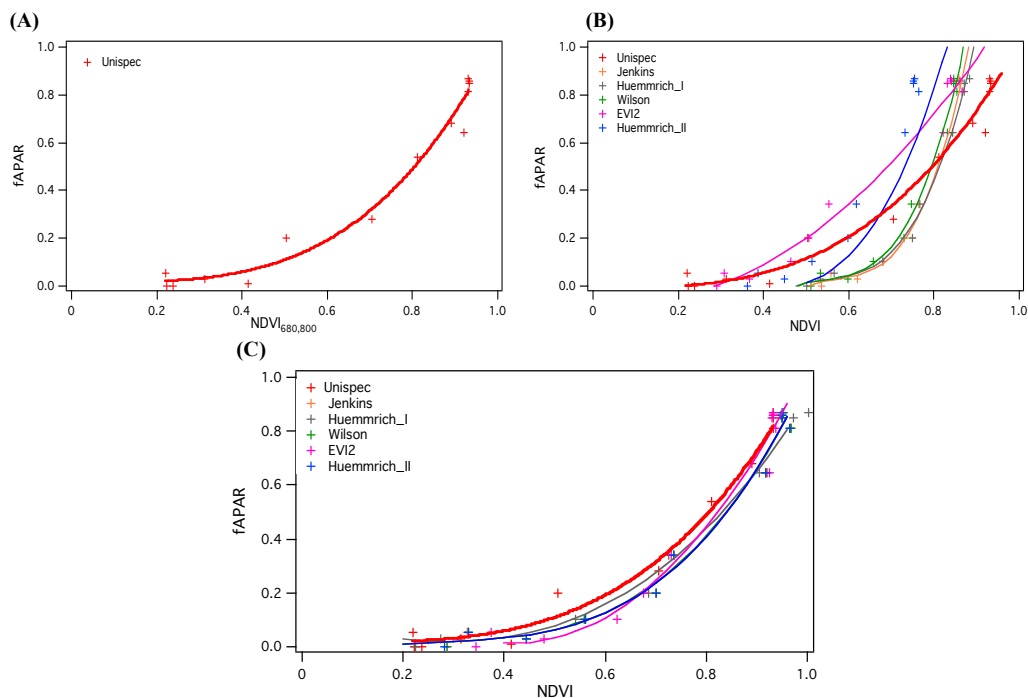


Figure 2-7: NDVI- fA_{PAR} relationships derived from mid-day (A) hyperspectral spectrometer and (B) broadband spot radiometers data. Pane (C) represents resulting functions after calibration of broadband values to represent narrowband hyperspectral value outputs.

2.4 Discussion:

Temperature, moisture content and light availability interact with plants' life-cycle events (Menzel et al. 2005; Kathuroju et al. 2007) and can be perceived as major drivers affecting ecosystem phenologic progression. These three variables have been show to significantly affect land-surface fluxes and account

for some of the dynamic changes observed in flux measurements (Goulden et al. 1997; Sellers et al. 1996). For our ecosystem, growth dynamics were closely linked to temperature and water balance as shown by the close link of GPP with VPD and temperature seasonal trends. VPD seemed to be a better indicator of water balance than relative humidity, seemingly correlating with the notion that VPD more accurately monitors variation in atmospheric humidity as temperature changes as proposed by Anderson et al. (1939). PPFD, VDP and temperature can be conceptually thought as analogous to the components of the LUE model, where light availability is a measure of A_{PAR} , and temperature and VPD affect the photosynthetic efficiency of the canopy.

The ability to use inexpensive spot radiometers to assess ecosystem state increases the feasibility of achieving continuous monitoring of the many diverse global ecosystems (Huemmrich et al., 1999; Balzarolo et al., 2011; Pastorello et al., 2011). The comparison of optical time series' to GPP can show if a simple remote sensing greenness product can track the general seasonal growth progression of the vegetation. Not all flux variability can be resolved by optical sensors as NDVI cannot capture the high-frequency changes in CO_2 , which are captured by eddy-covariance instruments. However, the high temporal resolution of two-band sensors does allow resolution of detailed seasonal patterns. A lack of temporal resolution of the hyperspectral dataset can lead to an inaccurate depiction of NDVI dynamics present throughout the growth season that are inherently resolved by continuous sampling of two-band sensors.

Results from correlation analysis of the proxy indices showed all of them as having a strong correlation with GPP values for the combined growing season. The low correlation between proxy NDVIs and GPP during the dormant stage (Table 2-2), likely related to the effects of low vegetation amounts, where canopy background effects are known to have a significant influence on optical measurements (Huete et al., 1985; Goward & Huemmrich, 1992; Price et al., 1992). Similarly low correlations found after disturbance events (Figure 2-5) were likely due to the presence of farm equipment and respiring vegetation left after harvesting. These canopy effects would have lingered until canopy closure, which occurred slightly into each of the green-up stages. These factors may have affected the NDVI proxy-GPP relationship during this stage, leading to a reduced correlation than was expected. Effects of canopy structure remained minimal for the rest of the growth season, as canopy closure was the predominant state of this ecosystem. However, in ecosystems where canopy structure was constant throughout the growth season we encounter weaker seasonal NDVI- productivity correlations (Gamon et al. 1995).

The comparison between proxy and definite NDVI values showed that, for the purposes of estimating fA_{PAR} and driving the LUE model, broadband derived greenness indices are all comparable to benchmark narrowband $NDVI_{680,800}$ measurements (Figure 2-6). The power function that characterize the EVI2 proxy- $NDVI_{680,800}$ relationship is likely due to the known saturation of $NDVI_{680,800}$ at high relative values (Huete et al., 1999), and is inherently corrected during EVI2 calculations (Rocha and Shaver, 2009). Further comparison of the broadband and

narrowband derived NDVI values showed proxy indices as having a much smaller range of values than our standard $NDVI_{680,800}$. This could be partly associated with differences in sensor composition and response. The radiometric and spectral characteristics that define each sensor will have an effect on the quantitative measure of light conditions, which have been shown to significantly affect spectral products such as NDIV calculations (Teillet et al., 1997; Tittebrand et al., 2009). Without knowing the specific spectral response, we cannot produce a first principle evaluation of broad and narrow band instruments which would allow a direct cross-comparison between the sensors. Without this information cross-comparison of sensors are based on empirical observations and comparisons.

Defining the $NDVI-fA_{PAR}$ relationship constitutes a first step to constructing an LUE model. Defining and comparing this relationship for each NDVI proxy expressions is vital to assessing the capability of using two-band sensors for constructing the model. Initial comparison of each of the proxy derived functions all showed a similar general pattern to that of the benchmark $NDVI_{680-800}fA_{PAR}$ relationship. However, each seemed to be offset by different amounts (Figure 2-7b). This variability is likely a function of the different methods by which each proxy has been calculated. Empirical normalization of the two-channel broadband data to narrow-band values using the one-to-one response relationships (Figure 2-6) reduced these differences and produced statistically equivalent functions.

The ability to properly track GPP seasonal dynamics with broadband-derived proxy NDVIs (Figure 2-5), the high correlation between proxy and

definite NDVI measurements (Figure 2-6), and the accurate characterization of the NDVI- fA_{PAR} relationship (Figure 2-7) are all positive results pointing to the possibility of using two-band sensors to derive a LUE model. Noting that all proxy indices gave very high correlations with GPP and NDVI_{680,800}, in subsequent chapters we chose to focus on a single proxy index. Proxy index NDVI_{Huemmrich_II} was chosen as it yielded a high correlation with GPP ($R^2 = 0.871$), provided simplicity in calculation, and the highest correlation to our benchmark NDVI_{680,800}. In subsequent sections of this thesis, NDVI_{Huemmrich_II} will be referred solely as “proxy NDVI”.

2.5 References Cited:

Adkinson, A.C., Syed, K. H., Flanagan, L.B. (2011). Contrasting responses of growing season ecosystem CO₂ exchange to variation in temperature and water table depth in two peatlands in northern Alberta, Canada. *Journal of Geophysical Research*, 116: 1-17.

Anderson, D. B. (1936). Relative humidity or vapor pressure deficit. *Ecology* 17: 277-282.

Aubinet M., Aubinet, M., Grelle, A., Ibrom, A., Rannik, Ü., Moncrieff, J., Foken, T., Kowalski, A.S., Martin, P.H., Berbigier, P., Bernhofer, Ch., Clement, R., Elbers, J., Granier, A., Grünwald, T., Morgenstern, K., Pilegaard, K., Rebmann, C., Snijders, W., Valentini, R., Vesala, T. (2000). Estimates of the annual net carbon and water exchange of forests: The EUROFLUX methodology. *Advances in Ecological Research* 30: 113-176.

Baldocchi D.D., Hicks B.B., and Meyers T.D. (1988). Measuring biosphere-atmosphere exchanges of biologically related gases with micrometeorological methods. *Ecology* 69: 1331-1340.

Baldocchi D.D. (2003). Assessing the eddy covariance technique for evaluating carbon dioxide exchange rates of ecosystems: past, present and future. *Global Change Biology* 9: 479-492.

Balzarolo, M., Anderson, K., Nichol, C., Rossini, M., Vescovo, L., et al. (2011). Ground-based optical measurements at European flux sites: a review of methods, instruments and current controversies. *Sensors*, 11: 7954-7981.

Churkina, G., Schimel, D., Braswell, B.H., Xiao, X.M. (2005). Spatial analysis of growing season length control over net ecosystem exchange. *Global Change Biology* 11:1777-1787.

Eklundh, L., Jin, H., Schubert, P., Guzinski, R., Heliasz, M. (2011). An optical sensor network for vegetation phenology monitoring and satellite data calibration. *Sensors*, 11: 7678-7709.

Field, C. B. (1991). Ecological scaling of carbon gain to stress and resource availability. Pages 35-65 in H. A. Mooney, W. E. Winner, and E. J. Pell, editors. *Responses of plants to multiple stresses*. Academic Press, London, England.

Fisher, J.I., Mustard, J.F., Vadeboncoeur, M.A. (2006) Green leaf phenology at Landsat resolution: scaling from the field to the satellite. *Remote Sensing of Environment*, 100: 265-279.

- Flanagan L.B., and Johnson B.G. (2005). Interacting effects of temperature, soil moisture, and plant biomass production on ecosystem respiration in a northern temperate grassland. *Agricultural and Forest Meteorology*, 130: 237-253.
- Gamon, J. A., Field, C.B., Goulden, M., Griffin, K., Hartley, A., Joel, G., Peñuelas, J., Valentini, R. (1995). Relationship between NDVI, canopy structure, and photosynthesis in three Californian vegetation types. *Ecological Applications*, 5: 28-41.
- Gamon, J.A., Rahman, A.F., Dungan, J.L., Schildhauer, M., and Huemmrich, K.F. (2006). Spectral Network (SpecNet): what is it and why do we need it? *Remote Sensing of Environment*, 103: 227–235.
- Gamon, J. A., Cheng, Y., Claudio, H., MacKinney, L., Sims, D. A. (2006b). A mobile tram system for systematic sampling of ecosystem optical properties. *Remote Sensing of Environment*, 103: 246-254.
- Gamon, J.A., Coburn, C., Flanagan, L.B., Huemmrich, K.F., Kiddle, C., Sanchez-Azofeifa, G.A., Thayer, D.R., Vescovo, L., Gianelle, D., Sims, D.A., Rahman, A.F., Pastorello, G.Z. (2011). SpecNet revisited: bridging flux and remote sensing communities. *Canadian Journal of Remote Sensing*, 36: 370-390.
- Garrity, S.R., Vierling, L.A., and Bickford, K. (2010). A simple filtered photodiode instrument for continuous measurement of narrowband NDVI and PRI over vegetated canopies. *Agriculture and Forest Meteorology*, 150: 489-496.
- Glenn, A. J. (2006), Growing season carbon dioxide exchange of two contrasting peatland ecosystems, M.Sc. thesis, Dep. of Biol. Sci., Univ. of Lethbridge, Lethbridge, AB, Canada.
- Glenn, A. J., Flanagan, L. B., Syed, K. H., and Carlson, P. J. (2006). Comparison of net ecosystem CO₂ exchange in two peatlands in western Canada with contrasting dominant vegetation, Sphagnum and Carex, *Agriculture and Forest Meteorology*, 140: 115–135.
- Goulden, M. L., Daube, B. C., Fan, S. M., Sutton, D. J., Bazzaz, A., Munger, J. W., et al. (1997). Physiological responses of a black spruce forest to weather. *Journal of Geophysical Research*, 102: 28987–28996.
- Goward, S. N., & Huemmrich, K. F. (1992). Vegetation canopy PAR absorbance and the Normalized Difference Vegetation Index: An assessment using the SAIL model. *Remote Sensing of Environment*, 39: 119–140.
- Holben, B. N. (1986). Characteristics of maximum-value composite images from temporal AVHRR data. *International of Journal Remote Sensing*, 7: 1417-1434.

- Huemmrich, K.F., Black, T.A., Jarvis, P.G., McCaughey, J.H., Hall, F.G. (1999) High temporal resolution NDVI phenology from micrometeorological radiation sensors. *J Geophys Res Atmos*, 104:27935–27944.
- Huete, A. R., Jackson, R. D., Post, D. F. (1985). Spectral response of a plant canopy with different soil backgrounds. *Remote Sensing of Environment*, 17: 37-53.
- Huete, A., and Justice, C. (1999). MODIS Vegetation Index (MOD 13) Algorithm Theoretical Basis Document. Greenbelt: NASA Goddard Space Flight Centre, <http://modarch.gsfc.nasa.gov/MODIS/LAND/#vegetation-indices>.
- Kumar, M., & Monteith, J. L. (1981). Remote sensing of crop growth. In H. Smith (Ed.), *Plants in the daylight spectrum*. New York: Academic Press. 134–144.
- Jenkins, J.P., Braswell, B.H., Frolking, S.E., Aber, J.D. (2002). Detecting and predicting spatial and interannual patterns of temperate forest springtime phenology in the eastern U.S. *Geophys Res Lett*, 29:2201.
- Jenkins, J.P., Richardson, A.D., Braswell, B.H., Ollinger, S.V., Hollinger, D.Y., Smith, M.L. (2007) Refining light-use efficiency calculations for a deciduous forest canopy using simultaneous tower-based carbon flux and radiometric measurements. *Agricultural Forest Meteorology*, 143:64–79.
- Kathuroju, N., White, M.A., Symanzik, J., et al. (2007). On the use of the advanced very high resolution radiometer for development of prognostic land surface phenology models. *Ecol Model*, 201:144-56.
- Landsberg, J.J. (1977). Some useful equations for biological studies. *Experimental Agriculture*, 13:273-286.
- Lloyd, J. and Taylor, J.A. (1994). On the temperature dependence of soil respiration. *Funct. Ecol.* 8: 315-323.
- Menzel, A., Estrella, N., and Testka, A. (2005). Temperature response rates from long-term phenological records. *Climate Res*, 30: 21-28.
- Moore, C.J. (1986). Frequency response corrections for eddy correlation systems. *Boundary-Layer Meteorol*, 37: 17-35.
- Moncrieff, J.B., Massheder, J.M., de Bruin, H., Elbers, J., Friborg, T., Heusinkveld, B., Kabat, P., Scott, S., Soegaard, H., and Verhoef, A. (1997). A system to measure surface fluxes of momentum, sensible heat, water vapour and carbon dioxide. *Journal of Hydrology*, 188: 589-611.

- Monteith, J. L. (1972). Solar radiation and productivity in tropical ecosystems. *Journal of Applied Ecology*, 9: 747-766.
- Monteith, J. L. (1977). Climate and the efficiency of cop production in Britain. *Phil. Trans. R. Soc. Lond. B*, 281: 277-294.
- Pastorello, G.Z., Sanchez-Azofeifa, A.G., Nascimento, M.A. (2011). Enviro-Net: From Networks to ground-based sensor systems to a web platform for sensor data management. *Sensors*, 11: 6454-6479.
- Prince, S. D. (1991). A model of regional primary production for use with coarse resolution satellite data. *International Journal of Remote Sensing*, 12:1312-1330.
- Richardson, A.D., Jenkins, J.P., Braswell, B.H., Hollinger, D.Y., Ollinger, S.V., and Smith, M.L. (2007). Use of digital webcam images to track spring green-up in a deciduous broadleaf forest. *Oecologia*, 152: 323–334.
- Rocha, A. V., and Shaver, G. R. (2009). Advantages of a twoband EVI calculated from solar and photosynthetically active radiation fluxes. *Agricultural and Forest Meteorology*, 149:1560–1563.
- Running, S.W., Nemani, R.R. (1991) Regional hydrologic and carbon balance responses of forests resulting from potential climate change. *Climate Change*, 19:349–368.
- Running S.W., Nemani, R.R., Heinsch, F.A., Zhao, M., Reeves, M., Hashimoto, H. (2004). A continuous satellite-derived measure of global terrestrial primary production. *Bioscience*, 54: 547-560.
- Schwartz, M.D. (1990). Detecting the onset of spring: a possible application of phenological models. *Climate Res*, 1:23-29.
- Schwartz, M. D. (1994). Monitoring global change with phenology: the case of the spring green wave. *Int. J. Biometeorology*, 38: 18-22.
- Schwartz, M.D., Reed, B.C., White, M.A. (2002). Assessing satellitederived start-of-season measures in the coterminous USA. *Int J Climatol*, 22:1793–1805.
- Sellers, P.J. (1987). Canopy reflectance, photosynthesis, and transpiration II. The role of biophysics in the linearity of their interdependence. *Remote Sensing of Environment*, 21: 143–183.
- Sellers, P. J., Bounoua, L., Collatz, G. J., Randall, D. A., Dazlich, D. A., Los, S. O., et al. (1996). Comparison of radiative and physiological effects of doubled atmospheric CO₂ on climate. *Science*, 271: 1402–1406.

- Syed, K. H., L. B. Flanagan, P. J. Carlson, A. J. Glenn, and K. E. Van Gaalen (2006). Environmental control of net ecosystem CO₂ exchange in a treed, moderately rich fen in northern Alberta, *Agric. For. Meteorol.*, 140: 97–114.
- Teillet, P.M., Staenx, K., Williams, D.J. (1997). Effects of Spectral, Spatial, and Radiometric Characteristics on Remote Sensing Vegetation Indices of Forested Regions. *Remote Sensing of Environment*, 61:139-149.
- Tittebrand, A., Spank, U., Bernhofer, C. (2009). Comparison of Satellite- and Ground-Based NDVI above Different Land-Use Types. *Theor. Appl. Climatol.*, 98:171-186.
- Webb, E.K., Pearman, G.I. and Leuning, R. (1980). Correction of flux measurements for density effects due to heat and water vapour transfer. *Q. J. R. Meteorol. Soc.* 106: 85-100.
- White, M.A., Thornton, P.E., Running, S.W. (1997). A continental phenology model for monitoring vegetation responses to interannual climatic variability. *Global Biogeochem Cycles*, 11:217–234.
- Wilson, T.P., and Meyers, T.P. (2007). Determining vegetation indices from solar and photosynthetically active radiation fluxes. *Agricultural and Forest Meteorology*, 144: 160–179.

Chapter 3 – Photochemical Reflectance Index as a proxy of light use efficiency

3.1. Introduction:

Conceptually, the LUE model is composed of two components 1) a structural component, described by changes in fA_{PAR} , and 2) a physiological component, portrayed by the light use efficiency term. Addressing the efficiency term of the LUE model from remote sensing has been more challenging than addressing the fA_{PAR} variable. As an indicator of xanthophyll cycle activity, PRI can reveal dynamic changes in photosynthetic efficiency at fine temporal and spatial scales (Gamon et al. 1992, 1993, Peñuelas et al., 1995). The xanthophyll cycle is particularly active under conditions of excess energy, *i.e.* departures from the linear, light-limited region of the photosynthetic light-response curve (Björkman and Demmig-Adams 1994). Therefore, it is during conditions involving transitions to excess light that PRI is likely to provide an accurate measure of xanthophyll cycle activity.

Comparisons between the PRI and LUE at the canopy level and stand level (Filella et al. 1996; Gamon et al., 2001; Nichol et al., 2000, 2002; Strachan et al., 2002; Rahman et al., 2004; Garbulsky et al., 2008; Goerner et al. 2011) often show a good correlation between these two variables, at least for individual ecosystems. However, deviation in the LUE-PRI relationship often occurs in response to different vegetation types, sun angle, view angle, canopy structure, and pigment pools sizes among other factors (Barton and North, 2001; Gamon et al., 2001; Sims et al., 2006; Hilker et al., 2008a,b; Filella et al., 2009; Garrity et

al., 2011; Gamon & Berry, 2012). Further complications arise from the different operational definitions of LUE, with some studies defining it based on incident PPFD or “PAR” (Nichol et al. 2000, 2003; Grace et al. 2007) and others defining it based on absorbed PPFD or “PAR” (Drolet et al., 2005, 2008; Hilker et al., 2008; Garbulsky et al., 2008; Goerner et al., 2009). Originally, light use efficiency was defined as a ratio of productivity to the amount of radiation intercepted by a crop to drive photosynthesis (Monteith, 1972; 1977). Later, authors have also calculated LUE based on absorbed light, which is presumably a more accurate estimate of light actually used for photosynthesis, and is closely related to intercepted LUE. The benefit of calculating LUE based on absorbed radiation (LUE_{Abs}) is that by accounting for the structural component of vegetation (fA_{PAR}), it can better isolate the physiological (efficiency) term. However, absorbed light, and the fraction of absorbed light used for photosynthesis, can be hard to measure, especially in tall, structurally complex vegetation. Consequently, LUE is often approximated using incident light (LUE_{Inc}). The effect of these two LUE expressions, and their effect on the PRI-LUE relationship, needs to be better understood.

Significant progress has been made in exploring the effects of light conditions on the LUE-PRI relationship (Hall et al, 2008; Hilker et al., 2008a,b; Middleton et al., 2009). Still, the majority of studies overlook how changes in pigment pools or canopy structure can alter the reflectance properties and associated PRI or LUE values, all of which can confound the LUE-PRI relationship. Many remote sensing studies seem to make the assumption that

fluctuations in PRI represent only short-term photoregulatory processes associated with the xanthophyll cycle and neglect long-term processes that can also affect the index. Studies have shown that constitutive PRI changes due to pigment pool size variation over a growth season can account for most of the PRI variation and potentially confound the LUE-PRI relationship (Stylinski et al., 2002; Sims et al., 2006; Filella et al., 2009; Garrity et al., 2011; Gamon & Berry, 2012). Similarly, changes in canopy or stand structure that affect reflectance patterns can also strongly influence PRI (Gamon et al., 1995; Barton and North, 2001).

Consequently, to understand the mechanism of PRI response, it is important to determine what the index is truly representing, taking into account the irradiance and the spatial and temporal dimension of PRI measurements within a specific ecosystem.

This study explored the suitability of PRI as a proxy for light use efficiency in an alfalfa agricultural field using the two commonly used LUE definitions (*i.e.* LUE_{Abs} and LUE_{Inc}). One goal was to consider the effect of LUE formulation on the PRI-LUE relationship. Also, we explicitly considered the effect of time scale by examining the LUE-PRI relationship both seasonally and diurnally. Garbulsky et al. (2011) suggested that highly productive crops would not have a significant relationship between PRI and LUE_{Abs} , as there is a strong net CO_2 uptake by the ecosystem and little excess energy or need for downregulation. Consequently, we expected that at the seasonal time scale, PRI would be a weak indicator of LUE_{Abs} and that light absorption would be the dominant term in the LUE model. At the diurnal time scale, assuming negligible

changes in vegetation structure, we expected PRI to act as a proxy of efficiency, as has been shown before (Gamon et al. 1992, 1993, Peñuelas et al., 1995)

3.2. Methods:

3.2.1 Study site:

All measurements were made in a homogeneous alfalfa field (*Medicago sativa*) located at the University of Alberta South Campus agricultural research farm; coordinates 53.497 N, -113.552 E. Monitoring occurred throughout the 2009 to 2011 growth season using 1) a 50m Tram system (Gamon, et al., 2006b), providing hyperspectral optical measurements from 2009-2011; 2) a 3 m phenology/ meteorological station, providing broadband optical measurements from 2009-2011; and 3) a 2.5m eddy covariance flux tower, providing atmospheric-biospheric CO₂ exchange measurements from 2009-2010. Further descriptions of the study site and measurement design can be found in chapter 2.

3.2.2 Hyperspectral tram reflectance:

Hyperspectral optical measurements were collected once a week throughout the first two growth cycles of the 2010 growing season, using the tram based robotic system described in chapter 2 of this thesis and in further detail by Gamon et al. (2006b). This involved the use of a dual channel field spectrometer (Unispec-DC, PP-Systems, Amesbury, Massachusetts, USA) (spectral range of 305-1130nm) collecting data every 1m along the 50m-length tram track. On some days, diurnal measurements were made by sampling every hour over the

collection day, as weather permitted. For practical reasons, these hourly measurements were focused on the middle of the photoperiod (*i.e.* 13:30 MDT) when solar elevation angles were relatively high (solar azimuth range of 97° to 257°), and did not include early morning or late evening sampling.

All raw reflectance data collected from the hyperspectral tram runs was corrected to actual target reflectance using a 99% reflective white standard panel (Spectralon, Labsphere Inc., North Sutton, NH). The correction procedure can be mathematically expressed as:

$$\rho_{\text{corrected}} = (R_{\text{target}}/I_{\text{downwelling}}) \times (I_{\text{downwelling}}/R_{\text{standard}}) \quad (1)$$

where $\rho_{\text{corrected}}$ represents corrected reflectance. The first term ($R_{\text{target}}/I_{\text{downwelling}}$) represents the raw reflectance, expressed as a ratio of the upwelling radiance to the downwelling irradiance over the alfalfa field target. The second term ($I_{\text{downwelling}}/R_{\text{standard}}$) represents the cross calibration value calculated as a ratio of the downwelling irradiance to the radiance of the standard panel (Gamon et al. 2006b). An assumption of this method is that the sky conditions are identical (or nearly identical) during target and panel readings. Using this formula, it is not necessary to apply a radiometric calibration, since the calibration coefficients cancel.

Corrected reflectance values were used to derive the photochemical reflectance index (PRI) as follows:

$$PRI = (\rho_{531} - \rho_{570}) / (\rho_{531} + \rho_{570}) \quad (2)$$

where “ ρ ” refers to reflectance and the subscripts refers to the specific spectral bands (531 nm and 570 nm) used for the index. On diurnal sampling days, for each of the hourly collections, PRI values were first calculated for each individual meter along the tram line and then averaged, resulting in a single PRI value per hourly collection period.

3.2.3 fA_{PAR} calculation:

A ceptometer (AccuPAR LP-80, Decagon, Pullman, Washington, USA) was used to measure upwelling and downwelling radiation properties above and below the alfalfa canopy. Measurements collected under the canopy were done as close to the base of the canopy as possible. However, due to the thickness of the instrument (approximately 1 cm) and unevenness of the ground, below-canopy measurements were collected approximately 2cm above the ground. This failure to capture extremely short vegetation could lead to artificially low early season fA_{PAR} measurements and consequently to false high LUE_{Abs} estimates, with diminishing error as the canopy grew taller. These errors were unavoidable with this instrument. Canopy light property measurements allowed the calculation of the fA_{PAR} values. This was calculated using the equation:

$$fA_{PAR} = 1 - t - r + r_s \quad (3)$$

where, t is the fraction of transmitted radiation, r is the reflected radiation from the canopy, and r_s is the soil reflectance component (AccuPAR user's manual, <http://www.decagon.com/manuals/LPman12.pdf>). Individual measurements were made every 5 meters along the track and were done in concert with hourly optical sampling. fA_{PAR} values were averaged to a single value for each hourly collection period. This allowed comparable fA_{PAR} spatial and temporal coverage to that of optical measurements.

3.2.4 Continuous fA_{PAR} and A_{PAR} measurements:

As previously outlined in chapter 2 of this thesis, the phenology station provided fully automated continuous measurements of the canopy reflectance (1 minute logging interval). Data collected from the broadband sensors on the tower were used to calculate a proxy normalized difference vegetation index (NDVI), calculated from the ratio of upwelling to downwelling radiation and outlined by the mathematical expression:

$$NDVI_{\text{proxy}} = (\rho_{\text{PYR}} - \rho_{\text{PAR}}) / (\rho_{\text{PYR}} + \rho_{\text{PAR}}) \quad (4)$$

where ρ_{PYR} is the radiation reflectance calculated from the ratio of upwelling to downwelling radiation using a silicon pyranometer (Onset Computer Corporation, Bourne, Massachusetts, USA, Massachusetts); and ρ_{PAR} is the total reflectance of photosynthetically active radiation (PAR) calculated from the ratio of upwelling

to downwelling PPFD. The high temporal resolution of the broadband data allowed near continuous diurnal NDVI proxy values through the season.

Through the use of the NDVI- fA_{PAR} relationships previously defined in chapter 2, NDVI_{proxy} values were converted into continuous seasonal fA_{PAR} values. Proxy NDVI values were first converted to NDVI_{680, 800} values using empirically derived regressions (see chapter 2). These converted NDVI values were then used to construct a NDVI- fA_{PAR} relationship. The resulting non-linear equation from the NDVI_{proxy}- fA_{PAR} curve ($y = 3.76 (\text{NDVI}_{\text{Huemmrich_II}})^{5.38}$; $R^2 = 0.92$) was then used to derive continuous fA_{PAR} values (every 1 minute) throughout the growing season (see chapter 2 for graphical representation of relationship).

Absorbed photosynthetically active radiation (A_{PAR}) was calculated as the product of continuous fA_{PAR} and PPFD:

$$A_{PAR} = fA_{PAR} \times \text{PPFD} \quad (5)$$

Combining continuous irradiance and fA_{PAR} values derived from the broadband optical sensors provided A_{PAR} values at one-minute time steps throughout the 2010 growing season.

3.2.5 LUE derivations:

To evaluate the impact of LUE formulation on the PRI-LUE relationship, two metrics of LUE were calculated. LUE values for the growth season based on absorbed radiation were computed as follows:

$$\text{LUE}_{\text{Abs}} = \text{GPP}/A_{\text{PAR}} \quad (6)$$

Additionally, LUE was also calculated based on incoming PPFD as opposed to absorbed light using the following equation:

$$\text{LUE}_{\text{Inc}} = \text{GPP}/\text{PPFD} \quad (7)$$

3.2.6 Linear mixing model:

A linear mixing model was used to explore the link between PRI and canopy structure by simulating the effect of different levels of canopy closure on PRI changes throughout the growing season. This model utilized brown soil and green canopy spectra from data collected during growth cycle #2 as end-members, and mixed different ratios of brown and green reflectance (assuming linear additive mixing). Spectral response from end members (100% and 0%) were defined and used to model the expected response of canopy cover levels of 0, 20, 40, 60, 80, and 100% closure. PRI values were calculated from each of the modeled spectra and compared to measured values from growth cycle #2. Linear mixing model allowed us to assess the link between seasonal PRI response and canopy structure.

3.2.7 Seasonal analysis of optical, fA_{PAR} and flux measurements:

For the seasonal analysis, PRI and fA_{PAR} were expressed as two different temporal aggregation periods. For time series analysis, midday PRI and fA_{PAR}

were calculated by averaging measurements taken during solar noon (~13:30 MDT). Therefore, each midday value represents the average PRI and fA_{PAR} values of approximately 20 minutes (time needed for tram and light bar sampling) centered on solar noon. Expressing PRI and fA_{PAR} as midday values was done to match the temporal aggregation (30 minutes) of flux measurements. For direct 1-to-1 correlation analysis, the entire PRI and fA_{PAR} datasets of the 2010 growth season were used. Each of the values in the dataset represents an average of each hourly sampling collected throughout the growth season.

All seasonal relationships of fluxes were derived using 30-minute aggregate midday values. Midday values were chosen to remove some of the variability associated with eddy covariance data. To match the temporal resolution of GPP, 30-minute averaged A_{PAR} values from midday were extracted for the entire growth season. Seasonal LUEs (absorbed and incident) were calculated using mid-day 30-minute averaged GPP and A_{PAR} values.

3.2.8 Diurnal Analysis of PRI as an LUE proxy:

Taking into account the limited amount of collection days available for diurnal analysis, we selected the most complete datasets that best represented the different canopy states encountered through out the growth season. Collection days 12/05/17, 12/06/12, and 12/06/28 represented mid green-up, mid mature-growth, and end of growth cycle (#1), respectively. Collection day 12/07/27 was representative of the transition between green-up and the mature growth phase of growth cycle #2. For each collection day, light response curves were prepared

using the 30-minute aggregated NEE values over the full day (daylight hours only) and compared to corresponding PPFD values at identical temporal periods. Each of the light curves was divided in two sections (prior and post solar noon, approximately 12:30 MST). The slope of each section was calculated and represented the photosynthetic quantum yield (α). To remove the effect of hysteresis on α calculations, only periods 2 hours away from solar noon and within the photoperiod were considered (*i.e.* from 04:30- 10:30 MST; and from 14:30-21:00 MST). For each of the light curve, the change in diurnal quantum yield ($\Delta\alpha$) was calculated by comparing the slope of each of the sections prior and post solar noon.

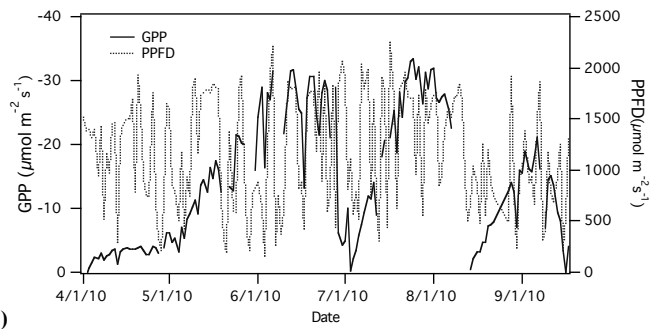
Diurnal analysis also compared PRI and PPFD responses for each of the four collection days. In this analysis, each PRI_{531,570} value represents an average of a single tram run collected at a given hour of the day. PPFD values were averaged over 30-minutes to match the temporal coverage of flux and tram collection periods. The change in diurnal PRI (Δ PRI) was calculated by comparing the maximum and minimal PRI values. Temporarily low PRI values that were caused by short periods of cloud cover were excluded from Δ PRI calculations.

3.3. Results:

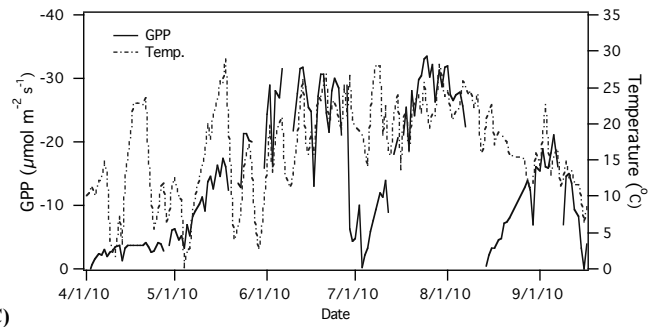
3.3.1 Analysis of seasonal patterns:

Seasonal changes in PRI roughly follow seasonal changes in productivity (Figure 3-1d). Some slight deviations between PRI and GPP were observed during mid green-up of the first growth cycle and could suggest physiological response to light conditions, temperature, VPD or a combination of these variables. As expected given the large change in canopy structure during the growing season, the fA_{PAR} seasonal pattern also closely tracked GPP (Figure 3-1e). Similarly, the seasonal pattern of LUE_{Inc} closely followed GPP (Figure 3-1f) and showed similar overall patterns to that of PRI and fA_{PAR} . However, this was not the case for LUE_{Abs} , where there was a negative association with the GPP seasonal patterns (Figure 3-1g). The progression of LUE_{Abs} values throughout the growth season shows a repeatable pattern occurring within each of the individual growth cycles (Figure 3-1g). The pattern consisted of high values during early green-up stage, followed by progressive decrease during mid green-up, and reaching a plateau during crop mature-growth stages. Clearly, the LUE calculation method has a significant effect on the resulting seasonal LUE pattern.

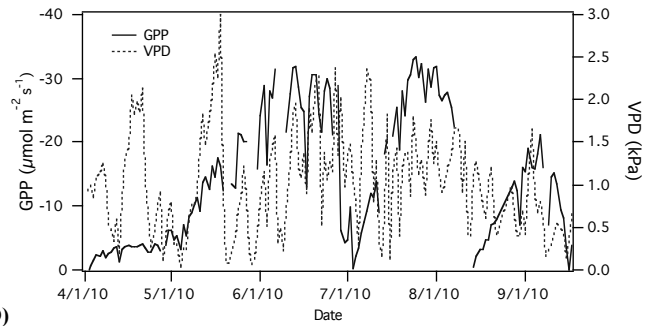
(A)



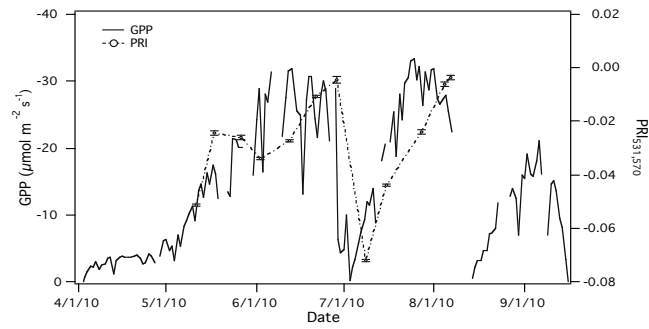
(B)



(C)



(D)



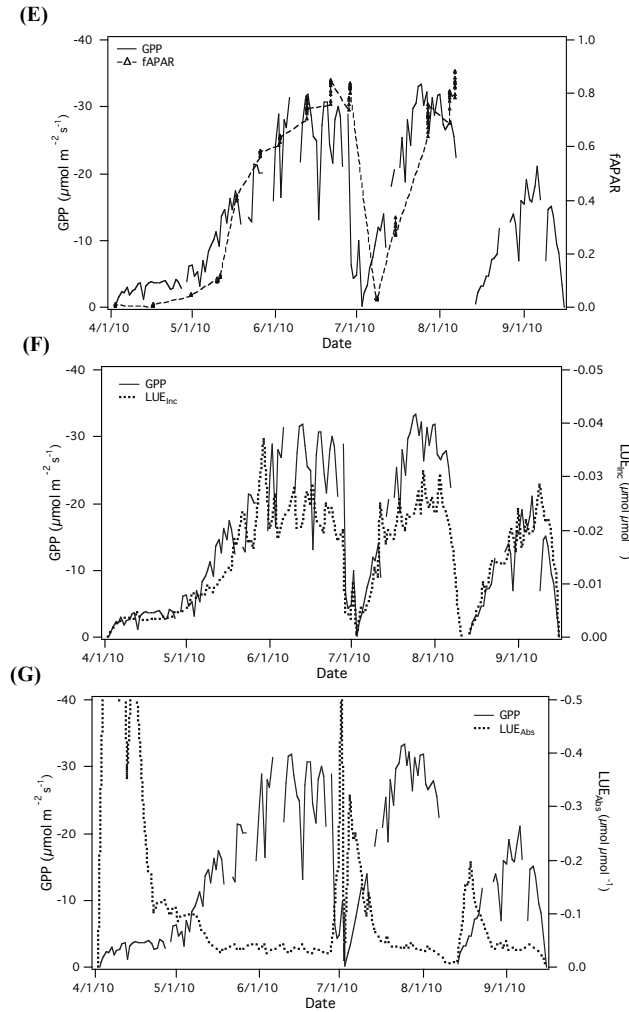


Figure 3-1: Time series of midday GPP and (A) irradiance, (B) temperature, (C) VPD, (D) PRI_{531,570}, (E) fA_{PAR} , (F) LUE_{Inc} , and (G) LUE_{Abs} .

Analysis of the PRI time series shows it generally followed fA_{PAR} (Figure 3-2a). Comparison of PRI to the LUE_{Inc} time series also revealed comparable seasonal patterns (Figure 3-2b). Conversely, comparison of the LUE_{Abs} and PRI time series revealed opposite seasonal patterns to one another (Figure 3-1c).

The seasonal time series of LUE_{Abs} appeared to be in the opposite direction to that of LUE_{Inc} . Generally, periods of high LUE_{Abs} values seemed to correspond to low LUE_{Inc} values, and vice versa. Comparison of the two datasets showed them as being negatively correlated ($R = -7.87$, $R^2 = 0.62$) (Figure 3-3).

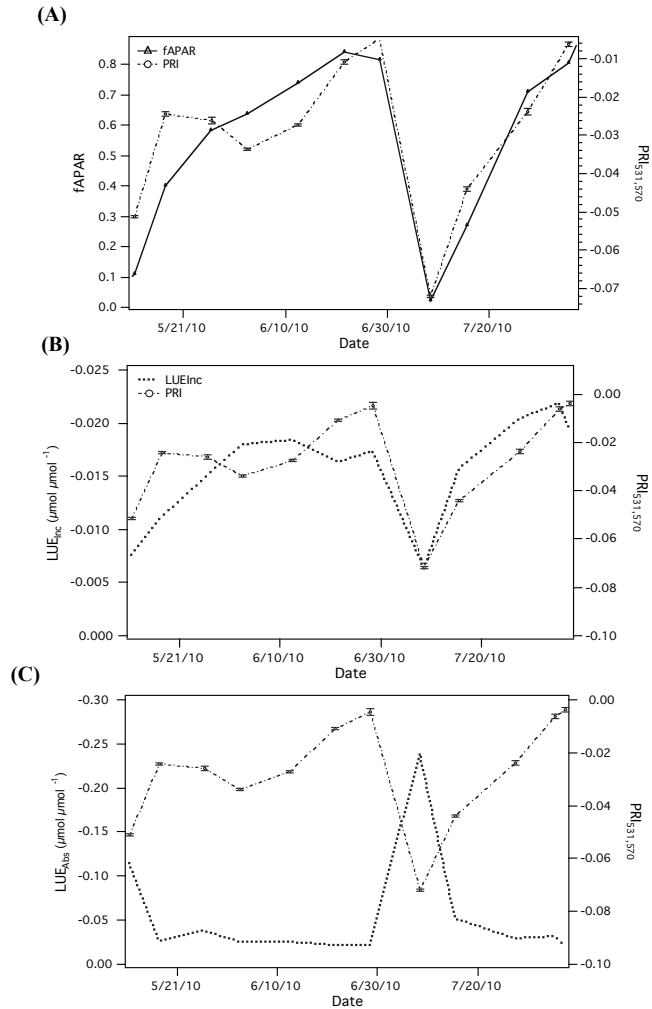


Figure 3-2: Comparison of hourly collected f_{APAR} , midday LUE_{Inc} and midday LUE_{Abs} to hourly collected $PRI_{531,570}$ seasonal time series.

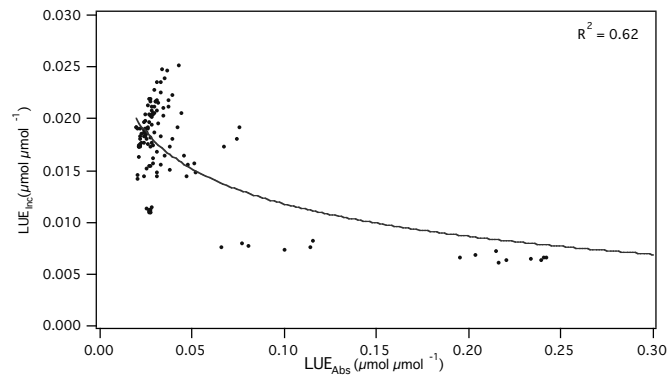


Figure 3-3: One-to-one correlation of absolute seasonal LUE_{Abs} and LUE_{Inc} values showing a negative exponential correlation ($R^2 = 0.62$).

3.3.2 Seasonal PRI comparison to PAR, fA_{PAR} , and A_{PAR} :

To further investigate the underlying reason for the opposing seasonal pattern of $PRI_{531,570}$ and LUE_{Abs} , correlations with other variables relating to the LUE model were also explored. The variables tested consisted of PAR, fA_{PAR} and A_{PAR} , as they represent the direct measure of downwelling irradiance (PPFD), the measure of vegetation structure, and a combination of structure and available PAR irradiance (PPFD), respectively. $PRI_{531,570}$ had a very low correlation to irradiance ($R^2 = 0.12$) (Figure 3-4a), and a higher but still weak association to A_{PAR} ($R^2 = 0.49$) (Figure 3-4b). However, there was a relatively strong correlation between $PRI_{531,570}$ and fA_{PAR} ($R^2 = 0.78$) (Figure 3-4c). One source of scatter in the PRI - fA_{PAR} relationship resulted from patchy canopy structure conditions during periods of open canopy. Also, early season fA_{PAR} values could be slightly lower as the light bar might have failed to capture all green material (green leaves and stems) near the ground and below the instrument.

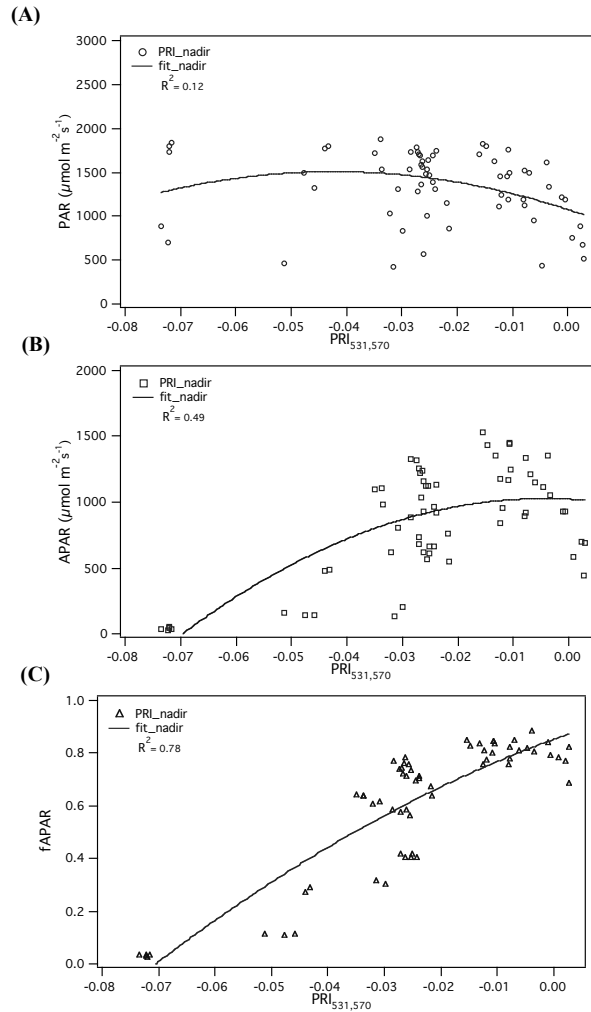


Figure 3-4: Pairwise correlation of $PRI_{531,570}$ derived from hyperspectral reflectance measurements and (A) PAR (PPFD), (B) A_{PAR} , and (C) f_{APAR} for the entire 2010 growing season.

3.3.3 Linear mixing model and correlations to canopy structure:

To further explore a possible functional link between PRI and green canopy structure, we simulated PRI for different levels of canopy closure using a linear mixing model. Using this model, we were able to confirm the influence that vegetation structure has on PRI values throughout the season. Results showed measured $PRI_{531,570}$ as having a strong correlation to modeled values (Figure 3-5b), further supporting the conclusion that seasonal PRI patterns were primarily driven by canopy structure, and not xanthophyll cycle activity *per se*.

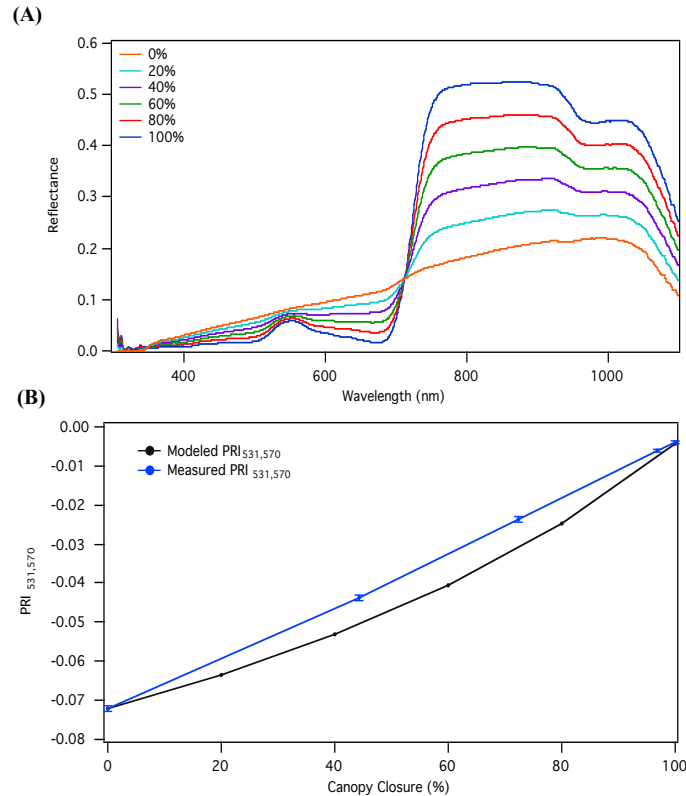


Figure 3-5: Spectral reflectance resulting from the linear mixing model for various percentages of canopy closure ranging from 0% to 100%. Modeled PRI values calculated from the idealized spectral reflectance, compared favorably to measured PRI values.

The strong influence of fA_{PAR} on PRI supports the notion that the index is dominated by changing green canopy structure over the course of the season. As a result when seasonal PRI (or fA_{PAR}) is plotted against the two LUE formulations (incident and absorbed PPFD basis), strong but opposite relationships emerge. A direct comparison between PRI and LUE_{Abs} (calculated for all collection times and periods) showed a strong correlation between the two ($R^2 = 0.92$) (Figure 3-6a). However, the positive relationship between PRI and LUE_{Abs} expected if the index was acting as a true proxy of efficiency does not emerge. As with our previous results, the response of the LUE_{Inc} -PRI correlation was opposite to that observed when using LUE values based on absorbed light. As both PRI and fA_{PAR} appeared to describe vegetation structure, we expected both to have similar

correlations to seasonal LUE. Indeed, the seasonal fA_{PAR} -LUE (absorbed and incident light based) relationships show a very similar pattern to those of the PRI-LUE relationships (compare Figure 3-6b to 3-6a).

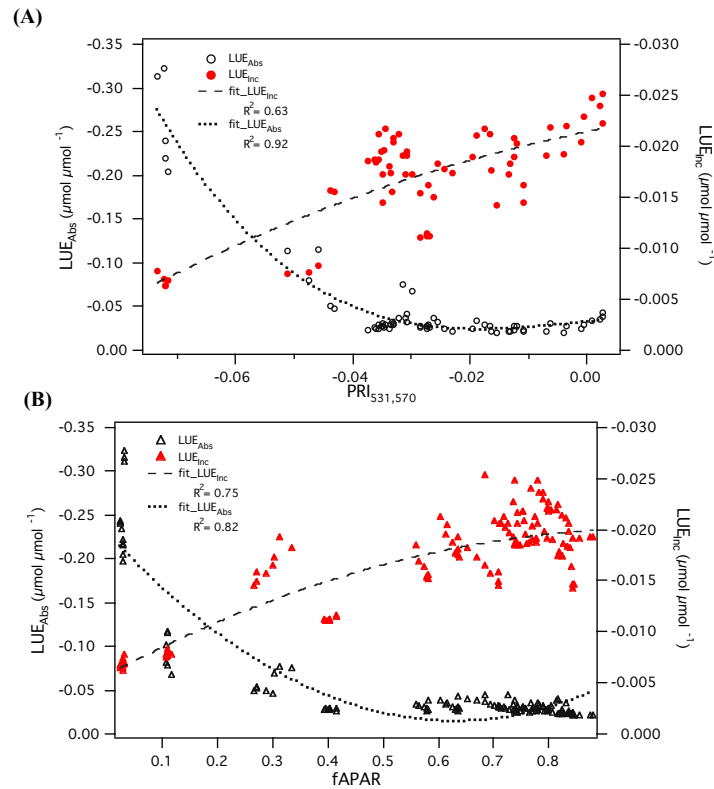


Figure 3-6: (A) Seasonal correlation between LUE (absorbed and incident light based) and PRI. (B) Seasonal correlation between LUE (through both methods) and fA_{PAR} . $PRI_{531,570}$ derived from hyperspectral reflectance measurements. fA_{PAR} calculated from light bar measurements.

3.3.4 Diurnal evaluation of PRI as a proxy of LUE

The original studies linking PRI to LUE were done at the diurnal time scale, where structural changes in canopy were small compared to those driven by photosynthetic downregulation in response to saturating light (Gamon et al. 1992, 1993; Peñuelas et al., 1995). Following this tradition, we explored patterns in diurnal PRI to determine if the index was able to track physiological changes at

this temporal scale for our alfalfa crop. A series of representative collection days that described the various canopy states encountered throughout the growth season are shown in Figure 3-7a. NEE light-response curves for each of these collection days allowed us to explore the actual physiological status of the vegetation independently of optical measurements. For collection day *A* and *D*, there seemed to be little diurnal variation in PRI (Figure 3-8e and 3-8h). Diurnal light-response curves of both of these days showed little deviation between the first and latter half of the day (Figure 3-8a and 3-8d). Analysis of the light curve for collection day *B* shows slight separation between the first and latter half of the day (Figure 3-8b). The point of hysteresis begins during solar noon (12:30 MST). The diurnal PRI pattern was closely associated with the light regime (Figure 3-8f). As PPFD increased from morning to solar noon, PRI values decreased. Following solar noon, PRI values continued to decrease slightly, but subsequently showed recovery late in the diurnal cycle. During collection day *C*, there was a significant separation in the NEE-light trajectory between the first and latter part of the day (Figure 3-8c). The point of hysteresis of the curve began around 12:00 MST, which correlated with the daily peak PPFD value ($1872 \mu\text{mol m}^{-2} \text{s}^{-1}$). The diurnal PRI trend, again, closely followed the light regime, declining as PPFD increased in the morning, then jumping up in response to midday cloud cover that extended from solar noon until 13:30 MST (Figure 3-8g). When looking at individual diurnal patterns of these collection days, there is evidence for classic midday decline in LUE in some cases (Figure 3-8f and 3-8g) but not all (Figure 3-8e and 3-8h). These cases of a midday PRI dip correspond to days with hysteresis in the

light response curves, indicating days where photosynthetic downregulation occurred.

For each of the collection days, quantum yield (α) was calculated for the first and second half of the diurnal cycle. By quantifying changes in diurnal α , we were able to directly measure diurnal changes in light-use efficiency. Comparison of $\Delta\alpha$ to Δ PRI (calculated from diurnal tram measurements) showed a strong correlation ($R^2 = 0.91$) (Figure 3-9). The linear relationship that emerges between $\Delta\alpha$ and Δ PRI confirms that, on a diurnal time scale, when changing canopy structure (ΔfA_{PAR} due to crop growth) is not an issue, the “classic” PRI response can be seen, even in ecosystems with high net CO_2 uptake such as crops. However, days with photosynthetic downregulation may not be visible in seasonal PRI trends, particularly if midday cloud cover masks these periods of midday depression (as in collection day C of Figure 3-7).

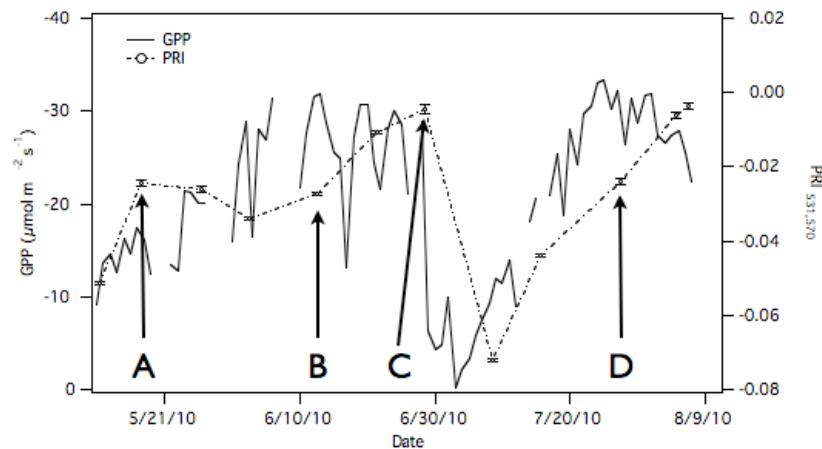


Figure 3-7: Seasonal trend of GPP and PRI. Letters “A, B, C, and D” corresponding to collection dates (12-05-17, 12-06-12, 12-06-28, and 12-07-27, respectively) used for diurnal analysis. This figure was derived from Figure 3-1D.

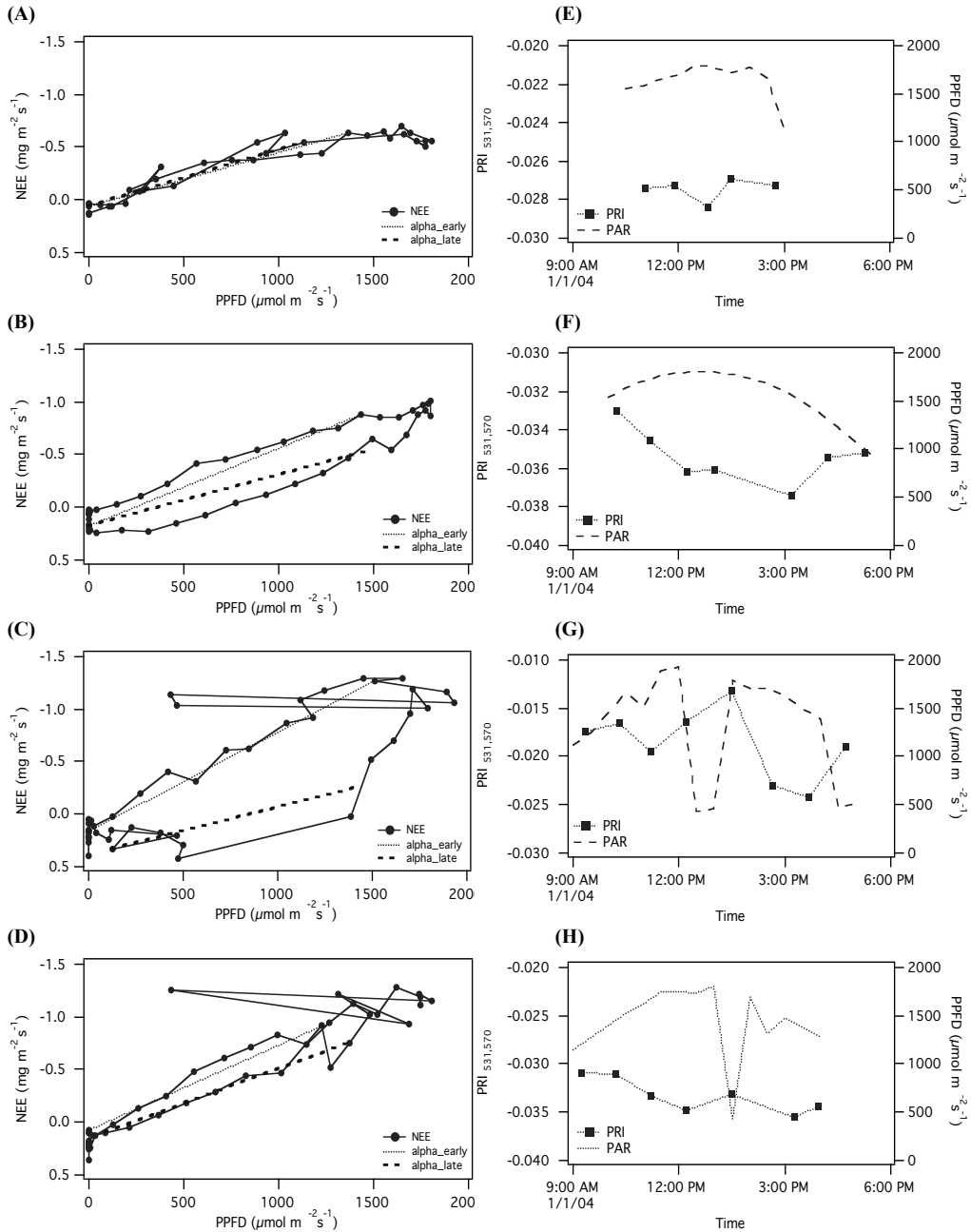


Figure 3-8: Analysis of diurnal patterns of light response curves for collection days (A) 12-05-17, (B) 12-06-12, (C) 12-06-28, and (D) 12-07-27 (listed as *A*, *B*, *C* and *D*, respectively, in Figure 3-6). Changes in diurnal PRI and PPFD for collection days (E) *A*, (F) *B*, (G) *C*, and (H) *D* are also illustrated. NEE points represent 30 minute running averages. Dashed lines in each light curve plot represent calculated quantum yield values (α) early (dotted line) and late (dashed line) in the day. Each PRI point is an average of 50 sample tram points collected hourly throughout the diurnal day. PPFD was collected every minute and averaged over 30 minutes to match the flux temporal resolution.

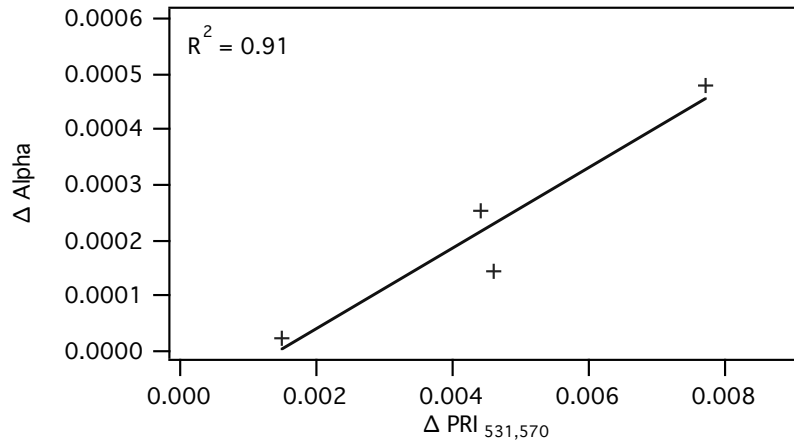


Figure3-9: Correlation between Δ quantum yield and $\Delta \text{PRI}_{531,570}$ derived from diurnal analysis.

4.4. Discussion:

Addressing the efficiency term through the LUE model can be quite challenging. As this study shows, using PRI as a proxy of efficiency at a seasonal time scale may be problematic for this alfalfa crop. As our results indicate, some of the complexities associated with monitoring LUE include the fact that LUE does not vary greatly throughout the season. LUE_{Abs} is generally flat during most of the growing season, except for early season where high GPP and small changes in canopy light interception (indicated by low NDVI and fA_{PAR} values) occur. Also, during this period of low cover, underestimated fA_{PAR} values can lead to false high LUE_{Abs} estimates, exaggerating the otherwise negligible PRI- LUE_{Abs} correlation. This low seasonal variability in LUE_{Abs} for most of the period of canopy closure makes it difficult to track using PRI. Most of the seasonal changes in PRI are associated with changes in vegetation structure (measured by fA_{PAR}), making it difficult to separate the effect of structural changes from physiological changes in the PRI signal. Our results also show that the improper definition of LUE (based on incident light) can confound the correlation between LUE and

PRI, making it appear like a meaningful correlation between these variables, when in fact this correlation is driven by changing canopy structure, which also influences PRI (as demonstrated in Figure 3-5), not just the A_{PAR} term.

At the seasonal scale, comparison of PRI to fA_{PAR} and LUE_{Abs} allowed us to identify the component (structural vs. physiological) that PRI most closely represents. The strong association between seasonal PRI and fA_{PAR} time series (Figure 3-2a) was the first indicator that, for this alfalfa crop, PRI was mostly an indicator of the ecosystem's structural component. Correlation between these two variables shows that 78% of the variability within this index can be explained by fA_{PAR} (Figure 3-4c). Thus, over seasonal time scales, PRI is a better indicator of canopy greenness and total chlorophyll content (analogous to NDVI) than a proxy of the physiological status of vegetation. The linear mixing model further demonstrated the mechanism of the strong association between seasonal PRI changes and canopy structural progression. Conceptually, this is analogous to other studies that show PRI being similarly confounded by pigment pool sizes, particularly over long time periods (Stylinski et al. 2002; Sims et al. 2006; Filella et al., 2009; Garbulsky et al. 2011; Gamon & Berry, 2012).

Even though the seasonal pattern largely shows PRI as being closely connected to the structural component, there is still evidence that the index can capture the physiological status of vegetation over short time scales through the activity of the xanthophyll cycle, as previously reported (Gamon et al. 1992, 1993, Peñuelas et al., 1995). Periods of deviation between the fA_{PAR} and PRI time series show evidence of slight physiological effects, beyond the structural

component, on the PRI signal. However, this divergence could be the result of using midday values for time series analysis. PRI patterns can be influenced, by short-term weather patterns, as the index is highly related to incoming radiation (Figure 3-8). Analysis of midday PPFD, VPD and PRI values collected over the growing season (see Figure 3-2) indicated that some of the variation in midday PRI was indeed caused by irradiance ($R^2 = 0.33$) and VPD ($R^2 = 0.22$), but these correlations were much weaker than the PRI- fA_{PAR} correlations shown in figure 3-6, so are not shown here. Conditions of variable cloud cover, as can normally be encountered during mid-day at our site, can lead to some of the variability in the PRI values not accounted for by fA_{PAR} in the overall seasonal PRI trend (see Figure 3-2).

At the diurnal time scale, PRI does indeed accurately track changes in LUE, even though this may not be noticeable over a seasonal time scale. This is due to: a) the strong influence of canopy structure on PRI, and b) the confounding effects clouds (and possibly reduced VPD) can have on PRI, which cause temporary recovery of PRI during when a cloud passes at midday, as shown in collection days C and D. All of this supports our original contention (first suggested by Garbulsky et al. 2011) that in a healthy, unstressed crop, LUE variation (and thus PRI) is not terribly useful as an LUE indicator, and thus the focus of the modeling effort for a crop like this should be primarily directed at capturing A_{PAR} and secondarily at LUE (PRI).

Analysis of the PRI patterns at the diurnal time scale shows evidence for the index's association with physiological activity, and thus with the efficiency

term of the LUE model, at least over short time scales (when canopy structure does not vary much). The decrease in PRI values observed on representative days *B* and *C*, indicate photosynthetic downregulation, presumably due to de-epoxidation towards the zeaxanthin state (Gamon et al. 2001). The variability in PRI values observed in day *C* is associated with cloud cover, causing the temporary decrease in excess light energy leading to a decrease need for non-photochemical quenching for this short time period; this causes the otherwise reduced PRI to be “invisible” for this date when examining the seasonal trend of midday values (e.g. Figure 3-2a). The minimal hysteresis in the light curve pattern in representative days *A* and *D*, suggest little diurnal downregulation on these dates. This is further supported by the minimal variability of PRI on these days, suggesting that substantial non-photochemical quenching did not occur since light availability did not exceed the saturation threshold of vegetation (Bjorkman and Demming-Adams, 1994). Alternatively, on days *B* and *C*, the separation in NEE light response between the initial and latter part of the day, and the parallel changes in PRI, indicates PRI was able to clearly detect this short-term stress associated with midday photosynthetic downregulation.

At the diurnal time scale, changes in leaf movement (heliotropic alfalfa leaves) can lead to measurable changes in diurnal vegetation structure. Yet, in comparison to the overall structure changes occurring throughout the growth season, structural changes due to leaf movement appeared to be minimal. This is confirmed by comparing the small changes in diurnal fA_{PAR} (max diurnal $\Delta fA_{\text{PAR}} = 0.05$) to the larger seasonal changes (approximately $\Delta fA_{\text{PAR}} = 0.73$). Therefore,

one can assume that changes in PRI, at the diurnal time scale, are primarily driven by downregulation in response to saturating light conditions, and not due to changing canopy structure. The parallel patterns between diurnal PRI and illumination in all diurnal analysis demonstrate that the degree of excess irradiance has a dominant effect on PRI dynamics over the short term as previously reported by Gamon et al. (2001, 2013). However, this was only apparent in the context of diurnal temporal periods, and was not clearly evident in the seasonal PRI patterns.

With the complexity of trying to distinguish the underlying mechanisms affecting PRI signal at the various temporal dimensions (seasonal, diurnal, etc.), the ability to interpret PRI in terms of light response curves provides a way to clearly identify if the variability in signal is attributed to physiological changes in light use efficiency. Our results show an example of this analysis at the diurnal level (Figure 3-6), however, due to limitations in the temporal coverage of tram data, this analysis could not be conducted for every day over the full season. Limitations in temporal dimension of the dataset call for the need for continuous PRI measurements if we are to fully characterize these effects. Similar to the two-band NDVI_{proxy} sensors discussed in chapter 2, automated PRI sensors would provide us with a detailed view of the dynamic changes occurring within an ecosystem, and would help define the drivers (*i.e.* structural or physiological) affecting Δ PRI at the seasonal and diurnal temporal scales (Garrity et al. 2010, Balzarolo et al. 2011). Skye Instruments Ltd. and Decagon Devices Inc. are two companies currently developing continuous PRI sensors for commercial

distribution. However, Skye PRI sensors are still poorly characterized and Decagon PRI sensors are still undergoing field-testing and development, hence more progress in sensor development may be needed before these sensors can be used to accurately measure PRI.

My findings support the contention that proper interpretation of PRI depends largely on the context, which includes time scale, type and condition of canopy, and irradiance. Consequently, even with the development of automated PRI sensors, we recommend that all PRI studies should be complemented with measurements of leaf pigments, canopy structure, PPFD, and photosynthesis (or net carbon flux) measurements. It is only through the complete suite of measurements that we can account for effects of different vegetation types, sun angle, view angle, canopy structure, pigment pools sizes, and level of downregulation, all of which are known to effect PRI (Barton and North, 2001; Gamon et al., 2001; Sims et al., 2006; Hilker et al., 2008a,b; Filella et al., 2009; Garrity et al., 2011; Gamon & Berry, 2012). Attaining a pure PRI signal that can serve as an indicator of efficiency, at all temporal scales, would leave us one step closer to deriving a purely remote sensing driven LUE model for assessing productivity in any terrestrial ecosystem.

5. References:

- Barton, C. V. M., North, P. R. J. (2001). Remote Sensing of canopy light use efficiency using the Photochemical Reflectance Index. Model and analysis. *Remote Sensing of Environment*, 78: 264-273.
- Balzarolo, M., Anderson, K., Nichol, C., Rossini, M., Vescovo, L. (2011). Ground-Based Optical Measurements at European Flux Sites: A Review of Methods, Instruments and Current Controversies. *Sensors*, 11: 7954-7981
- Björkman, O. and Demmig-Adams, B. (1994). Regulation of photosynthetic light energy capture, conversion and dissipation in leaves of higher plants. In: Schulze E-D and Caldwell MM (eds) *Ecophysiology of Photosynthesis*, pp 17–47. Ecological Studies 100. Springer-Verlag, Berlin.
- Féret, J.B., François, C., Asner, G.P., Gitelson, A.A., Martin, R.E., Bidel, L.P.R., Ustin, S.L., le Maire, G., & Jacquemoud, S. (2008). PROSPECT-4 and 5: advances in the leaf optical properties model separating photosynthetic pigments. *Remote Sensing of Environment*, 112: 3030-3043.
- Filella, I., Amaro, T., Araus, J. L., & Peñuelas, J. (1996). Relationship between photosynthetic radiation-use efficiency of Barley canopies and the photochemical reflectance index (PRI). *Physiologia Plantarum*, 96: 211–216.
- Filella, I., Porcar-Castell, A., Munné-Bosch, S., Bäck, J., Garbulsky, M., & Peñuelas, J. (2009). PRI assessment of long-term changes in carotenoids/chlorophyll ratio and short-term changes in de-epoxidation state of the xanthophyll cycle. *International Journal of Remote Sensing*, 30: 4443–4455.
- Gamon, J.A., Peñuelas, J., and Field, C.B., (1992). A narrow-waveband spectral index that tracks diurnal changes in photosynthetic efficiency. *Remote Sensing of Environment*, 41: 35-44.
- Gamon, J.A., Filella, I., Peñuelas, J. (1993) The dynamic 531-nanometer Δ reflectance signal: a survey of twenty angiosperm species. Yamamoto HY , Smith CM (Eds). *Photosynthetic Responses to the Environment*. American Society of Plant Physiologists, Rockville. pp. 172-177.
- Gamon, J.A., Roberts, D.A., Green, R.O. (1995) Evaluation of the photochemical reflectance index in AVIRIS imagery. In: Green RO (Ed) *Proceedings of the Fifth Annual JPL Airborne Earth Science Workshop*, Pasadena, 23-26 January 1995. JPL Publication 95-1:55-58.
- Gamon, J. A., Field, C. B., Fredeen, A. L., & Thayer, S. (2001). Assessing photosynthetic downregulation in sunflower stands with an optically-based model. *Photosynthesis Research*, 67: 113–125.

- Gamon, J.A., & Berry, J.A. (2012). Facultative and constitutive pigment effects on the Photochemical Reflectance Index (PRI) in sun and shade conifer needles. *Israel Journal of Plant Sciences*, 60: 85–95.
- Gamon, J.A. & Bond, B. (2013). Effects of irradiance and photosynthetic downregulation on the photochemical reflectance index in Douglas-fir and ponderosa pine. *Remote Sensing of Environment*, 135: 141-149.
- Garbulsky, M. F., Peñuelas, J., Papale, D., & Filella, I. (2008). Remote estimation of carbon dioxide uptake of a Mediterranean forest. *Global Change Biology*, 14: 2860-2867.
- Garbulsky, M. F., Peñuelas, J., Gamon, J. A., Inoue, Y., & Filella, I. (2011). The photochemical reflectance index (PRI) and the remote sensing of leaf, canopy and ecosystem radiation use efficiencies: A review and meta-analysis. *Remote Sensing of Environment*, 115: 281-297.
- Garrity, S.R.; Vierling, L.A.; Bickford, K. A., (2010). Simple Filtered Photodiode Instrument for Continuous Measurement of Narrowband NDVI and PRI over Vegetated Canopies. *Agricultural and Forest Meteorology*, 150: 489-496.
- Garrity, S. R., Eitel, J. U. H., & Vierling, L. A. (2011). Disentangling the relationships between plant pigments and the photochemical reflectance index reveals a new approach for remote estimation of carotenoid content. *Remote Sensing of Environment*, 115: 628-635.
- Goerner, A., Reichstein, M., Tomelleri, E., Hanan, N., Rambal, S., Papale, D., Dragoni, D., Schullius, C. (2011). Remote sensing of ecosystem light use efficiency with MODIS-based PRI. *Biogeosciences*, 8: 189-202.
- Hilker, T., Coops, N. C., Hall, F. G., Black, T. A., Wulder, M. A., Nesic, Z., et al. (2008). Separating physiologically and directionally induced changes in PRI using BRDF models. *Remote Sensing of Environment*, 112: 2777-2788.
- Jacquemoud, S., & Baret, F. (1990), PROSPECT: a model of leaf optical properties spectra. *Remote Sensing of Environment*, 34: 75-91.
- Nichol, C. J., Huemmrich, K. F., Black, T. A., Jarvis, P. G., Walthall, C. L., Grace, J., et al. (2000). Remote sensing of photosynthetic-light-use efficiency of boreal forest. *Agricultural and Forest Meteorology*, 101: 131-142.
- Nichol, C. J., Lloyd, J., Shibistova, O., Arneth, A., Roser, C., Knohl, A., et al. (2002). Remote sensing of photosynthetic-light-use efficiency of a Siberian boreal forest. *Tellus Series B-Chemical and Physical Meteorology*, 54: 677-687.
- Monteith, J. L. (1977). Climate and the efficiency of crop production in Britain. *Phil. Trans. R. Soc. Lond. B*. 281: 277-294.

- Peñuelas, J., Filella, I., and Gamon, J. A. (1995). Assessment of photosynthetic radiation-use efficiency with spectral reflectance. *New Phytol* 131: 291–296.
- Rahman, A. F., Cordova, V. D., Gamon, J. A., Schmid, H. P., & Sims, D. A. (2004). Potential of MODIS ocean bands for estimating CO₂ flux from terrestrial vegetation: A novel approach. *Geophysical Research Letters*, 31: L10503.
- Sims, D. A., Luo, H., Hastings, S., Oechel, W. C., Rahman, A. F., & Gamon, J. A. (2006). Parallel adjustments in vegetation greenness and ecosystem CO₂ exchange in response to drought in a Southern California chaparral ecosystem. *Remote Sensing of Environment*, 103: 289-303.
- Strachan, I. B., Pattey, E., & Boisvert, J. B. (2002). Impact of nitrogen and environmental conditions on corn as detected by hyperspectral reflectance. *Remote Sensing of Environment*, 80: 213–224.
- Stylinski, C. D., Gamon, J. A., & Oechel, W. C. (2002). Seasonal patterns of reflectance indices, carotenoid pigments and photosynthesis of evergreen chaparral species. *Oecologia*, 131: 366–374.

Chapter 4 – Effects of Temporal aggregation on LUE model accuracy

4.1 Introduction:

The LUE model allows the direct integration of optical measurements with flux measurements. Integration of optical and flux measurements can avoid some of the limitations associated with each independent method. Remote sensing provides the ability to sample in sites that are not ideal for eddy covariance technique including ecosystems with high heterogeneity or with clear topographic relief. However, criticism arises from the LUE model's dependence on empirical observation. Integration of optical sampling with eddy covariance can strengthen our understanding of the mechanisms underlying the LUE model.

One of the primary goals involving remote sensing and flux dataset integration has been the validation of terrestrial carbon exchange estimated from satellite products using net ecosystem carbon exchange values from the global flux network as a reference (Rahman et al., 2004; Turner et al., 2005; Heinsch et al., 2006; Sims et al., 2006; Coops et al., 2007). With progress in this area, research priorities have continued to focus into exploring individual ecosystem processes by partitioning net ecosystem carbon exchange into its component fluxes: gross primary productivity and ecosystem respiration. The integration of optical with flux measurements can provide an additional method for the partitioning of fluxes, thus helping provide further insight into ecosystem functioning (Gamon, 2006). The evaluation of the individual components allow

for a more mechanistic understanding of carbon cycle dynamics (Falge et al., 2002; Law et al., 2002).

One of the challenges of integrating optical and flux data arises from the different time and space scales of optical and flux measurements. To achieve meaningful integration of remote sensing with flux data, an in-depth assessment exploring the temporal aggregation requirements needed to build relationships that properly represent the physiological status of plant canopies is necessary. Recently, Sims et al. (2005) observed a strong correlation between midday satellite based gross CO₂ and daily aggregated carbon flux at a variety of sites. However, the low temporal resolution associated with satellite based measurements makes it difficult to fully explore the effect data aggregation has on the accuracy of integration. Field optical sampling provides an experimental platform for the integration of optical and flux measurements (Gamon et al. 2006).

The main objectives of this chapter are to: 1) explore the effect of aggregation on the terms of the LUE model, both individually and combined and 2) determine the optimal aggregation period that will allow the most accurate prediction of fluxes from optical measurements. This case study will hope to establish some of the issues associated with developing an accurate LUE model that can be compared and integrated with flux derived productivity measurements.

4.2 Methods:

4.2.1 Study site:

The homogeneous alfalfa field (*Medicago sativa*) was located at the University of Alberta South Campus agricultural research farm; coordinates 53.497 N, -113.552 E. Monitoring occurred throughout the 2009 to 2011 growth seasons at various extents using 1) a 50m tram system (Gamon, et al., 2006b), providing a sampling platform for hyperspectral optical measurements from 2009-2011; 2) a 3 m phenology/ meteorological station, providing broadband optical measurements from 2009-2011; and 3) a 2.5m eddy covariance flux tower, providing atmospheric-biospheric CO₂ exchange measurements from 2009-2010. For more information on these methods, refer to chapter 2.

4.2.2 Eddy-covariance derived GPP:

The eddy covariance (EC) technique (Baldocchi et al., 1988, Moncrieff et al., 1997; Aubinet et al., 2000; Baldocchi, 2003) was used to measure net ecosystem CO₂($\mu\text{mol m}^{-2} \text{s}^{-1}$), latent heat (LE) (W m^{-2}), and sensible heat (H) (W m^{-2}) fluxes over the study field. Fluxes were measured at 10Hz and averaged over 30 minute aggregation periods throughout 2009 and 2010 growing seasons. High frequency eddy covariance data were processed using the post-acquisition software EdiRe (University of Edinburgh) program. Flux of CO₂ was expressed as the product of mean air density and the covariance between instantaneous vertical wind velocity and concentration fluctuations (details outlined in chapter 2 of this thesis).

Partitioning of measured net ecosystem exchange (NEE) ($\mu\text{mol m}^{-2} \text{s}^{-1}$) into gross primary productivity (GPP) ($\mu\text{mol m}^{-2} \text{s}^{-1}$) and total ecosystem respiration (TER) ($\mu\text{mol m}^{-2} \text{s}^{-1}$) was performed using the light-response curve method (Flanagan and Johnson, 2005; Glenn et al., 2006a; Glenn et al. 2006b; Syed et al., 2006; Adkinson et al., 2011). This method first involves fitting a non-linear regression using the following equation:

$$\text{NEE} = - \frac{A_{max} \alpha \text{PPFD}}{A_{max} + \alpha \text{PPFD}} + R_{10} Q_{10}^{(T-10/10)} \quad (3)$$

where A_{max} is the maximum carbon assimilation ($\mu\text{mol m}^{-2} \text{s}^{-1}$), or GPP, at infinite PPFD ($\mu\text{mol m}^{-2} \text{s}^{-1}$); α is the apparent quantum yield derived from the slope of the light-response curve ($\text{mol CO}_2 \text{ mol}^{-1} \text{PPFD}$); R_{10} represents the ecosystem respiration rate at 10°C ($\mu\text{mol m}^{-2} \text{s}^{-1}$); Q_{10} is the respiration temperature response coefficient during temperature changes of 10°C ; and T is the atmospheric temperature near the ground ($^\circ\text{C}$). For further details regarding partitioning of fluxes refer to chapter 2.

4.2.3 Vegetation indices:

The vegetation index NDVI was derived from hyperspectral reflectance measurements. NDVI was used as a proxy for fA_{PAR} (Kumar & Monteith, 1981; Sellers et al., 1987; Prince, 1991; Goward & Huemmrich, 1992). The index was constructed as follows:

$$\text{NDVI}_{680,800} = (\rho_{800} - \rho_{680}) / (\rho_{800} + \rho_{680}) \quad (4)$$

where “ ρ ” refers to reflectance and the subscripts refers to the specific spectral bands used (800 nm and 680nm).

Data collected from the broadband sensors on the phenology station were used to calculate a proxy normalized difference vegetation index (NDVI), derived based on the concept presented by Huemmrich et al. (1999). It was constructed from the ratio of upwelling to downwelling radiation and outlined by the mathematical expression:

$$\text{NDVI}_{\text{proxy}} = (\rho_{\text{PYR}} - \rho_{\text{PAR}}) / (\rho_{\text{PYR}} + \rho_{\text{PAR}}) \quad (5)$$

where ρ_{PYR} is the total radiation reflectance calculated from the ratio of upwelling to downwelling radiation using a silicon pyranometer (Onset Computer Corporation, Bourne, Massachusetts, USA, Massachusetts); and ρ_{PAR} is the total reflectance of photosynthetically active radiation (PAR) calculated from the ratio of upwelling to downwelling PAR radiance and irradiance (PPFD) using a quantum sensor (Onset Computer Corporation, Bourne, Massachusetts, USA, Massachusetts). The high temporal resolution of the 2-channel broadband data, logging every minute and averaged over 30 minute aggregation periods, allowed near-continuous diurnal NDVI proxy values through the season. Refer to Chapter 2 of this thesis for further detail.

4.2.4 fA_{PAR} and A_{PAR} values and derivations:

The fraction of absorbed photosynthetically active radiation (fA_{PAR}) absorbed by the alfalfa canopy was measured hourly in concert with optical sampling and calculated as previously outlined in chapter 2 of this thesis. Through the use of the previously defined $NDVI_{680,800}-fA_{PAR}$ and $NDVI_{proxy}-fA_{PAR}$ relationships, continuous fA_{PAR} values were calculated. Figure 4-1 shows the detailed methodology describing the process used to derive these values. $NDVI_{680,800}$ and $NDVI_{proxy}$ and fA_{PAR} midday values were used to determine $NDVI_{proxy}-fA_{PAR}$ and $NDVI_{680,800}-fA_{PAR}$ seasonal trends. Comparison between the two showed the proxy $NDVI$ based relationship to have a similar pattern to that of the benchmark $NDVI_{680,800}-fA_{PAR}$ relationship, but with a slight offset (see detailed analysis in chapter 2). To remove the offset, proxy $NDVI$ values were empirically corrected to match those of measured $NDVI_{680,800}$ and then used to construct a new $NDVI-fA_{PAR}$ relationship. The resulting non-linear equation from the $NDVI_{Huemmrich_II}-fA_{PAR}$ curve was then applied to all the $NDVI_{proxy}$ values, resulting in continuous fA_{PAR} values at one-minute intervals for the entire growth season. Continuous absorbed photosynthetically active radiation (A_{PAR}) values, at one-minute intervals, were a product of continuous fA_{PAR} values and directly measured PPFD logged every minute throughout the growing season.

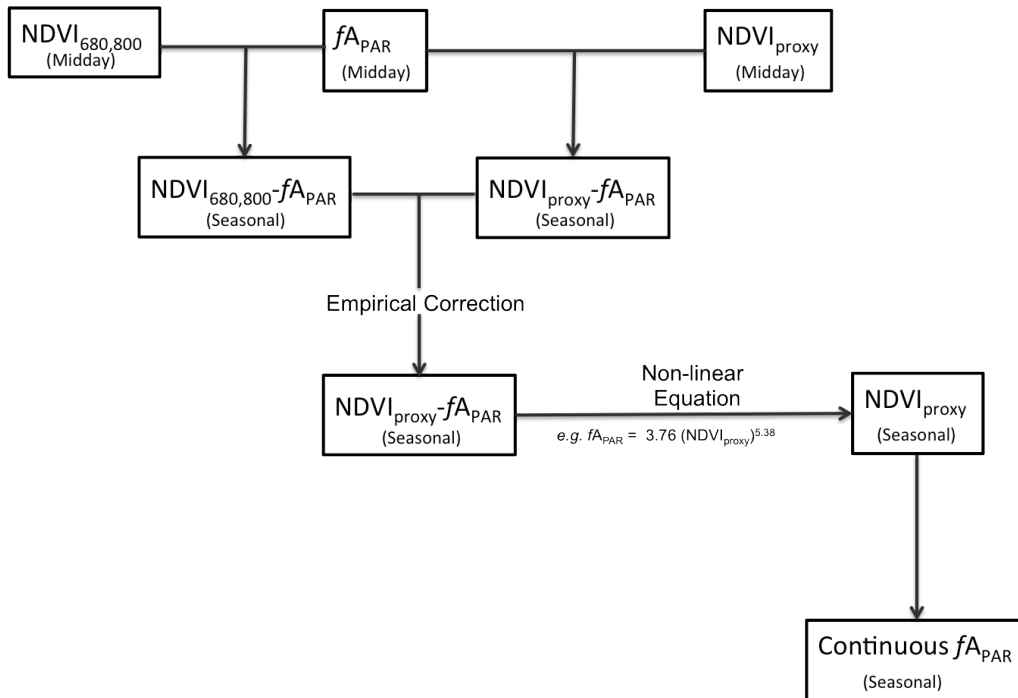


Figure 4-1: Flow chart depicting the method used to calculate continuous fA_{PAR} derived from the measured $NDVI_{680,800}-fA_{PAR}$ relationship. Comparison between the $NDVI_{680,800}$ and $NDVI_{proxy}$ values allowed the empirical correction of the 2-channel broadband data for the 2010 growth season. The power equation describing the empirically corrected $NDVI_{proxy}-fA_{PAR}$ relationship was applied to all $NDVI_{proxy}$ values collected throughout the season, allowing the calculation of continuous fA_{PAR} values for the entire 2010 growth season.

4.2.5 Temporal aggregation of LUE model variables:

A detailed assessment of the effect of temporal aggregation on the terms of the LUE model, both individually and combined, was performed to determine how best to integrate the flux and optical data streams. For temporal aggregation analysis, the LUE model equation was expressed as:

$$\begin{array}{c}
 \text{[----- III -----]} \\
 \text{GPP} = (fA_{PAR} \times PAR) \\
 \text{[IV] [I] [II]} \\
 \text{[----- V -----]}
 \end{array} \quad (7)$$

where the product of (I) the fraction of absorbed photosynthetically active radiation (fA_{PAR}), and (II) photosynthetically active radiation (PAR) is equivalent

to (III) the absorbed photosynthetically active radiation (A_{PAR}); and can be directly compared to (IV) gross primary productivity (GPP). Conventional expressions of the LUE model contain an efficiency term (ϵ), however, as discussed in chapter 3, due to the low influence of the physiological constituent on the overall seasonal productivity at our test site, this term was disregarded. Also, the low temporal coverage of PRI measurements prevented us from applying the same analysis to efficiency. Each of the variables in the LUE model were aggregated through averaging over increasing periods from 1 to 24 hours around midday values for each day of the growth season. Roman numerals I-V refer to the sequence in which the terms were aggregated, and indicate whether these terms were aggregated individually (I, II, IV) or in combination (III, V).

Aggregation by averaging fA_{PAR} was done using previously calculated continuous fA_{PAR} values. We should note that the NDVI- fA_{PAR} relationship built on midday values was used to calculate continuous fA_{PAR} values. To better illustrate this, a conceptual depiction of this process can be seen in figure 4-2 (top panel). Although there are some drawbacks to this method, the approach provided continuous fA_{PAR} values for all times of the day throughout the entire growth cycle. Aggregation effect on fA_{PAR} (method I of equation 7) was evaluated by aggregating continuous fA_{PAR} values (original logged at 1 minute intervals) while maintaining all other variables of the LUE model constant. fA_{PAR} values were aggregated over periods ranging from 30 minutes, matching the flux aggregation, to 24 hours. An LUE model was driven from each of the aggregation periods and

modeled GPP was compared to calculated GPP values. Figure 4-3b provides a flowchart of the aggregation methodology specific for continuous fA_{PAR} .

PAR values were collected at one-minute intervals. Measurements were aggregated over periods ranging from 30minutes to 24 hours. To test the aggregation effect on PAR, a series of LUE models were derived from each of the PAR aggregation periods, while maintaining all other variables at a designated constant aggregation period, and comparing the resulting model values to GPP (Figure 4-3a). The same general process was used to assess the effect of A_{PAR} and GPP aggregation (Figure 4-3c and 4-3d respectively). The fifth aggregation method comprised of a combination of all variables (Figure 4-3e). An optimal aggregation period was determined for each iteration, and was defined as the temporal aggregation period resulting in the highest coefficient of determination value. This was done for each of the three growth cycles within the 2010 growth season.

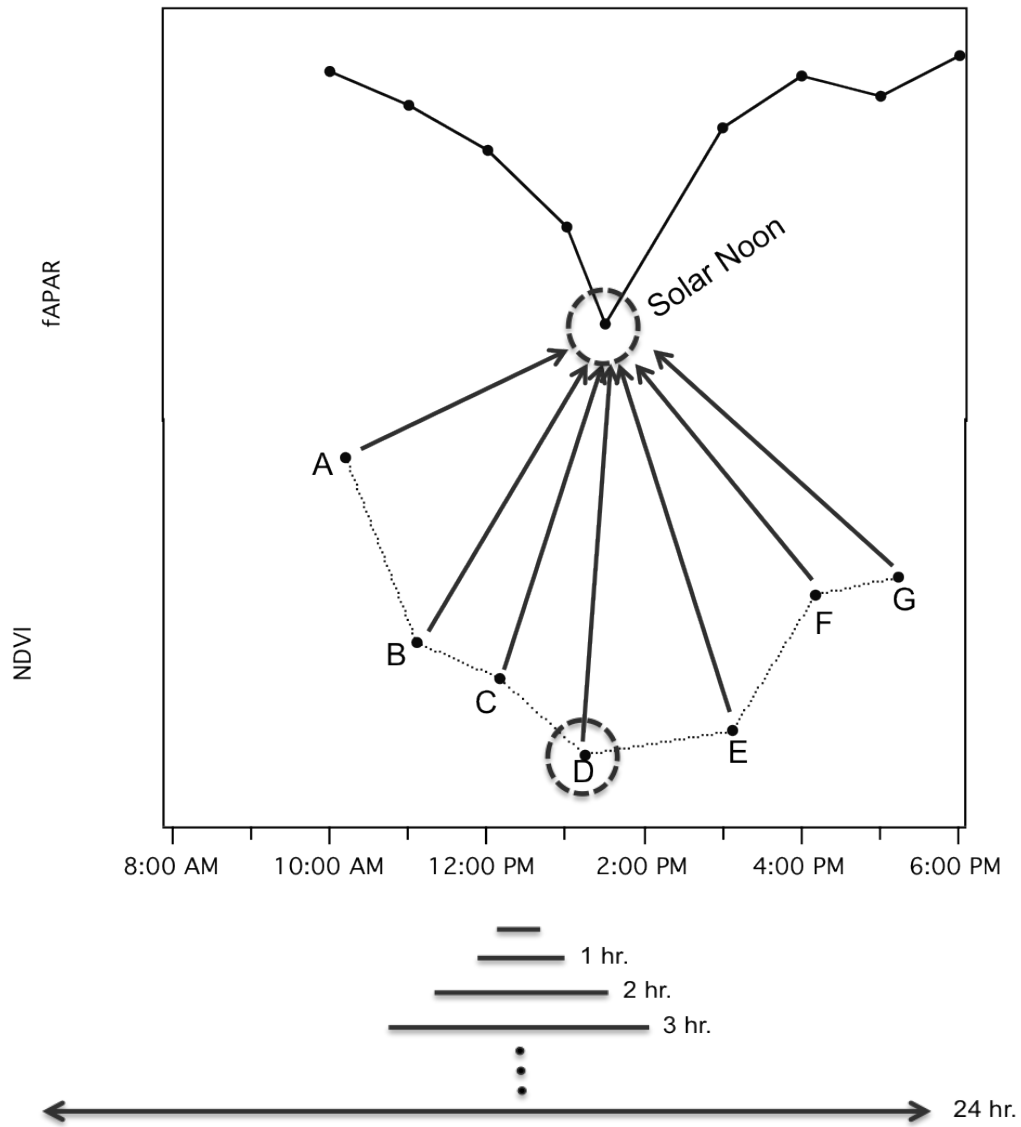
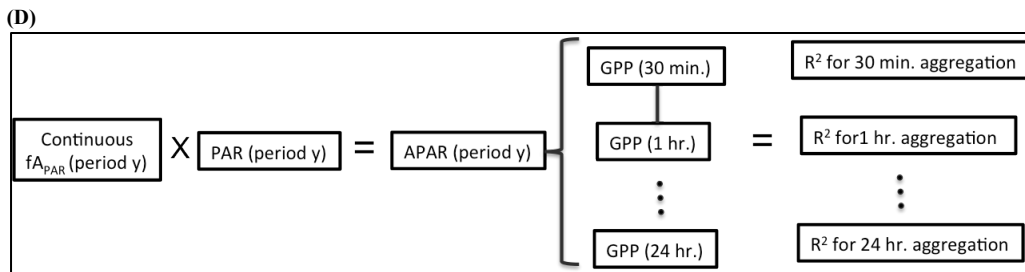
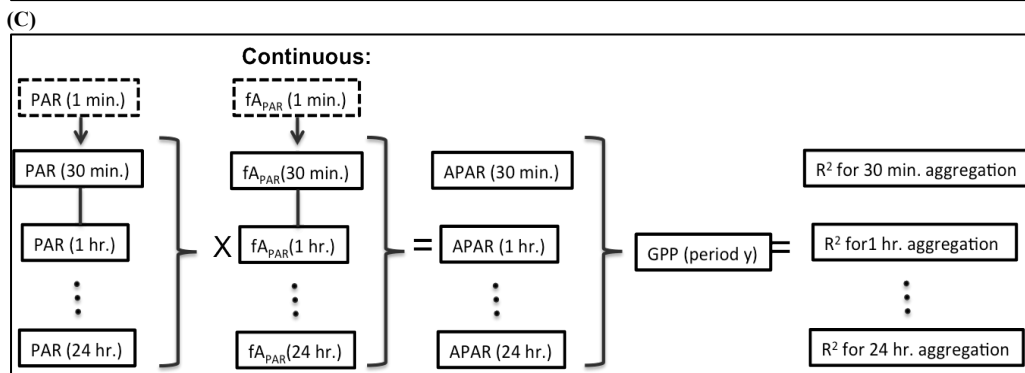
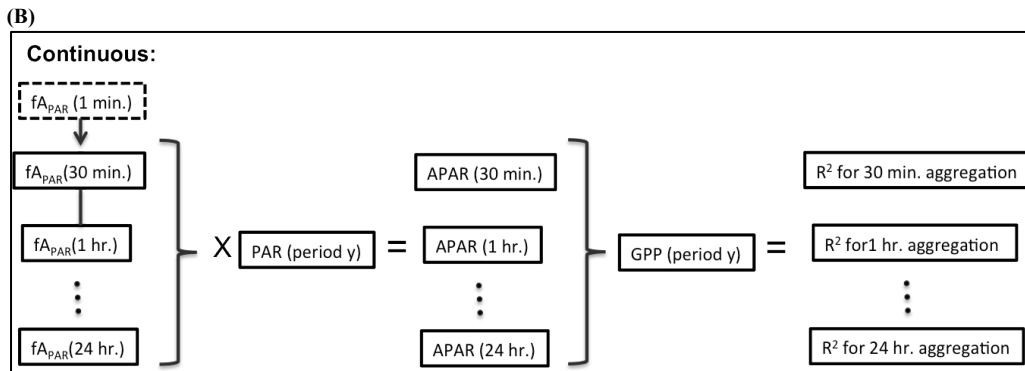
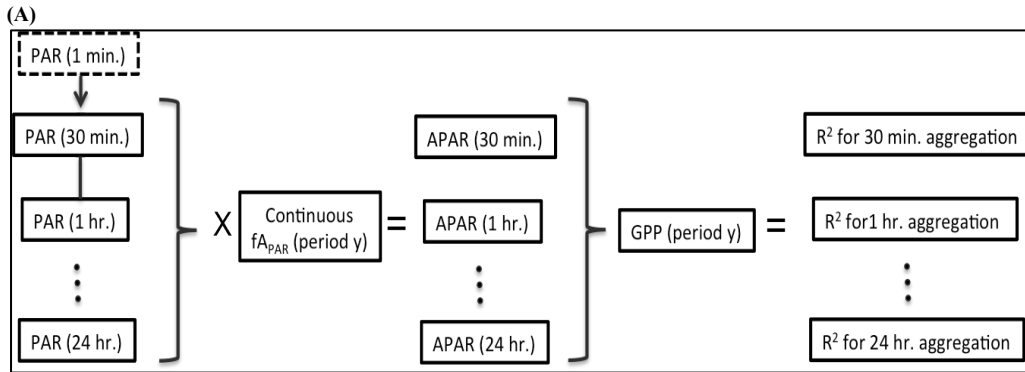


Figure 4-2: Conceptual model showing how NDVI_{proxy} data were associated with fA_{PAR} measurements during the calculation of continuous fA_{PAR} values. To construct the $NDVI_{680,800} \sim fA_{PAR}$ relationship, continuous NDVI_{proxy} measurements were compared only to midday values. The bottom panel is meant to represent the aggregation periods varying from 30 min. to 24 hours, centered on solar noon (approximately 13:30 MDT).



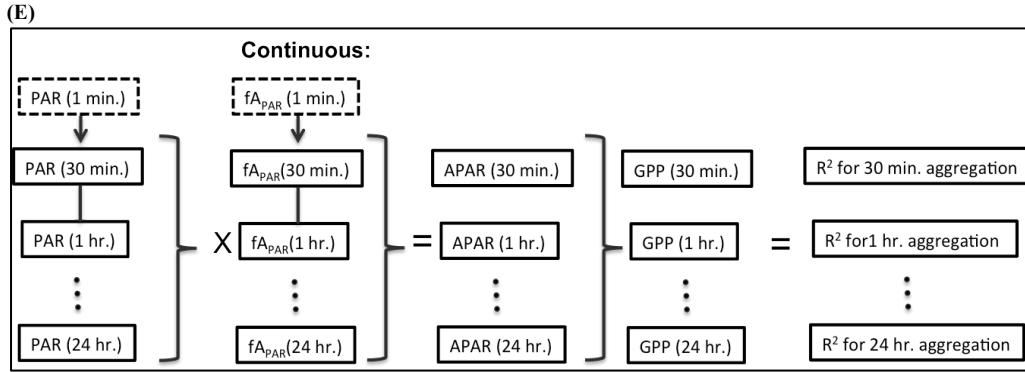


Figure 4-3: Work flows for aggregation of (A) PAR, (B) fA_{PAR} , (C) A_{PAR} , (D) GPP, and (E) all variables.

4.3 Results:

4.3.1 Temporal aggregation of each LUE model variable:

The initial qualitative assessment of the effect of aggregation on each of the LUE variables is easily illustrated by observing changes in their time series patterns (Figure 4-4). Aggregation of each of the LUE variables reduced variability inherent in continuous data, yielding clearer diurnal and seasonal patterns. The quantitative impact of temporal aggregation on model accuracy was determined by calculating coefficients of determination (R^2 values) for each of the aggregation period iterations within each aggregation method.

Evaluation of the impact of PAR aggregation for the growth cycle #1 (Figure 4-5a) shows a significant initial increase in accuracy during the first 4 hours of aggregation (R^2 range of 0.96-0.83, $\Delta R^2 = 0.13$). This upsurge is then followed by very slight increases, reaching a maximum $R^2 = 0.97$ that correlated to an optimal aggregation time period of 9 hours. Following peak accuracy, we observed a slightly decreasing plateau continuing until maximum aggregation period (24 hours). Very similar overall PAR aggregation effect patterns were observed for growth cycles #2 and #3, but the R^2 values were lower. Testing of

the fA_{PAR} variable for the first growth cycle showed negligible sensibility to aggregation, having a maximum $\Delta R^2 \approx 0.003$ throughout the entire aggregation period (Figure 4-5b). The optimal aggregation period was determined to be 12 hours, but the lack of sensibility to aggregation makes it hard to confidently resolve a definite optimal period. Similarly flat aggregation patterns were observed for growth cycles #2 and #3 but the R^2 values declined with each subsequent cycle. The general pattern for aggregation of A_{PAR} within each growth cycle was as expected, as it appears to be a combination of patterns observed from the PAR and fA_{PAR} aggregation methods. As in the PAR aggregation patterns, we observed an initial increase in R^2 values, followed by a plateau (Figure 4-5c).

Aggregation of flux-derived GPP showed an initial high responsiveness to aggregation, showing a $\Delta R^2 = 0.09$ (R^2 range of 0.96-0.87) within the first five aggregation hours. This was followed by slow continuous increases in R^2 values, until reaching optimal aggregation periods of 5 hours in all growth cycles, after which we observed a continuous slow decrease in values as flux variability increases and boundary layer conditions deteriorate (Figure 4-5d). Aggregation method V, where all terms were varied, showed patterns similar to both method III and IV. In growth cycles #1 and #2, again we observed an initial high sensitivity to aggregation continuing until peak accuracy, followed by a slow continuous decrease in R^2 values. For growth cycle #3, no initial rise in accuracy was observed.

When each of the aggregation methods was compared to one another, through all growth cycles, aggregation method V showed the greatest accuracy,

defined by the comparison of R^2 values for each aggregation method. Also, inter-comparison of growth cycles showed overall decreasing accuracy from cycle #1 to cycle #3 as these cycles become shorter and individual stages less distinct.

Optimal aggregation periods for each cycle and aggregation method are summarized in Table 4-1.

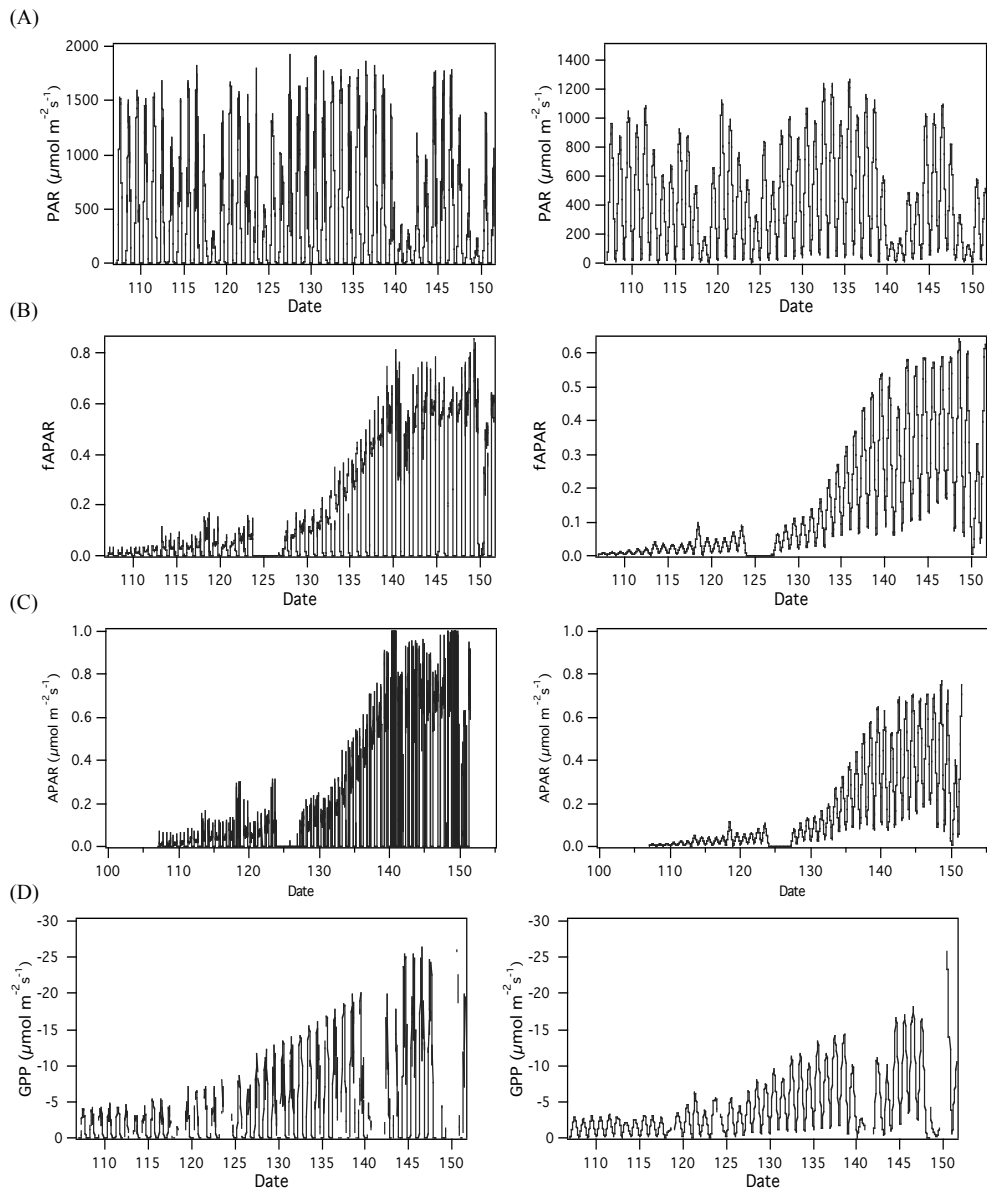
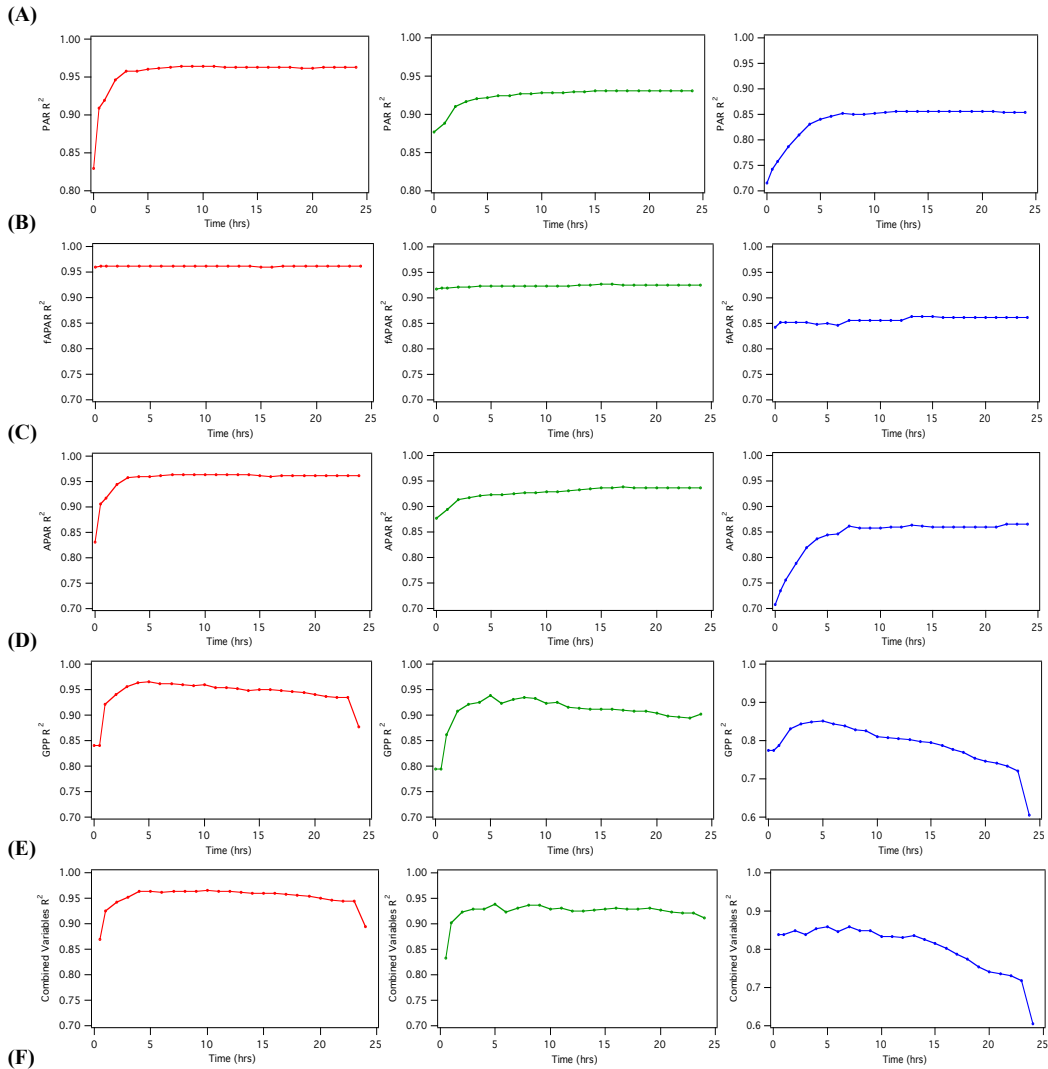


Figure 4-4: Comparison of the effect of aggregation through averaging on the time series of variable (A) PAR, (B) $f\text{APAR}$, (C) APAR , and (D) GPP aggregated over 30 minutes (left panels) and 12 hours (right panels). Aggregation reduces noise and generates a clearer pattern of diurnal changes.



(F) Figure 4-5: Coefficient of determination as a function of aggregation period (hours) for LUE model variables (A) PAR, (B) f_{APAR} , (C) A_{PAR} , (D) GPP and (E) all variables aggregated in concert; for growth cycle #1 (red), growth cycle #2 (green), and growth cycle #3 (blue) within the 2010 growth season.

Table 4-1: Resulting optimal aggregation periods for each of the aggregation methods. Individual periods were calculated for each of the three growth cycles within the 2010 growth season and a composite of the entire growth season.

Growth Cycle	PAR	fA_{PAR}	A_{PAR}	GPP	All Parameters
2010 GC#1	9 hr.	12 hr.	9 hr.	5 hr.	10 hr.
2010 GC#2	16 hr.	15 hr.	15 hr.	5 hr.	8 hr.
2010 GC#3	14 hr.	14 hr.	13 hr.	5 hr.	7 hr.
Full Season	15 hr.	16 hr.	15 hr.	4 hr.	9 hr.

4.3.2 Optical vs. flux productivity comparisons based on optimal aggregation periods:

To further explore the integration of optical and flux measurements, a series of optically driven LUE models, using the previously defined optimal aggregation periods of PAR, fA_{PAR} , and A_{PAR} , were compared to optimally aggregated GPP (9hrs., 12 hrs., and 9hrs. for GC#1, respectively) (see Table 4-1 for all aggregation periods). This was done for each of the three growth cycles as well as a composite of the entire 2010 growth season. Each of the models can be thought of as increasing in complexity and starting with PAR, fA_{PAR} , and A_{PAR} variables as drivers. The LUE model based on PAR showed little association with GPP ($R^2 = 0.19$ for growth cycle #1) (Figure 4-6a). The relationship showed significant dispersion in values and no clear seasonal trajectory throughout each of the three growth cycles. The model driven by fA_{PAR} showed a strong positive non-linear correlation to GPP ($R^2 = 0.85$ for growth cycle #1) (Figure 4-6c). A strong seasonal trajectory started to become defined showing a clear positive correlation between canopy greenness and GPP. Deviations in the relationship were attributed to periods directly following strong precipitation events, where flux measurements and calculated productivity appeared to be undervalued. The

final and more complex A_{PAR} driven LUE model showed the greatest correlation to productivity ($R^2 = 0.97$ for growth cycle #1) (Figure 4-6d). The very clear seasonal trajectory appeared to be non-linear for each of the growth cycles, as A_{PAR} values seemed to increase while productivity plateaued.

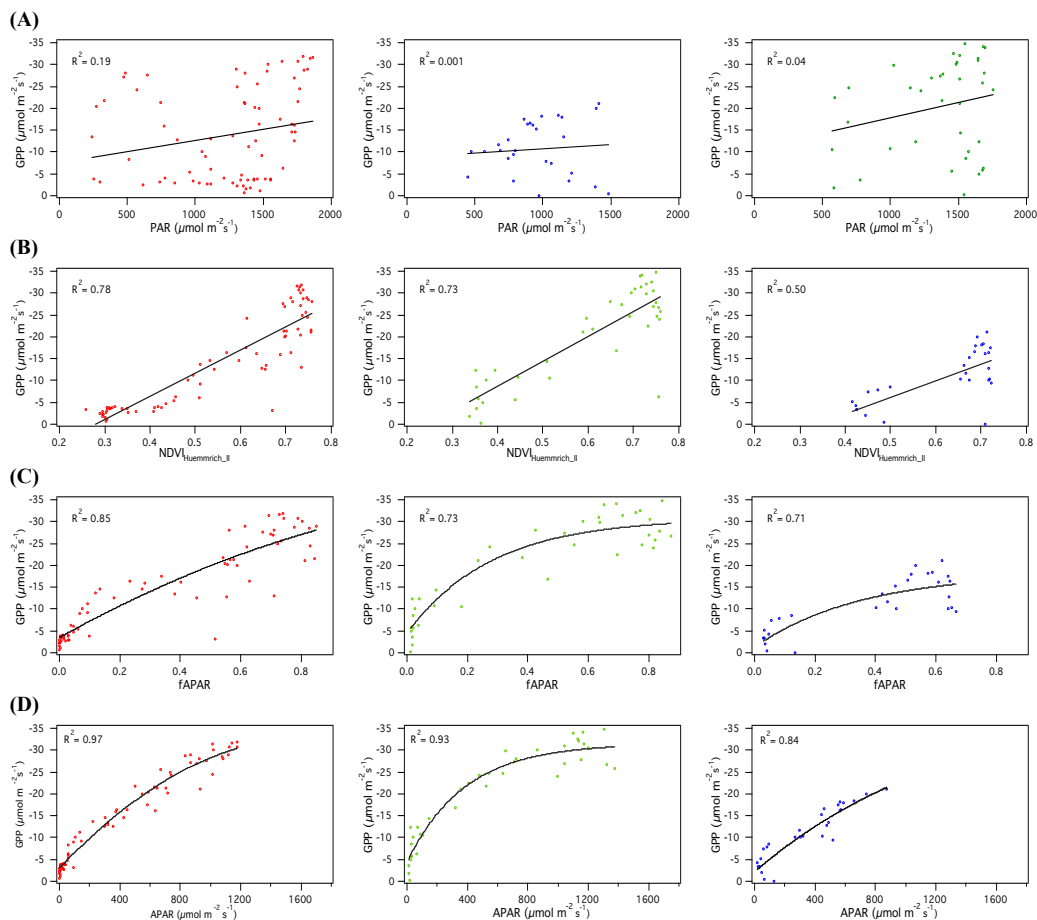


Figure 4-6: Comparison between measured GPP and optically derived representation of productivity through (A) PAR, (B) $NDVI_{Huemmrich_II}$, (C) fA_{PAR} , and (D) A_{PAR} for growth cycle #1 (red), growth cycle #2 (green), and growth cycle #3 (blue) within the 2010 growth season.

For each model, the three growth cycles showed patterns that were generally comparable. This was specially the case with the PAR-GPP comparisons, where the data set ranges seemed to all fall within one other's (Figure 4-7a). Comparisons of fA_{PAR} -GPP growth cycle relationships showed the first and third cycles as following a similar seasonal trajectory, while the second

cycle had slightly higher GPP per fA_{PAR} values (Figure 4-7b). The seasonal trajectory difference of cycle #2 became more pronounced in the A_{PAR} -GPP correlations (Figure 4-7c) and is supported by greater average GPP values during this time period, relative to the other cycles. When looking at the A_{PAR} -GPP relationships for each of the individual growth cycles, there is some evidence of hysteresis (trajectory not shown).

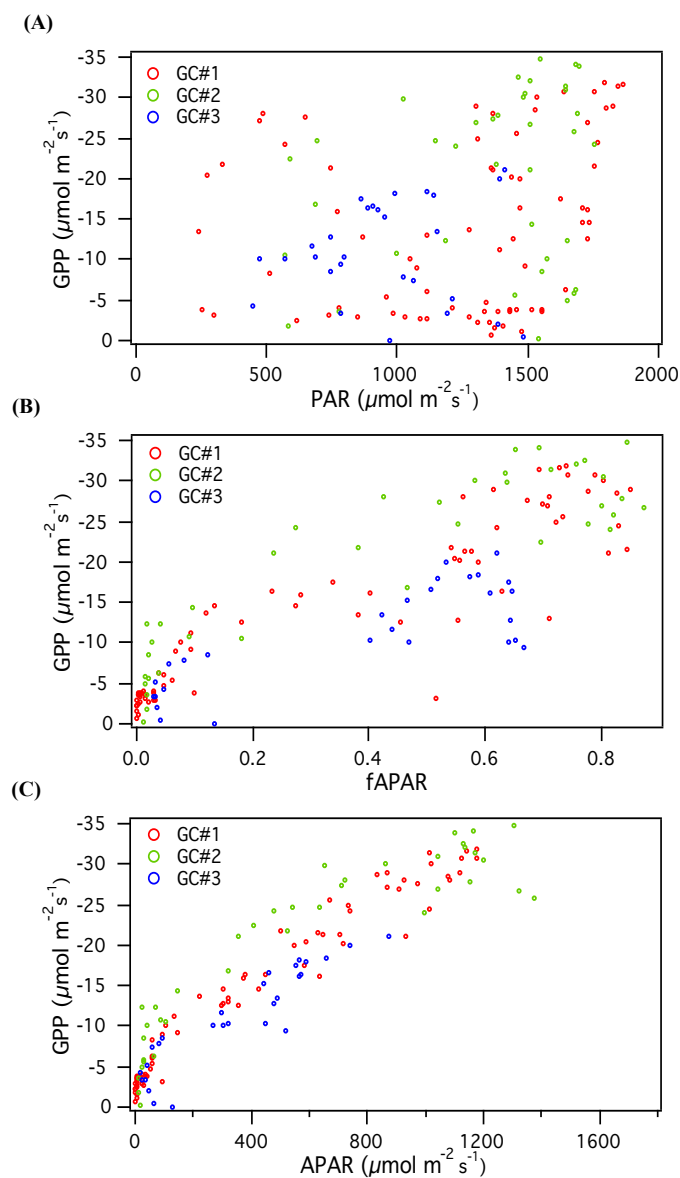


Figure 4-7: Seasonal comparison of all combined growth cycles between measured GPP and optically derived representation of productivity through (A) PAR, (B) fA_{PAR} , and (D) A_{PAR} .

Using an optimally aggregated A_{PAR} driven LUE model for each growth cycle and the complete growing season, optical based productivity values were calculated and compared to optimally aggregated GPP (9hrs, 15hrs, 13hrs, and 15hrs for GC#1, GC#2, GC#3, and full season, respectively). Time series plots of productivity for each of the growth cycles allowed us to assess if modeled GPP could resolve the seasonal dynamics encountered throughout the 2010 growth season. Assessment of the first growth cycle showed very close association between the modeled and measured GPP (Figure 4-8a). Major deviations between the measured and modeled values was observed during the start of the season and continued until green-up initiated. During green-up and maturity, modeled GPP accurately tracks the seasonal dynamics observed in measured values. Furthermore, the continuous A_{PAR} dataset allowed the calculation of continuous productivity values, even during periods where the flux dataset contained gaps due to precipitation or instrument malfunction events. Comparison between modeled and measured GPP during the second and third growth cycles showed similar results (Figures 4-8b and 4-8c, respectively). Divergences mainly occurred during recovery following harvesting events but correlations returned during green-up and maturity phases.

Due to variation in optimal aggregation periods between growth cycles, modeling of the entire 2010 growth season was performed by first determining the optimal aggregation period of all combined growth seasons (15hrs, 16hrs, 15hrs, 4hrs, and 9hrs for PAR, fA_{PAR} , A_{PAR} , GPP, and all variables combined, respectively). Also, multiple model iterations using single growth season average

aggregations were tested and resulted in the same time series pattern, changing only the model's scale ranges. From the evaluation of the entire season, we were able to observe a deviation between the modeled and measured GPP during the second growth cycle. Modeled values seem to underestimate productivity throughout this second cycle, especially considering that this cycle was the most productive due to high total precipitation during this period.

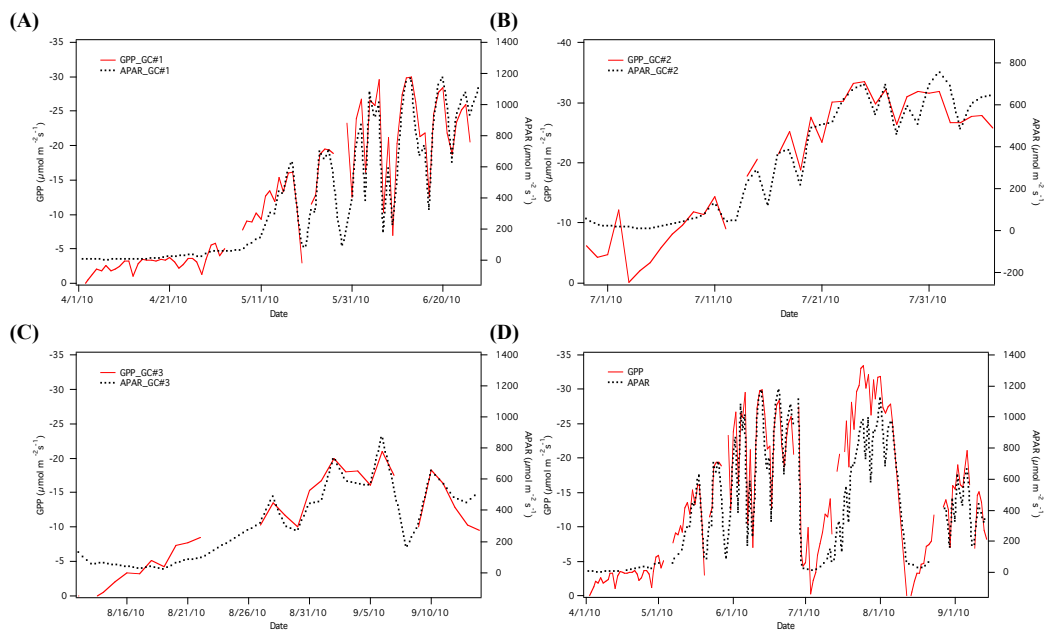


Figure 4-8: Time series of measured GPP and A_{PAR} derived productivity for (A) growth cycle #1, (B) growth cycle #2, (C) growth cycle #3, and (D) the entire 2010 growth season.

4.4 Discussion:

As this study shows, the method by which data is treated to derive the LUE model directly influences its overall accuracy. More specifically, temporal aggregation can lead to significant changes in model accuracy (Figure 4-5).

Furthermore, our results indicate that aggregation does not only impact optically

derived variables but also those derived from eddy covariance fluxes (Figure 4-5e). This illustrates the importance of understanding the impact of data manipulation and determining optimal approaches by which remote sensing and flux measurements can be integrated and result in accurate ecosystem productivity measurements.

The aggregation exercise not only provides a road map as to how to construct the most accurate model based on optimal periods, it also provided insight as to the effect each variable has on the overall model. PAR showed high sensitivity to aggregation, most likely due to the changing conditions encountered at our experimental site around mid-day, where clouds frequently appeared near solar noon. Optimal aggregation periods for each of the growth cycles seem to suggest that variability in PAR would be best dealt with by aggregating over a period approximating the diurnal photoperiod allowing minimization of variability through averaging. fA_{PAR} variability seemed to be insensitive to aggregation (Figure 4-1b). The lack of variability is most likely a function of the method used to calculate continuous fA_{PAR} using $NDVI_{proxy}$ values. By comparing all $NDVI_{proxy}$ values to only midday fA_{PAR} measurements, we remove the diurnal variability that would otherwise be maintained if each NDVI measurement was compared to its corresponding fA_{PAR} measurement. Future analysis should include an evaluation of the two methods and the effect on aggregation results and the overall model accuracy. We should also note that the lack of stress in this agricultural field (relative to many natural ecosystems – see chapter 3) would also contribute to the low diurnal variability. It is important to note that an even with

the absence of variability, the high R^2 values observed in the $fA_{\text{PAR}}\text{-GPP}$ relationships demonstrate that fA_{PAR} as an essential variable within the LUE model.

At our alfalfa agricultural site, we found that variability associated with incoming radiation affected the temporal aggregation patterns in an A_{PAR} driven LUE model (Figure 4-5c). However, this would not be the same case in all biomes. Temporal aggregation patterns of fA_{PAR} would most likely be much more variable in ecosystems or development stages where canopy structure plays a significant role. In such ecosystems, the interaction between changing solar angles and structure would lead to greater variability in diurnal illumination and fA_{PAR} patterns. It is therefore important that effects of temporal aggregation be explored for each particular ecosystem and, if possible, phenological stage. Determining optimal aggregation periods for each model variable, can provide some insight into the underlying mechanisms driving the productivity within an ecosystem.

While it is known that productivity is mainly driven through the variation in canopy A_{PAR} and secondly through variation in efficiency (Field et al., 1995), the relative magnitudes will differ between ecosystems. Due to the difficulty using PRI as a proxy of LUE (see results from chapter 3 of this thesis), efficiency could not be easily determined through optical sampling in our study. However, assessing the model variance not explained through A_{PAR} helped to indirectly determine the proportion by which ϵ might have influenced the LUE model. At our site, the majority of the model variance (between 84%-97%) was explained by the structural (A_{PAR}) component of the LUE model (Figure 4-6d). This was

expected due to the high rate of photosynthetic rate and the lack of water and nutrient stress for most of the growing season in this alfalfa field. Presumably, the remaining variance represents the physiological component associated with light use efficiency or can be attributed to error.

A detailed assessment of the seasonal trends within each growth cycle provides insight into how structure and physiology play changing roles during different phenological stages. The non-linear correlations of each of the A_{PAR} -GPP relationships suggest that productivity cannot solely be explained by the structural component. Departure from linearity seems to occur in all growth cycles during the transition from green-up to maturity stages, where productivity continues to increase at rates greater than that of canopy growth. This would suggest that during the late phenological stages, there is a changing influence of physiological status and limitations on productivity. The onset of non-linearity seems to occur earlier and be more evident in growth cycle #2 than the other cycles. This, along with results showing growth cycle #2 as having the greatest slope when comparing the individual A_{PAR} -GPP relationships, as well as displaying maximum total GPP, indicate that efficiency is greatest for this cycle. Maximum LUE values in this cycle could be associated with high water availability due to frequent precipitation events. The lack of an efficiency term in our LUE model would explain the separation between the modeled and measured GPP seasonal time-series observed for growth cycle #2 (Figure 4-8d). In cycles #1 and #3, efficiency seems to play less of a role in driving productivity; therefore

time-series analysis shows modeled values as accurate estimates of productivity (Figure 4-8d).

These observations call for incorporation of an efficiency term in ecosystems where closed-canopy or slow-growing vegetation is predominant. In ecosystems such as evergreen forests, where photosynthetic rate is often low and nutrient and water availability may be limited, the light use efficiency term will most likely represent a much larger source of total model variance (Field et al., 1995). Even though an agricultural site does not contain the same complexities encountered in other ecosystems, the methods and analysis discussed here can be used as a working model when assessing more dynamic ecosystems.

The combination of this accurate LUE model with flux measurements can allow us to explore certain ecosystem components in more detail. For instance, the ability to accurately model GPP dynamics of through remote sensing can provide a novel approach to partition fluxes. Partitioning is important to better understand the dynamics of the carbon cycle and respiration as well as to develop biochemical models (Baldocchi et al., 2001; Baldocchi 2003). Additionally, optical data can also help better inform carbon fluxes by providing a tool for gap filling periods of missing data. Flux data series typically contains gaps due to instrument malfunction as occurs during precipitation events. Optical sampling is less susceptible to such disturbances, hence accurate values of optically modeled GPP, in association with fluxes measurements, can be used to gap fill missing flux data periods. Examples of this can be see in Figure 4-8, modeled productivity values were able to accurately complement missing productivity data. These

examples illustrate how combining optical and flux measurements can help achieve a more comprehensive understanding of biospheric- atmospheric flux interactions.

4.5 References Cited:

Baldocchi, D.D. (2003). Assessing the eddy covariance technique for evaluating carbon dioxide exchange rates of ecosystems: past, present and future. *Global Change Biology*, 9: 479-492.

Baldocchi, D.D., Falge, E., Gu, L.H., Olson, R., Hollinger, D., Running, S., et al., (2001). FLUXNET: A new tool to study the temporal and spatial variability of ecosystem scale carbon dioxide, water vapor, and energy flux densities. *Bulletin of the American Meteorological Society*, 82: 2415-2434.

Coops, C., Hilker, T., Hall, F.G., Nichol, C.J., Drolet G.G. (2010). Estimation of light-use efficiency of terrestrial ecosystems from space: a status report. *Bioscience*, 60: 788-797.

Falge, E., Baldocchi, D., Tenhunen, J., Aubinet, M., Bakwin, P., Berbigier, P., Bernhofer, C., Burba, G., Clement, R., Davis, K.J. (2002). Seasonality of ecosystem respiration and gross primary production as derived from FLUXNET measurements. *Agricultural and Forest Meteorology*, 113: 53-74.

Field, C.B., Randerson, J.T., and Malmstrom, C.M., (1995). Global net primary production: combining ecology and remote sensing. *Remote Sensing of Environment*, 51:74-88.

Gamon, J. A., Rahman, A.F., Dungan, J.L., Schildhauer, M., Huemmrich, K.F. (2006). Spectral Network (SpecNet) – What is it and why do we need it?. *Remote Sensing of Environment*, 103: 227-235.

Heinsch F. A., Zhao, M., Running, S. W., Kimball, J. S., Nemani, R. R., Davis, K. J., et al. (2006). Evaluation of remote sensing based terrestrial productivity from MODIS using regional tower eddy flux network observations, *IEEE Trans. Geosci. Remote Sens.*, 44: 1908-1925.

Huemmrich, K.F., Black, T.A., Jarvis, P.G., McCaughey, J.H., Hall, F.G. (1999)High temporal resolution NDVI phenology from micrometeorological radiation sensors. *J Geophys Res Atmos*, 104:27935–27944.

Law, B.E., Falge, E., Gu, L., Baldocchi, D.D., Bakwin, P., Berbigier, P., Davis, K., Dolman, A.J., Falk, M., Fuentes, J.D. (2002). Environmental controls over carbon dioxide and water vapor exchange of terrestrial vegetation. *Agricultural and Forest Meteorology*, 113: 97-120.

Rahman, A.F., Cordova, V.D., Gamon, J.A., Schmid, H.P, Sims, D.A. (2004). Potential of MODIS ocean bands for estimating CO₂ flux from terrestrial vegetation: A novel approach. *Geophysical Research Letters*, 31.

Sims, D.A., Rahman, A.F., Cordova, V.D., Baldocchi, D.D., et al. (2005). Midday values of gross CO₂ flux and light use efficiency during satellite overpasses can be used to directly estimate eight-day mean flux. *Remote Sensing of Environment*, 101: 1-12.

Sims, D. A., Rahman, A.F., Cordova, V.D., El-Masri, B.Z., Baldocchi, D.D., Flanagan, L.B., Goldstein, A.H., Hollinger, D.Y., Misson, L., Monson, R.K., Oechel, W.C., Schmid, H.P., Wofsy, S.C., Xu, L. (2006). On the use of MODIS EVI to assess gross primary productivity of North American ecosystems. *Journal of Geophysical Research*, 112: 1633-1646.

Turner, D. P., Ritts, W. D., Cohen, W. B., Maeirsperger, T. K., Gower, S. T., Kirschbaum, A. A., et al. (2005), Site-level evaluation of satellite-based global terrestrial GPP and NPP monitoring, *Global Change Biology*, 11: 666–684.

Chapter 5 – General Discussion and Conclusion

This thesis is largely a test of optical methods in the context of the LUE model. A foundational assumption of this thesis was that optical monitoring (proximal remote sensing) at a comparable scale of the flux tower footprint can improve our understanding of the controls on carbon flux (Gamon et al. 2006, 2010). The LUE model is a product of the structural component (described by changes in A_{PAR}) and a physiological component (described through the efficiency term). Field et al. (1995) suggested that productivity (or GPP) is primarily driven through the variation in canopy A_{PAR} and secondly through variation in efficiency. Our results agree with this Field et al. (1995), showing that, at our site, the majority of the variance in GPP (approx. 78%) was explained by the structural (fA_{PAR}) component of the LUE model. This was expected due to the high rate of photosynthetic rate and the lack of water and nutrient stress associated with agricultural fields. In other ecosystems such as evergreen forests, where photosynthetic rate is low and nutrient and water may be limited, the light-use efficiency term is bound to represent a much larger source of total variance in carbon flux (Field et al., 1995).

Others have indicated that the amount by which each component of the LUE model contributes to the overall productivity will differ between ecosystems. For example, in a comparison of ecosystems, Garbulsky et al. (2011) suggested that ecosystems with high CO_2 assimilation and little excess energy or need for downregulation like a healthy crop system would not show a significant relationship between PRI and LUE_{Abs} . This is consistent with our finding that over

the full growing season in alfalfa, PRI is driven primarily by changes in canopy structure (as measured by fA_{PAR}) and is only weakly associated with LUE_{abs} .

In earlier diurnal studies, PRI was shown to be an accurate proxy of LUE_{Abs} (Gamon et al., 1992, 1993; Peñuelas et al., 1995). However, interpretation of PRI can become difficult at large temporal and spatial scales, where many factors such as effects of canopy structure, pigment pool changes, view and illumination angles can confound the PRI-LUE relationship (Barton & North, 2001, Styliniski et al., 2002; Sims et al., 2006; Filella et al., 2009; Garrity et al., 2011; Gamon & Berry, 2012). In our study, we found that at the seasonal time scale, PRI is indeed confounded by changes in vegetation structure. The effect associated with structural changes is so large that it hindered us to from identifying the underlying physiological changes defined by light use efficiency. However, at the diurnal level, where changes in vegetation structure are reduced, PRI accurately tracks changes in LUE, as has been shown in previous studies (Gamon et al. 1992, 1993, Peñuelas et al., 1995). This shows that even in an ecosystem with strong CO_2 uptake, PRI reveals changing physiological activity, when considered over the appropriate time scale. Our results demonstrate that the interpretation of PRI depends largely on the context in which the index is being analyzed. Factors such temporal and spatial scale, type and condition of canopy, and irradiance must be considered to ensure that PRI is acting like a suitable proxy of light use efficiency. Without this, it is still possible to get a correlation between PRI and GPP or other photosynthetic measures, but the explanation of

the correlation may be confounded by multiple factors, as shown in this study, and as reported by Barton and North (2001).

The ability to interpret PRI in terms of light response curves provides a way to clearly identify the variability in signal attributed to physiological changes in light use efficiency. This analysis helped identify periods of excess light energy (Björkman and Demming-Adams, 1994) when the xanthophyll cycle de-epoxidation is likely to play an important role in influencing the PRI signal.

Applying this method repeatedly over the growing season would help separate the PRI signal into the structural component and the subtler physiological component. Due to the need for frequent sampling, such measurements are hard to accomplish using the periodic tram sampling methods used here. Automated two-band PRI sensors could provide the necessary temporal coverage that would allow us to implement the light response curve method across the full growing season. While such PRI sensors are now available (Garrity et al. 2010; Balzarolo et al. 2011; Eklundh et al. 2011), more work is needed to characterize these sensors.

To make any association between a vegetation index and efficiency, LUE must be expressed in its correct form. As our results show, defining LUE based on incident light instead of absorbed light leads to an opposite and potentially incorrect conclusion that PRI is detecting changes in physiological activity, when, in fact, it is reflecting changes in canopy structure of rapidly growing vegetation. This misrepresentation of LUE can lead to misunderstanding of the controls on carbon flux, especially in ecosystems where productivity is primarily driven by structural changes in vegetation. It is likely that the literature is full of such false

correlations, Since many authors have chosen to calculate LUE on an incident light basis, while not measuring pigments or canopy structure, it is likely that misinterpretation of PRI abounds, confusing our ability to reveal the underlying mechanisms controlling carbon fluxes. We recommend that, to be able to test any vegetation index as a proxy of efficiency, it is crucial that LUE be calculated by its correct definition *i.e.* based on absorbed light, particularly in situations where canopy structure is likely to change and confound the interpretation of PRI.

The empirical calibration of two-band radiometer data with hyperspectral data can be used as example of how different optical datasets can be integrated to produce a unified signal (in our case, a common fA_{PAR} metric) for use in the LUE model. The integration of data sources allows us to take advantage of the benefits associated with each measurement method, while minimizing their disadvantages. For example, the lack of temporal resolution in our hyperspectral data and the low spectral resolution of two-band sensors can be both overcome through empirical cross-calibrations, allowing integration of the data streams. The ability to use inexpensive spot radiometers to assess ecosystem carbon flux increases the feasibility of achieving continuous monitoring of the many diverse global ecosystems (Huemmrich et al., 1999, Gamon et al. 2010). The rich temporal resolution associated with automated two-band sensors allowed us to capture the seasonal dynamic changes in vegetation structure that would have otherwise been unnoticed through occasional or periodic field collection methods such as the tram collections. The strong correlation between $NDVI_{proxy}$ and our benchmark

NDVI_{680,800}, and the strong correlation with fA_{PAR} , show that simple and inexpensive 2-channel radiometers can be used to drive the LUE model.

The concept of data source integration can be explained using a funnel analogy (Figure 5-1). For this concept, we can think of each data source as an input that can be combined with others to produce a single LUE model expression. One of the main advantages of data integration would be the production of a single LUE model that accommodates and incorporates multiple data sources into a single, uniform output.

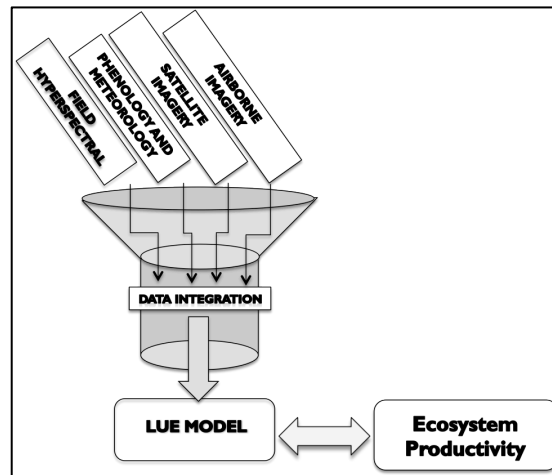


Figure 5-1: Hypothesized funnel concept describing the progress of integrating different data sources. Integration results in a single expression of the LUE model that can then be compared to ecosystem productivity.

The way data is treated when deriving the LUE model will directly influence its overall predictive capabilities. Our results demonstrate that aggregation can be important. In this study, the need for spatial aggregation was minimized by the uniform stand structure and the sampling methods that allowed a large sampling area. Our study shows that temporal aggregation can lead to significant changes in model accuracy. Also, our results indicate that aggregation

not only affects variables derived from optical measurement but also those derived from eddy covariance. Therefore, it is essential to determine how the different data sources affect the accuracy of the LUE model.

Additionally, this study demonstrated a method for conceptually integrating optical and flux data by comparing diurnal changes in PRI to changes in the slope of the light response curve. This kind of methodological integration can help us understand the relative importance of structural vs. physiological controls on ecosystem carbon fluxes. In this case, structural controls (fA_{PAR}) dominated, but this would not be the case for all ecosystems. For example, in evergreen ecosystems, where physiological downregulation can exert a significant influence over fluxes, we would expect light-use efficiency to become a more important model variable (Running and Nemani 1988; Runyon et al., 1994; Gamon et al., 1995). Further work should focus on expanding these methods of analyses across different ecosystems to help reveal contrasting controls on carbon fluxes and develop improved LUE models, as has been proposed (Gamon et al. 2006, 2010)

Take Home Messages:

- The ability to properly track GPP seasonal dynamics with broadband-derived proxy NDVIs, the high correlation between proxy and benchmark (narrow-band) NDVI measurements, and the accurate characterization of the NDVI- fA_{PAR} relationship are all positive results pointing to the utility

of using automated two-band sensors to derive a LUE model. More work is needed to develop and test similar PRI sensors.

- In alfalfa, seasonal $PRI_{531,570}$ changes are primarily influenced by structural changes (illustrated as fA_{PAR} variation over time) which concealed the underlying physiological changes associated with occasional photosynthetic downregulation on the diurnal scale.
- An incorrect derivation of LUE, based on incident light, can lead to incorrect positive correlations between efficiency and PRI. Properly defining LUE as LUE_{ABS} should help avoid this problem.
- Within a single day, even in ecosystems primarily influenced by canopy structure, the underlying physiological changes quantified through light response curve analysis are strongly correlated with PRI changes. This method of integrating light-response curves derived from eddy covariance with dynamic optical properties illustrates a powerful way to demonstrate the physiological influence on PRI against a background of structural changes affecting this index.
- Integration of flux and optical data using the LUE model can help with partitioning of flux data and gap-filling periods of missing flux data.
- Temporal aggregation of data can significantly affect the LUE model accuracy.

Future research:

There are additional areas where future research would allow further testing and refinement of the LUE model. One of these areas includes the further comparisons of two-channel NDVI and PRI sensors against benchmark spectrometer measurements. While this study used empirical methods of calibrating such sensors, another approach might be to use the sensor radiometric response functions to better characterize such sensors. There is a particular need to characterize new two-band sensors used to monitor PRI. Automated PRI sensors would facilitate the application of the light response curve method, allowing the partitioning of the seasonal PRI signal into that which is affected by structure vs. due to physiological changes by using light response curves. This would allow us to better evaluate the correlation between PRI and changes in efficiency at the seasonal level.

One of the biggest remaining questions of this study is related to data aggregation. Our results illustrate a limited subset of the many different aggregation periods and methods that could be used. There is a need to expand the concept of data aggregation by methodically exploring the effect of different aggregation periods on the overall LUE model accuracy. This could lead to an improved LUE model that uses an optimal method by which optical data could best predict productivity. Also additional models that allow estimations of ecosystem productivity should be also explored. These may include models driven by fluorescence index (Zarco-Tejada et al., 2000) as well as the chlorophyll index (Gitelson et al., 2006).

Further studies might also consider expanding this analysis to other types of ecosystems, where vegetation structure changes do not have such a strong influence on productivity, such as in evergreens. Networks such as the FLUXNET and SpecNet could be used to further explore the integration of flux and optical data across various ecosystems. To help achieve this, better methods of data management will be needed due to the large volumes of data involved. Unlike current data systems that focus on flux or spectral data alone, data systems that facilitate integration of flux and spectral data must be developed. Such studies could help us understand contrasting controls on carbon flux, and could also evaluate whether a universal LUE model parameterization is possible.

References Cited:

- Baldocchi, D.D., Hicks, B.B., and Meyers, T.D. (1988). Measuring biosphere-atmosphere exchanges of biologically related gases with micrometeorological methods. *Ecology*, 69: 1331-1340.
- Baldocchi, D.D., Finnigan, J.J., Wilson, K.W. et al., (2000). On measuring net ecosystem carbon exchange in complex terrain over tall vegetation. *Boundary Layer Meteorology*, 96: 257-291.
- Barton, C. V. M., & North, P. R. J. (2001). Remote Sensing of canopy light use efficiency using the Photochemical Reflectance Index. Model and analysis. *Remote Sensing of Environment*, 78: 264-273.
- Björkman, O. and Demmig-Adams, B. (1994). Regulation of photosynthetic light energy capture, conversion and dissipation in leaves of higher plants. In: Schulze E-D and Caldwell MM (eds) *Ecophysiology of Photosynthesis*, pp 17–47. *Ecological Studies* 100. Springer-Verlag, Berlin.
- Braswell, B.H., Schimel, D.S., Linder, E., and Moore III, B. (1997). The response of global terrestrial ecosystems to interannual temperature variability. *Science*, 278:870-873.
- Balzarolo, M., Anderson, K., Nichol, C., Rossini, M., Vescovo, L. (2011). Ground-Based Optical Measurements at European Flux Sites: A Review of Methods, Instruments and Current Controversies. *Sensors*, 2011: 7954-7981
- Eklundh, L., Jin, H., Schubert, P., Guzinski, R., Heliasz, M., (2011). An optical sensor network for vegetation phenology monitoring and satellite data calibration. *Sensors*, 11: 7678-7709.
- Field C.B., Randerson J.T., Malmstrom C.M. (1995). Global net primary production: combining ecology and remote sensing. *Remote Sensing of Environment*, 51:74-88.
- Field C.B., Behrenfeld M.J., Randerson J.T. and Falkowski P. (1998). Primary production of the biosphere: Integrating terrestrial and oceanic components. *Science*, 281: 237-240.
- Filella, I., Porcar-Castell, A., Munné-Bosch, S., Bäck, J., Garbulsky, M., & Peñuelas, J. (2009). PRI assessment of long-term changes in carotenoids/chlorophyll ratio and short-term changes in de-epoxidation state of the xanthophyll cycle. *International Journal of Remote Sensing*, 30: 4443-4455.
- Foken, T.H., Wichura, B. (1995). Tools for quality assessment of surface-based flux measurements. *Agricultural and Forest Meteorology*, 78: 83-105.

Gamon, J.A., Peñuelas, J., and Field, C.B. (1992). A narrow-waveband spectral index that tracks diurnal changes in photosynthetic efficiency. *Remote Sensing of Environment*, 41: 35–44.

Gamon, J.A., Filella, I., Peñuelas, J. (1993). The dynamic 531-nanometer Δ reflectance signal: a survey of twenty angiosperm species. Yamamoto HY , Smith CM (Eds). *Photosynthetic Responses to the Environment*. American Society of Plant Physiologists, Rockville. pp. 172-177.

Gamon, J.A., Field, C.B., Goulden, M.L., Griffin, K.L., Hartley, A.E., Joel, G., Peñuelas, J. and Valentini, R. (1995). Relationships between NDVI, canopy structure and photosynthesis in three Californian vegetation types. *Ecol Appl*, 5: 28-41.

Gamon, J.A., Rahman, A.F., Dungan, J.L., Schildhauer, M., and Huemmrich, K.F. (2006a). Spectral Network (SpecNet): what is it and why do we need it? *Remote Sensing of Environment*, 103: 227-235.

Gamon, J.A., Coburn C., Flanagan L.B., Huemmrich K.F., Kiddle C., Sanchez-Azofeifa G.A., Thayer D.R., Vescovo L., Gianelle D., Sims D.A., Rahman A.F., and Pastorello G.Z. (2010). SpecNet revisited: bridging flux and remote sensing communities, *Canadian Journal of Remote Sensing*, 36: 376-390.

Gamon, J. A., & Berry, J. A. (2012). Facultative and constitutive pigment effects on the Photochemical Reflectance Index (PRI) in sun and shade conifer needles. *Israel Journal of Plant Sciences*, 60: 85-95.

Garbulsky, M. F., Peñuelas, J., Gamon, J. A., Inoue, Y., & Filella, I. (2011). The photochemical reflectance index (PRI) and the remote sensing of leaf, canopy and ecosystem radiation use efficiencies: A review and meta-analysis. *Remote Sensing of Environment*, 115: 281-297.

Garrity, S.R.; Vierling, L.A.; Bickford, K. A. (2010). Simple Filtered Photodiode Instrument for Continuous Measurement of Narrowband NDVI and PRI over Vegetated Canopies. *Agricultural and Forest Meteorology*, 150: 489-496.

Garrity, S.R., Eitel, J.U.H., & Vierling, L.A. (2011). Disentangling the relationships between plant pigments and the photochemical reflectance index reveals a new approach for remote estimation of carotenoid content. *Remote Sensing of Environment*, 115: 628–635.

Gitelson, A.A., Viña, A., Verma, S., Rundquist, D.C., Arkebauer, T. et al. (2006). Relationship between gross primary production and chlorophyll content in crops: implications for the synoptic monitoring of vegetation productivity. *Journal of Geophysical Research*, 111.

Heinsch F. A., Zhao, M., Running, S. W., Kimball, J. S., Nemani, R. R., Davis, K. J., et al. (2006). Evaluation of remote sensing based terrestrial productivity from MODIS using regional tower eddy flux network observations, *IEEE Trans. Geosci. Remote Sens.*, 44: 1908-1925.

Huemmrich, K.F., Black, T.A., Jarvis, P.G., McCaughey, J.H., & Hall, F.G. (1999). High temporal resolution NDVI phenology from micrometeorological radiation sensors. *Journal of Geophysical Research*, 104: 935-944.

Massman W.J., Lee X., (2002). Eddy covariance flux correlations and uncertainties in long term studies of carbon and energy exchanges. *Agricultural and Forest Meteorology*, 113: 121-144.

Peñuelas, J., Filella, I., and Gamon, J.A. (1995). Assessment of photosynthetic radiation-use efficiency with spectral reflectance. *New Phytologist*, 131: 291-296.

Schimel D.S., (1995). Terrestrial biogeochemical cycles: global estimates with remote sensing. *Remote Sensing of Environment*, 51: 49-56.

Sims, D.A., Luo, H., Hastings, S., Oechel, W.C., Rahman, A.F., & Gamon, J.A. (2006). Parallel adjustments in vegetation greenness and ecosystem CO₂ exchange in response to drought in a Southern California chaparral ecosystem. *Remote Sensing of Environment*, 103: 289-303.

Stylinski, C.D., Gamon, J.A., & Oechel, W.C. (2002). Seasonal patterns of reflectance indices, carotenoid pigments and photosynthesis of evergreen chaparral species. *Oecologia*, 131: 366–374.

Reich, P.B., Turner, D.P., Bolstad, P. (1999). An approach to spatially distributed modeling of net primary production (NPP) at the landscape scale and its application in validation of EOS NPP products. *Remote Sensing of Environment*, 70: 69–81.

Running, S.W. and Nemani, R.R. (1988). Relating seasonal patterns of the AVHRR vegetation index to simulated photosynthesis and transpiration of forests in different climates. *Remote Sensing of Environment*, 24: 347-367.

Running S.W., Nemani, R.R., Heinsch, F.A., Zhao, M., Reeves, M., Hashimoto, H. (2004). A continuous satellite-derived measure of global terrestrial primary production. *Bioscience*, 54: 547-560.

Running, S.W. (2008). Ecosystem disturbance, carbon, and climate. *Science* 321: 652–653.

Runyon, J., Waring, R.H., Goward, S.N. and Welles, J.M. (1994). Environmental limits on net primary production and light-use efficiency across the Oregon Transect. *Ecol Appl*, 4: 226–237.

Turner, D. P., Ritts, W. D., Cohen, W. B., Maeirsperger, T. K., Gower, S. T., Kirschbaum, A. A., et al. (2005), Site-level evaluation of satellite-based global terrestrial GPP and NPP monitoring, *Global Change Biology*, 11: 666–684.

Zarco-Tejada, P.J., et al. (2000). Chlorophyll fluorescence effect of vegetation apparent reflectance: II. laboratory and airborne canopy-level measurements with hyperspectral data. *Remote Sensing of Environment*, 74: 596-608.

Zhao, M., Heinsch, F. A., Nemani, R.R., and Running, S. W. (2005), Improvement of the MODIS terrestrial gross and net primary production global data set, *Remote Sensing of Environment*, 95: 164-176.